Fluorescence Tools to Identify Novel SERCA Activators

A DISSERTATION
SUBMITTED TO THE FACULTY OF THE GRADUATE SCHOOL
OF THE UNIVERSITY OF MINNESOTA
BY

Simon Joseph Gruber

IN PARTIAL FULFILLMENT OF THE REQUIREMENTS
FOR THE DEGREE OF
DOCTOR OF PHILOSOPHY

David D. Thomas, Adviser

August 2013

Acknowledgements

I first want to thank my advisor, **Dr. David Thomas**, for helping me decide to pursue graduate school and providing the best possible lab experience. Dave has allowed me to pursue my interests and provided guidance along the way, always willing to try new things and let me learn by trial and error. Everyone that comes through this lab knows how hard Dave works and the example he sets every day makes me want to be a better scientist. I would not be where I am today without the Dave Thomas and the more time I spend in the lab, the more excited I am about my future career in science.

I would like to thank my committee, **Dr. Joseph Metzger**, **Dr. Reuben Harris**, **Dr. Anja Bielinsky**, **Dr. Alex Lange** and **Dr. Gianluigi Veglia**, for all the guidance and support you have given me, especially regarding the presentations I have given over the years. I have had frequent interactions with the Metzger, Harris, and Veglia labs over the years. Whether I am asking them for advice about protein expression in a cell line, learning about phospholamban, or trying to understand how things work in an intact heart, collaborators and neighboring UMN labs have always been there to help.

Through my projects, I had the opportunity to work closely with **Dr. Razvan Cornea** and **Dr. Mike Autry**. I am thankful for both of these mentors and I am sure I am a better scientist because of them. Mike is one of the most knowledgeable scientists I have ever met, and he operates with more integrity than anyone. Mike wants the right answer and he accepts no compromises or incomplete experiments. He is a hard worker and an inspiration to be around, and I have no doubt he has a positive influence on my graduate career. Razvan got me started in the Thomas lab working on a drug screening

project and has encouraged me to stay involved with as many projects as possible. Razvan has great scientific instincts and I have always seen his success as something I aspire to attain. When I first started in the lab, my graduate student mentor **Dr. Elizabeth Lockamy** was going through some old drawers and throwing away all the "garbage". I have always had a tough time throwing away things that may be useful at some point in the future, so when Razvan walked by and started digging through the trash and lamenting the loss of a label maker from the 80's and other equipment he was never going to use, I knew we would get along great. Elizabeth taught me everything I needed to know to get started in the Thomas lab and how to stay in Dave's good graces. I would not have been as successful in the Thomas lab without Elizabeth to show me around and help me deal with all kinds of little problems. I am thankful for her mentorship and friendship.

Jesse McCaffrey, **Tyler Miller**, and **Dr. Brett Colson** are good friends that made the graduate school experience more pleasant. I would not have been able to eat lunch by myself or handle the everyday issues of working in a big lab without you guys.

Sarah Blakely and **Octavian Cornea** know that I could not have done anything without their help arranging trips to conferences, applying for grants, and dealing with everyday issues in and around the lab. I also would have failed to register for classes or even know what program I was in without the help of **Darlene Toedter** in the BMBB office. I am thankful for all of their help over the years.

There are many undergraduates that have assisted me over the years, and each showed a dedication to the lab that impressed me. They saved me time with routine tasks

Dedication

To my family, Josh, Pam, Sarah, and Ben Gruber

Abstract

One of the universal hallmarks of heart failure is defective calcium cycling. The calcium concentration in a muscle cell must be high to cause contraction and low to allow relaxation, and most of the calcium removal is accomplished by the intracellular membrane pump known as the sarco-endoplasmic reticulum calcium ATPase (SERCA). When SERCA activity is too low in cardiac muscle, the heart does not fully relax and fill with blood, so the next contraction cannot pump enough blood through the body. The ubiquity of calcium cycling dysfunction in heart failure and other muscle diseases has made SERCA a major target for novel heart failure therapeutics since the late 1990s. All of the work presented in this thesis focuses on methods to activate SERCA as a treatment for heart failure.

SERCA is regulated by phospholamban (PLB) in heart muscle, preventing the enzyme from being fully active all the time but allowing maximal activity when the body demands. Some methods of activating SERCA seek to remove the inhibitory effects of PLB, either partially or fully. In this thesis, PLB mutants are investigated as potential gene therapy vectors. PLB mutants that are less inhibitory but still bind to SERCA could allow the enzyme to be more active if they displace endogenous PLB. A FRET assay using genetically engineered fluorescent fusions of SERCA and PLB expressed stably in a human cell line was used to measure the ability of different mutants to compete for SERCA binding.

Fluorescently labeled SERCA and PLB were also reconstituted in an in vitro lipid bilayer system to screen for small-molecule compounds that activate SERCA. Several

compounds were found to decrease SERCA-PLB FRET and many of these turned out to be SERCA activators that improved myocyte contractility. However, none of the compounds were specific to the SERCA-PLB interaction.

Finally, an intramolecular FRET assay was developed to detect changes in the relative distance between cytoplasmic domains within SERCA in living cells. This assay was used to screen a small-scale compound library to show that FRET between SERCA domains is sensitive to both activators and inhibitors of SERCA function. All of these FRET assays are being followed up in the Thomas lab to identify potential SERCA activators for heart failure and other diseases.

Table of Contents

List of Figures

List of Equations

Chapter 1 - Introduction

1.1. Calcium Regulation in Muscle

Muscles contract when the cytosolic calcium concentration is high and relax when it is low. The physical mechanism of muscle contraction begins when an action potential reaches the outer membrane of a muscle cell. The action potential depolarizes the sarcolemmal membrane and triggers L-type Ca^{2+} channels that are closely linked to ryanodine receptors (RyR) in the sarcoplasmic reticulum (SR). RyRs release large amounts of Ca^{2+} from the SR, allowing sarcomeric proteins to contract, and the Ca^{2+} is pumped back into the SR by the sarco/endoplasmic reticulum calcium ATPase (SERCA). SERCA utilizes energy from hydrolyzing one molecule of ATP to pump two Ca^{2+} ions against a 4-log concentration gradient, and it is most active when the cytosolic $[Ca^{2+}]$ is high [1].

Muscle can be broadly broken down into three categories: smooth, skeletal, and cardiac. Skeletal muscle is further broken down into fast and slow-twitch muscle. Most muscle proteins are expressed as different isoforms with different properties in each type of muscle. For example, fast skeletal muscle contracts much more rapidly than smooth muscle because the calcium cycling and contractile proteins work faster. Cardiac muscle is highly specialized to meet the continuously changing demands on the heart [2].

SERCA in cardiac muscle is regulated by phospholamban (PLB), a single-pass transmembrane protein that inhibits SERCA when the $[Ca^{2+}]$ is low [3, 4]. This inhibition is relieved when PLB is phosphorylated at Ser-16 by protein kinase A (PKA) or at Thr-17 by calcium/calmodulin kinase II (CaMKII) [5, 6]. PKA phosphorylation of PLB is

promoted by β-adrenergic stimulation and is a crucial part of the body's 'fight or flight' response [7].

1.2. SERCA

1.2.1. SERCA Isoforms

Ca^{2+} pumps are present in both prokaryotic and eukaryotic organisms and have been evolutionarily conserved for millions of years [8]. Higher eukaryotes have greater numbers and diversity of many ion pumps, and mammals encode SERCA pumps in genes on three separate chromosomes in addition to other Ca^{2+} pumps expressed in the Golgi apparatus or plasma membranes [9]. The SERCA1 gene *ATP2A1* is primarily expressed as the 994-amino acid splice-variant SERCA1a in fast-twitch skeletal muscle and is only spliced into SERCA1b embryonically. SERCA1a is readily purified from skeletal muscle of rabbits or pigs and is the most frequently studied isoform. SERCA1a is 84% homologous to SERCA2a, the cardiac splice variant of the SERCA2 gene *ATP2A2*. SERCA2b is expressed at a high level in smooth muscle but also at low levels in all tissues as a 'housekeeping protein' [10], and SERCA2c is a poorly studied splice variant of unknown importance [11, 12], but a recent study suggests it may play a role in cardiac Ca^{2+} signaling [13]. SERCA2a and SERCA2b are identical for the first 993 amino acids but have different C-terminal tails resulting from alternative splicing at the last exon. SERCA2a transcripts encode only four additional amino acids for a total of 997 residues, while the C-terminal tail of SERCA2b has 49 amino acids and forms an extra helical domain that modulates affinity for Ca^{2+} and turnover rate [14]. SERCA2a is remarkably well preserved across mammalian species, with fewer than nine amino acid differences between humans and pigs, rabbits, dogs, or mice [15]. Mutations in the *ATP2A2* gene are

2

implicated in Darier's Disease, a skin disorder that is inherited in an autosomal dominant fashion [16]. Although these mutations sometimes manifest in coding regions of the gene, altering the sequence of SERCA2a and SERCA2b, Darier's Disease is not associated with cardiac symptoms and no *ATP2A2* mutations are linked to inherited cardiomyopathies.

The third SERCA gene, *ATP2A3*, is spliced into at least six different variants, a-f [17]. The SERCA3 variants have been studied only recently following successful cloning and generation of specific antibodies and their physiological role is still unknown. Evidence has begun to emerge that they may play a part in regulating small but distinct pools of Ca^{2+} in the cytoplasm and even the nucleus of many different cell types, including cardiomyocytes [13, 18]. The work in this thesis is primarily focused on SERCA2a, the cardiac isoform, but also involves SERCA1a because it has been characterized to a greater extent and is much easier to express and purify.
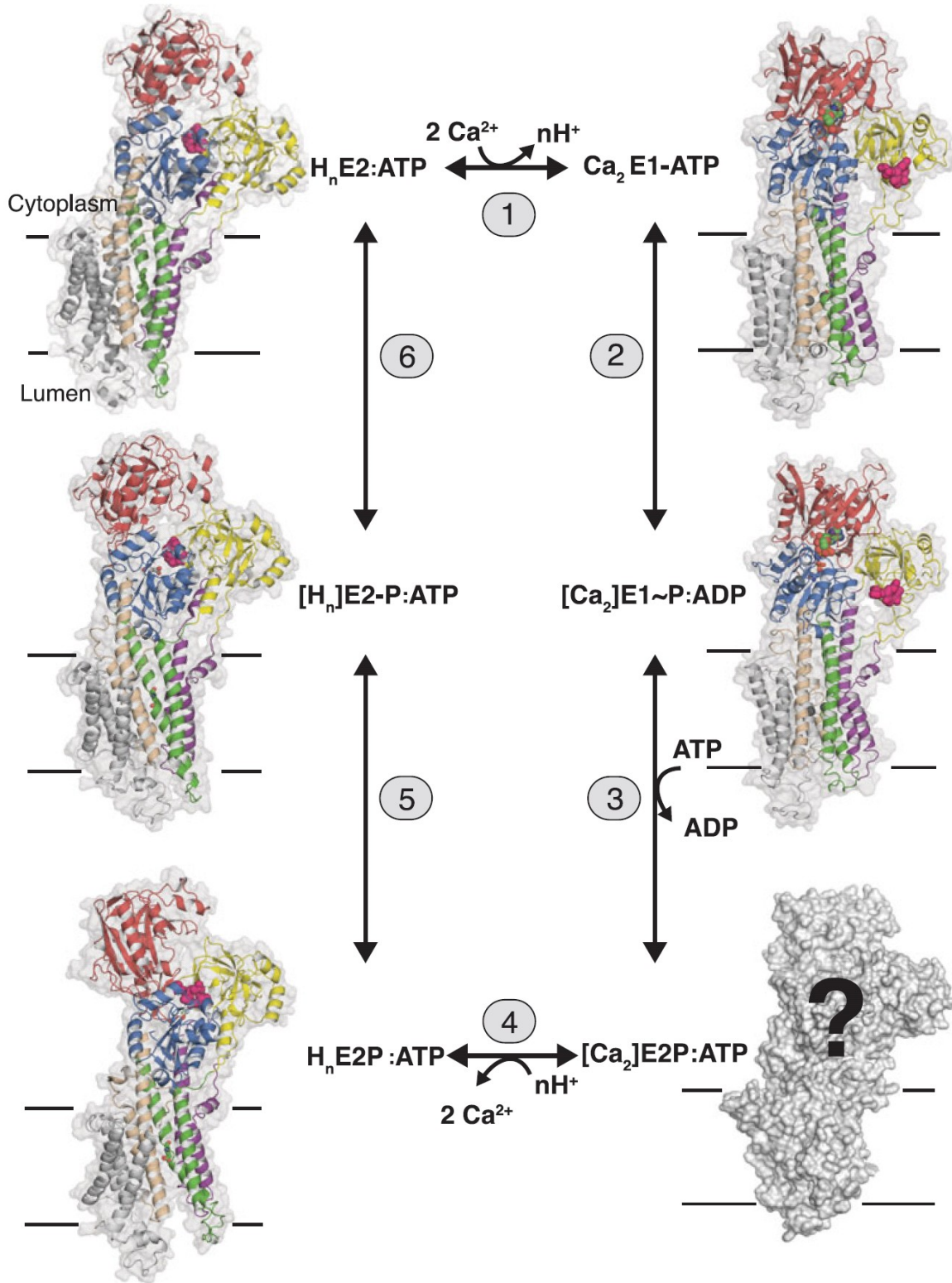
Figure 1. SERCA enzymatic cycle. Many SERCA crystal structures have been associated with a particular enzyme intermediate, highlighting the large-scale structural rearrangements that are seen in the cytoplasmic domains. From [19].

4

1.2.2. SERCA Enzymatic Cycle

The ability of the Ca^{2+}-ATPase to move ions against such a strong concentration gradient, and with great specificity for Ca^{2+} over other divalent cations, made SERCA the subject of intense study since its identification as a Ca^{2+} pump by David MacLennan in 1970 [20]. Many biochemical and structural states have been characterized, but the mechanism by which SERCA and other membrane pumps utilize the energy from ATP hydrolysis to move ions against their concentration gradient is still only partially understood.

SERCA has two Ca^{2+}-binding sites that are well defined by mutagenesis studies carried out mostly by the MacLennan lab [21-24]. SERCA oscillates between a high Ca^{2+}-affinity state (E1) and a low Ca^{2+}-affinity state (E2), and couples this oscillation to structural rearrangements that result in binding Ca^{2+} in the cytosol and releasing it in the ER/SR lumen [25-27]. The enzymatic cycle begins with the dephosphorylated, ATP-bound enzyme in the E1 state binding 2 Ca^{2+} ions cytosol (step 1 in **Figure 1**). SERCA hydrolyzes the ATP to phosphorylate itself and ADP is released as SERCA shifts into the E2 state and releases the Ca^{2+} ions in the ER/SR lumen, binding a new molecule of ATP (steps 2 and 3). Two to three H^+ ions are bound in place of the Ca^{2+} and counter-transported into the cytosol (step 4). This counter transport and shift back into the high Ca^{2+} affinity E1 state is accompanied by dephosphorylation and phosphate release (steps 5 and 6) [19].

1.2.3. SERCA Structure

Primary transporters like SERCA use chemical energy to move something against an unfavorable gradient. Many of these transporters utilize the energy stored in phosphate

bonds of molecules like ATP and share significant structural properties. ATP hydrolyzing enzymes are categorized as F-, V-, P-type or ABC transporters, based on functional and structural homology [28]. SERCA is classified as a P-type ATPase because it phosphorylates itself during its enzymatic cycle. P-type ATPases are mostly cation pumps or lipid flipases and also include the Na^+/K^+-ATPase, H^+/K^+-ATPase, and heavy metal Cu^+-ATPase [29]. All of the P-type ATPases have transmembrane domains consisting of bundles of α-helices that guide cargo across the membrane, and cytoplasmic domains that hydrolyze ATP and coordinate movement of the transmembrane helices. SERCA is one of the most well studied primary transporters and was the first P-type ATPase to be yield a high-resolution crystal structure [30].
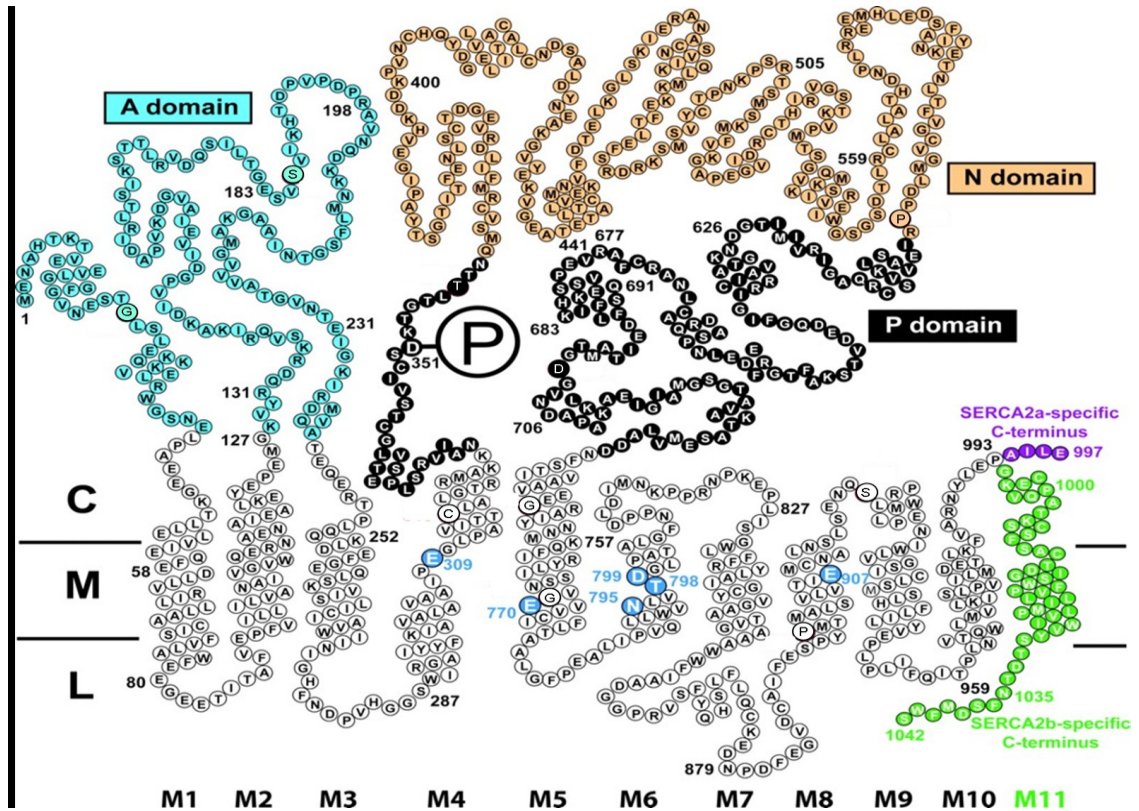
Figure 2. SERCA domain structure. SERCA is structurally homologous to many other ion pumps, consisting of ten transmembrane helices (white) and three cytosolic domains (A domain in cyan, N domain in orange, P domain in black). SERCA2b has an extra transmembrane helix and luminal extension (green) that are involved in stabilizing the Ca^{2+}-bound conformation. Ca^{2+}-binding residues in the transmembrane domain are in blue. Figure adapted from [31].

Most SERCA isoforms, including SERCA1a and SERCA2a, have ten transmembrane helices and three cytoplasmic domains (**Figure 2**). SERCA2b has an extra transmembrane helix and lumenal extension that slow conformational changes in the cytoplasmic domains and increase Ca^{2+} binding affinity, giving this isoform unique kinetic properties that are most useful in slow-twitch muscle or non-muscle tissue [14, 32] Key residues involved in Ca^{2+} binding are indicated in **Figure 2**.

The three cytoplasmic domains of SERCA form the 'headpiece'. The nucleotide binding domain (N domain) binds ATP and phosphorylates an aspartic acid residue (D351 in SERCA1a) in the phosphorylation (P) domain. The actuator (A) domain

coordinates movement of the N and P domains and undergoes significant rotational movements to coordinate the dephosphorylation of SERCA [33, 34].

Most of information about the three dimensional structure of SERCA comes from X-ray crystallography data, though individual domains have been studied by NMR with similar results [35]. These structures added depth to a significant body of SERCA mutagenesis research that had identified residues likely to be involved in ligand binding or biochemical transitions such as ATP hydrolysis and phosphate release [36-38]. SERCA1a purified from rabbit SR or recombinantly expressed and purified from yeast has been used to obtain numerous crystal structures with different inhibitors or ATP analogs bound, but no structure of SERCA2a or other isoforms has been reported. Most of the structures have been assigned to different biochemical states of the enzyme based on the ligands used to stabilize the crystals (**Figure 1**) [39]. Comparing crystal structures in various states reveals changes in the arrangement of transmembrane helices when Ca^{2+} binds and large rearrangements of the cytoplasmic domains with binding of Ca^{2+} or ATP.

It remains controversial whether crystal structures truly represent the conformation of the enzyme in its native states. Ligands added to generate crystals could perturb the structure, and crystallization can stabilize a structure that is not a favored state under physiological conditions. Thapsigargin (TG) was present in many early crystals, and the resulting structures showed a very compact headpiece arrangement [40]. Newer crystals in the absence of TG yielded virtually identical structures, and FRET studies with a double-labeled SERCA expressed in HEK cells or myocytes have shown that TG actually causes the headpiece to adopt a much more open conformation than seen in

crystals ([41] and Chapter 5). Crystallography predicted a significant opening of the headpiece upon Ca^{2+} binding, but FRET experiments carried out by Dr. Deb Winters in the Thomas lab revealed that this opening did not occur in native membranes [42]. Despite these limitations, crystal structures have been a powerful tool in connecting the enzymatic cycle of SERCA with the structural changes that facilitate efficient and specific Ca^{2+}-transport.

1.3. PLB

1.3.1. PLB Structure and Dynamics

PLB is a single-pass transmembrane protein that regulates SERCA in cardiac muscle by reducing its apparent calcium affinity ($1/K_{Ca}$) without inhibiting its maximal rate at high $[Ca^{2+}]$. PLB has three phosphorylation sites at S10, S16, and T17 that are phosphorylated by PKC, PKA, and CamKII, respectively [43]. Phosphorylation at either S16 or T17 reduces PLB inhibitory potency, but the PKA site is thought to be more important physiologically because it is more clearly under adrenergic control [44].

There is no crystal structure of PLB, but NMR has shown that both primary phosphorylation sites, S16 and T17, are at the end of the cytoplasmic helix next to a loop
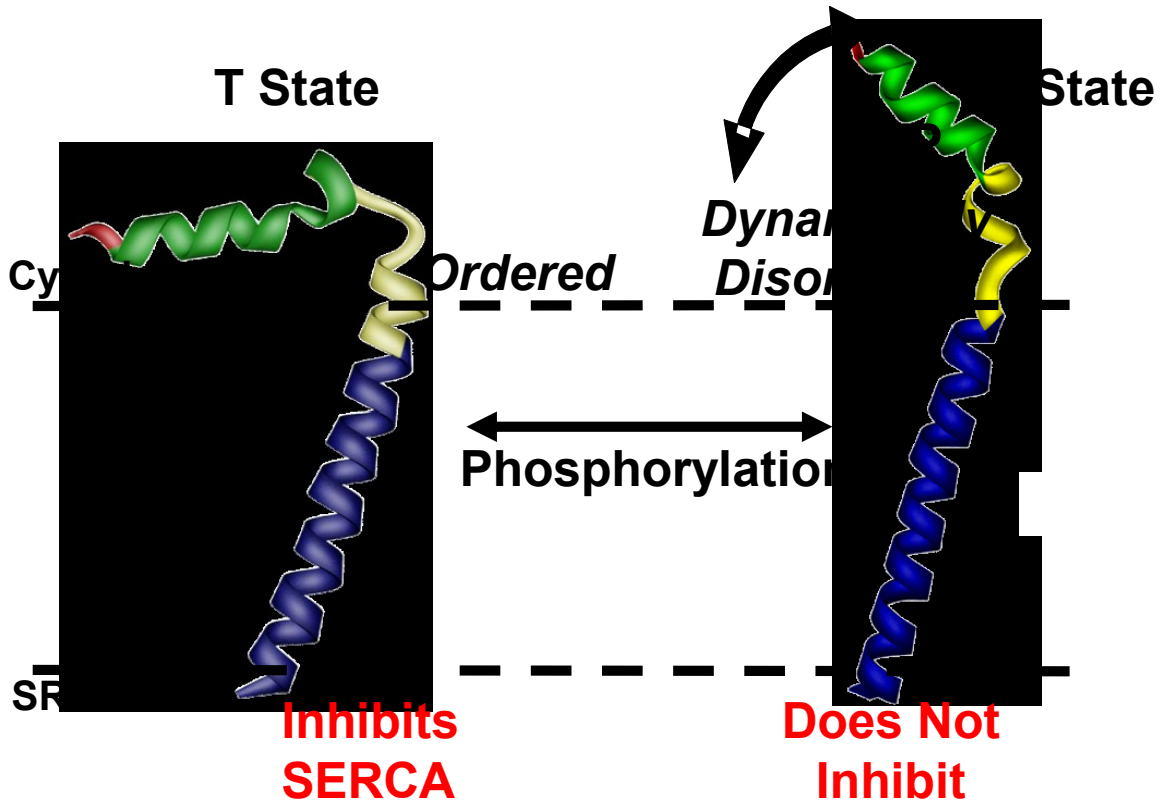
Figure 3. PLB structure and dynamics. PLB structures determined by NMR are color coded by domain: cytoplasmic helix Ia in green, transmembrane domain (II) in blue, and cytoplasmic helix 1b and the loop in yellow. Phosphorylation of PLB induces an order-to-disorder transition in the cytoplasmic helix that is associated with relief of SERCA inhibition.

connecting it to a transmembrane helix (**Figure 3**). In **Figure 3**, the cytoplasmic helix, domain Ia (residues 1-17), is green, and the transmembrane helix, domain II (residues 33-52), is blue. The loop between the helices (residues 18-22) and the second cytoplasmic helix, domain Ib (residues 23-32), are colored yellow. PLB exists in at least two structural states, a tense (T) state in which the cytoplasmic helix is highly ordered and interacts with the membrane surface, and a relaxed (R) state in which the cytoplasmic

helix becomes disordered and extends away from the membrane surface (**Figure 3**) [45]. PLB phosphorylation shifts the equilibrium of these two states in favor of the more disordered R state, as shown by NMR and EPR [46-48]. Thus phosphorylation induces an order-to-disorder transition in the cytoplasmic domain of PLB. MD simulations show that the phosphorylated state is stabilized by an intramolecular salt bridge that includes the phosphorylated serine [49]. The importance of tight control of SERCA phosphorylation in the heart is evidenced by a cardiomyopathic mutation in PLB, an arginine-to-cysteine substitution at position 9 that is thought to be pathogenic because it cannot be phosphorylated by PKA [50] (see section 1.5.2 "PLB-linked cardiomyopathies").

PLB oligomerizes via a leucine/isoleucine zipper formed between transmembrane helices to make a pentamer [51, 52] that is thought to be a storage form of PLB [53] but may also form a pore that allows ion conductance [54, 55]
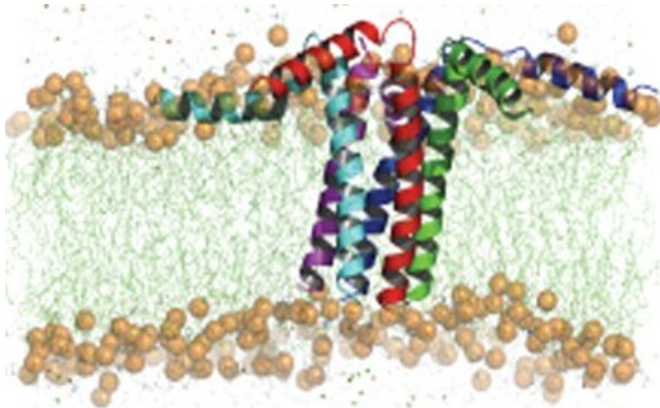
Figure 4. PLB pentamer structure in a lipid bilayer. Verardi *et al.* solved the structure of pentameric PLB by a hybrid solution/solid-state NMR method and performed molecular dynamic simulations of the structure in a lipid membrane. From [51]

(**Figure 4**). PLB oligomerization can be inhibited by mutating some of the zipper residues, but the 'AFA' mutant that replaces three cysteine residues at positions 36, 41, and 46, with alanine, phenylalanine, and alanine, respectively, is frequently used to study monomeric PLB structure and function.

1.3.2. PLB Regulation of SERCA

At the level of the SR in cardiac muscle where PLB is expressed, contractility is primarily regulated by cAMP-dependent activation of Ca^{2+} transport back into the SR by SERCA. PLB phosphorylation relieves all [56] or most [46] SERCA inhibition, leading to increased Ca^{2+} load in the SR, improved relaxation during diastole, and greater contractility in systole. The PLB:SERCA molar ratio in heart has been measured for several animals with reported values ranging from 1-5 [44, 57]. Quantitative measurements of S16 phosphorylation in pig cardiac muscle showed that while the PLB:SERCA ratio is variable, the ratio of unphosphorylated PLB to SERCA is unchanged between animals (~2.3:1), suggesting that S16 phosphorylation is tightly controlled to tune cardiac function [58].

The mechanism by which PLB regulates SERCA has been the subject of debate for several decades. Some cross-linking studies have been interpreted to suggest that relief of SERCA inhibition, by either high $[Ca^{2+}]$ or PLB phosphorylation, requires dissociation of PLB from SERCA [59, 60]. However, several lines of evidence, including FRET and co-immunoprecipitation, show clearly that PLB remains bound to SERCA even when phosphorylated by PKA [46, 48, 61-63] or when $[Ca^{2+}]$ is micromolar [64, 65]. Thus most existing evidence is consistent with an allosteric regulation model, in which phosphorylated PLB binds to SERCA in a distinct, non-inhibitory mode. This model is supported by evidence that PLB phosphorylation shifts the *R-T* equilibrium in favor of the extended *R* state [45, 47], correlating with inhibition relief. Karim *et al.* also demonstrated that anchoring the cytoplasmic helix to the lipid membrane, eliminating the *R* state, prevents inhibition relief [46]. In recent work from the Thomas lab, charged

lipids were used to attract or repel the cytoplasmic domain of PLB from the membrane, thus stabilizing the *T* or *R* state, respectively [66]. As predicted, positively charged lipids were found to repel the positively charged cytoplasmic domain, promoting the non-inhibitory *R* state of PLB and activating SERCA at physiological $[Ca^{2+}]$, while negatively charged lipids had the opposite effects. Studies in 2D crystals are consistent with this order-to-disorder transition upon PLB phosphorylation, but this change was not seen in a mutant that remains inhibitory even when phosphorylated, illustrating the coupling of function and structural dynamics [56]. Furthermore, the transmembrane domain of PLB alone is inhibitory, but inhibition cannot be relieved without the cytoplasmic helix, highlighting the importance of phosphorylation and cytoplasmic dynamics for PLB regulation of SERCA [67].

Much of the insight gained into the SERCA-PLB interaction comes from PLB mutagenesis and studies in reconstituted membrane systems. Proline 21 was initially
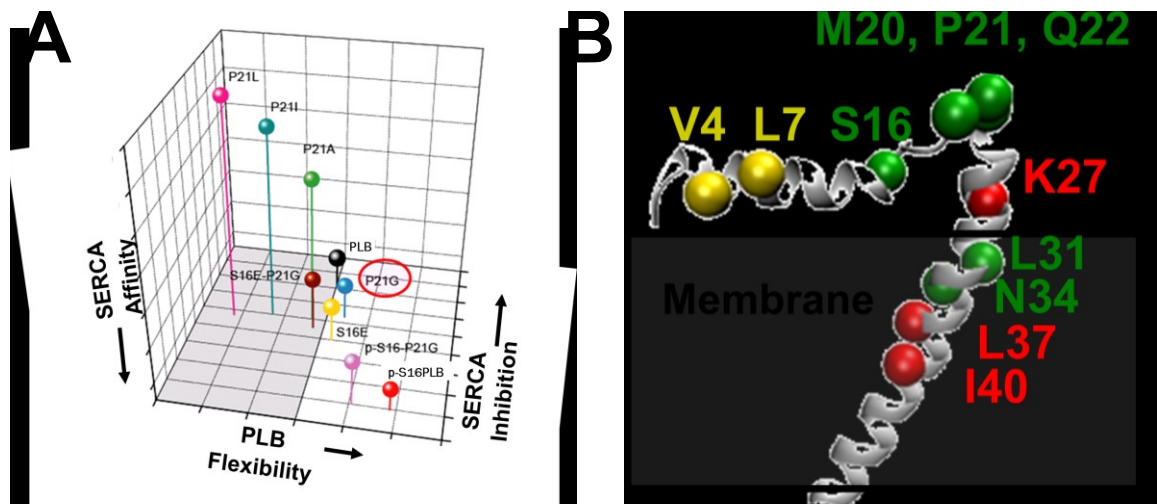
Figure 5. PLB mutations affect SERCA regulation. (**A**) Correlation between inhibitory potency, SERCA affinity, and cytoplasmic domain mobility in a series of P21 PLB mutants [68]. (**B**) Sites that are candidates for directed mutagenesis reduce inhibitory potency (green), increase association with SERCA (red), or reduce membrane interaction to promote the less inhibitory R state.

identified as important for PLB regulation [69]. Ha *et al.* made a series of mutations at this site showing that it could be used to 'tune' the mobility of the cytoplasmic domain, and correlated that mobility with inhibitory potency and affinity for SERCA (**Figure 5A**) [68, 70]. They found that increased dynamics, presumably corresponding to population of the R state, can decrease SERCA inhibition without decreasing affinity for SERCA. These observations led to the PLB mutant project discussed in Chapter 3 of this thesis. **Figure 5B** shows some of the sites being investigated to make mutants that bind tightly to SERCA and are less inhibitory.

1.4. SERCA-PLB Complex

The structure of the SERCA-PLB complex has been investigated with many different experimental approaches. Crystal structures of SERCA1a purified from rabbit muscle are abundant, but no structure for SERCA2a or a complex with PLB exists. Toyoshima and MacLennan have developed models of the SERCA1a-PLB complex based largely on molecular docking simulations, crosslinking, and NMR data [71, 72]. The absence of a SERCA2a crystal structure in the literature has made modeling the SERCA2a-PLB complex unachievable thus far.

The complex structures generated by Toyoshima and MacLennan show PLB in a groove between the M2 and M9 transmembrane helices of SERCA1a, also interacting with M4 and M6 (**Figure 6**). This site was explored because crystallography data seems to show that the groove appears and disappears as SERCA oscillates between the E1 and E2 structures. Chemical crosslinks between certain sites on SERCA and PLB are ablated by high [Ca^{2+}], leading many researchers in the field to conclude that PLB dissociates from SERCA when inhibition is relieved, either by the phosphorylation of PLB

Figure 6. SERCA-PLB complex. Model generated in [71] is based on SERCA crystal and PLB NMR structures, cross-linking data, and molecular simulations.

15

or by high $[Ca^{2+}]$ [73-76]. Other groups, including the Thomas lab, hypothesize that PLB remains bound to SERCA throughout the enzymatic cycle and that crosslinks no longer form because the complex has adopted a different conformation with PLB no longer in range of the ~1.5 nm crosslinking agents. Thus, the models may be valid for unphosphorylated PLB, but the structure of SERCA in complex with phosphorylated PLB is virtually unknown.

1.5. Calcium Dysregulation and Disease

1.5.1. Calcium Cycling in Muscle Diseases

Abnormal intracellular Ca^{2+} cycling is a hallmark of many muscle and non-muscle

diseases [78]. One of the key defects in both human and experimental heart failure (HF)

is depressed SR function of cardiac myocytes, often associated with changes in the

expression or activity of SERCA or other key Ca^{2+} handling proteins (**Figure 7**) [79-81].
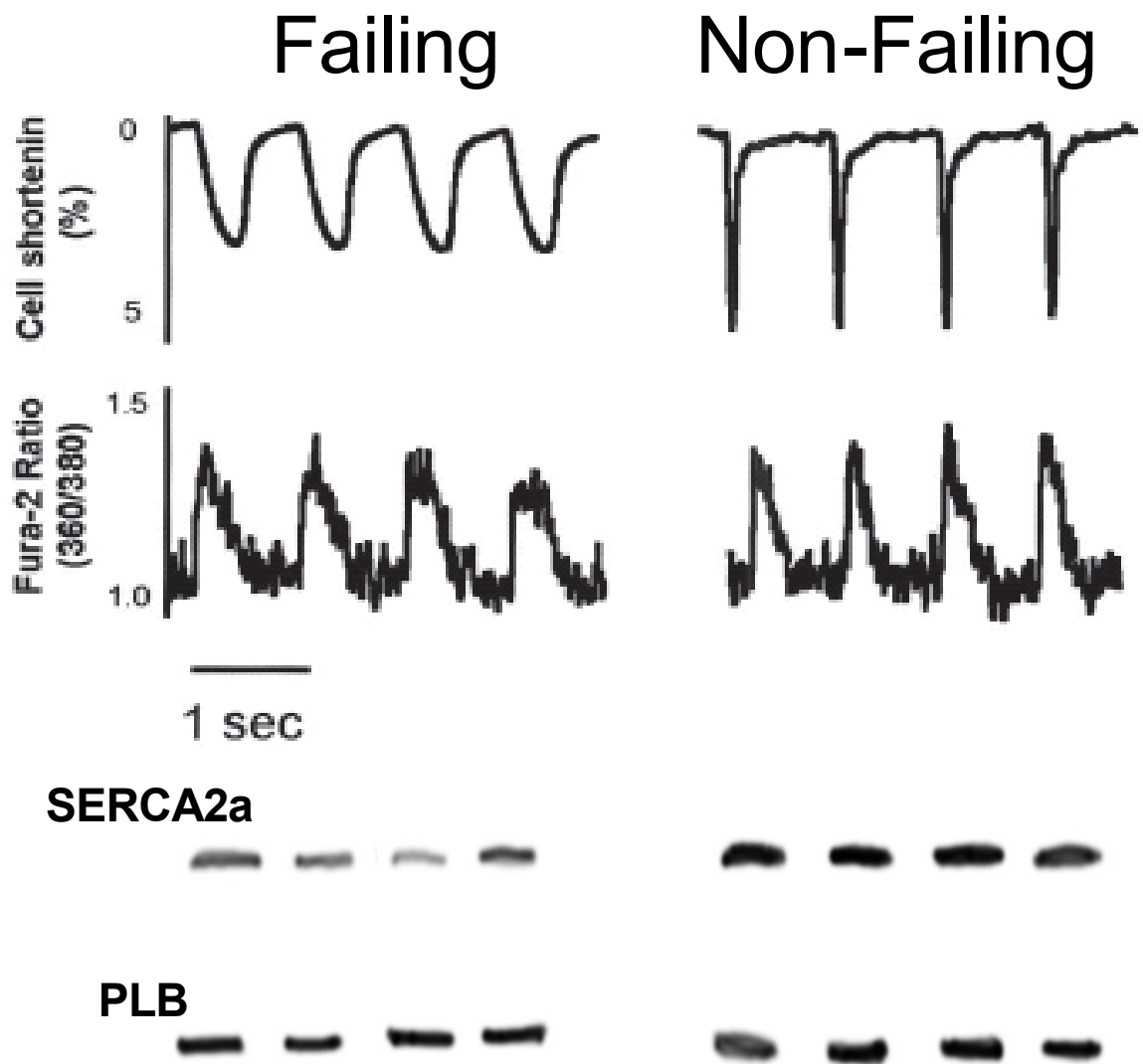
Figure 7. SERCA expression and activity in HF. Ca^{2+} transients from myocytes taken from failing and healthy human hearts show reduced Ca^{2+} cycling and reduced SERCA expression in failing hearts. Figure adapted from [77].

Deficient SR Ca^{2+} uptake prevents the heart muscle from fully relaxing and filling with blood for the next contraction, contributing to the pathology of HF. Although the causes of HF are diverse (gene mutations, ischemia, infection, heart attack, etc.), SERCA dysfunction is a near-universal symptom [82]. Many therapeutic routes to restore Ca^{2+} handling to treat HF have been investigated in recent years, and several of them are discussed in **section 1.6**.

SR dysfunction also plays a role in muscular dystrophy (MD), a disease that is caused by mutations in proteins that link the plasma membrane to the contractile apparatus of muscle cells. When the link does not function properly, the plasma membrane can become 'leaky', allowing ions like Ca^{2+} to pass through and disrupt normal Ca^{2+} regulation. Recent work with the *mdx* mouse model of MD found reduced SERCA activity, contributing to high intracellular [Ca^{2+}] levels, which can trigger stress responses and shut down muscle cells [83-85]. Increasing SERCA levels in the mice via gene therapy improved MD pathology [86] and many additional studies are underway, including a project in the Thomas lab to identify small molecule activators of the skeletal isoform SERCA1a.

Although several mutations in the SERCA1 and SERCA2 genes are linked to non-muscle disorders such as Brody's disease and Darier's disease [16], no known mutations have been identified in HF or MD patients. It is unclear whether SERCA deficiency is primarily a cause or an effect of these diseases, but work with animal models and human patients has made it clear that the disease phenotypes can be improved by activating SERCA and restoring intracellular Ca^{2+} handling.

18

SERCA2a expression is also reduced in muscle as a result of aging [87], and oxidative damage that accrues with age can also damage SERCA and reduce specific activity [88].

1.5.2. PLB-Linked Cardiomyopathies

Unlike to the SERCA2 gene, mutations in both the coding and non-coding portion of the human PLB gene are linked to diverse forms of HF. Mutations in the PLB promoter region that increase the expression PLB can cause SERCA to be over-inhibited, causing HF to develop over a number of decades [89-91]. Mutations in the PLB amino acid sequence also highlight the need for tunable control of Ca^{2+} cycling in muscle cells. The pathological mutation R9C prevents PLB from being phosphorylated by PKA at S16 [50, 92], and it has been suggested that newly identified R9H and R9L mutations cause disease by the same mechanism [93]. Two additional mutations, an R14 deletion and a premature stop codon at L39, produce a PLB that does not even interact with SERCA and mislocalizes to the plasma membrane where it could be affecting the activity of other ion pumps or even forming ion channels [94-97]. Taken together, these genetic mutations demonstrate the importance of SERCA and PLB in maintaining Ca^{2+} homeostasis to prevent the development of disease over time.

1.5.3. SERCA and Diabetes

The importance of SERCA function for proper muscle regulation is well established in the literature, but recent evidence has begun to point to the non-muscle SERCA2b isoform as a target for diabetes therapy. The etiology of type II diabetes is complex, but obesity clearly plays a major role in the development of diabetes [98]. Obesity-linked insulin resistance is connected to local inflammation of adipose tissue,

which produces a metabolic state characterized by oxidative stress, mitochondrial dysfunction, and ER stress.

Reactive oxygen species (ROS) couple ER stress and mitochondrial dysfunction with intracellular Ca^{2+} homeostasis. Elevated ROS causes oxidation of the ER Ca release channel (IP$_3$R) and/or SERCA, ultimately inhibiting Ca^{2+} handling [99]. Ca^{2+} leakage from the ER and decreased Ca^{2+}-reuptake by SERCA increases the basal cytoplasmic Ca^{2+} level, which in turn causes mitochondrial dysfunction and further increases ROS levels, activating the unfolded protein response and eventually apoptosis. The hypothesis that restoring (lowering) the basal cytoplasmic Ca^{2+} level can break the ERS-MD axis and prevent progression to diabetes has been supported by results showing improvement in a diabetic mouse model when SERCA2b, the non-muscle isoform, is overexpressed [100, 101]. The Thomas lab is currently pursuing a strategy to find SERCA2b-activating compounds as a potential therapy for Diabetes based on work presented in Chapter 5.

1.6. Heart Failure Treatment Strategies Targeting Calcium-Handling Proteins

Many diverse approaches are currently being pursued to develop novel therapeutics for HF. Some of the well-known methods that target Ca^{2+}-handling proteins are briefly discussed.

1.6.1. Blocking PLB Expression and Dephosphorylation

The labs of Kranias and Hajjar have pioneered the field of cardiac therapies relating to SERCA and PLB. Because SERCA activity is known to be low in HF, one of the first methods investigated to improve SERCA activity was inhibiting PLB. Blocking PLB expression in myocytes isolated from failing human hearts using anti-sense RNA improved the contractile parameters [102], leading to experiments in a rat myocardial

infarction model where HF progression was halted [103] and preliminary safety studies in dogs that identified cellular toxicity as an adverse effect [104]. Furthermore, blocking the expression of PLB may not be an ideal therapeutic route because a complete lack of SERCA regulation and adrenergic control is also pathogenic [95].

A similar strategy investigated by the Kranias group is preventing the dephosphorylation of PLB by overexpressing an inhibitor of the phosphatase that dephosphorylates PLB [105, 106]. This method has shown great promise in animal HF models and is being developed by NanoCor Therapeutics, a small biotech company co-founded by Kranias and Hajjar.

1.6.2. Pseudophosphorylating PLB

Another method that has shown promise in animal models is gene therapy to express a pseudophosphorylated PLB mutant, S16E. This mutant is less inhibitory than wild-type PLB but lacks adrenergic control because the native phosphorylation site is no longer present. S16E gene therapy successfully mitigated HF progression following myocardial infarction in both rats [107] and sheep [108]..

1.6.3. SERCA Overexpression

Gene therapy to overexpress SERCA2a in the heart is by far the most successful method to increase Ca^{2+} cycling in HF patients to date. The Hajjar lab has published dozens of articles showing that SERCA overexpression improves contractile parameters in isolated myocytes [77], small animal models [110], and large animal models [111]. This work led to the founding of Celladon, Inc. and clinical trials to develop the gene
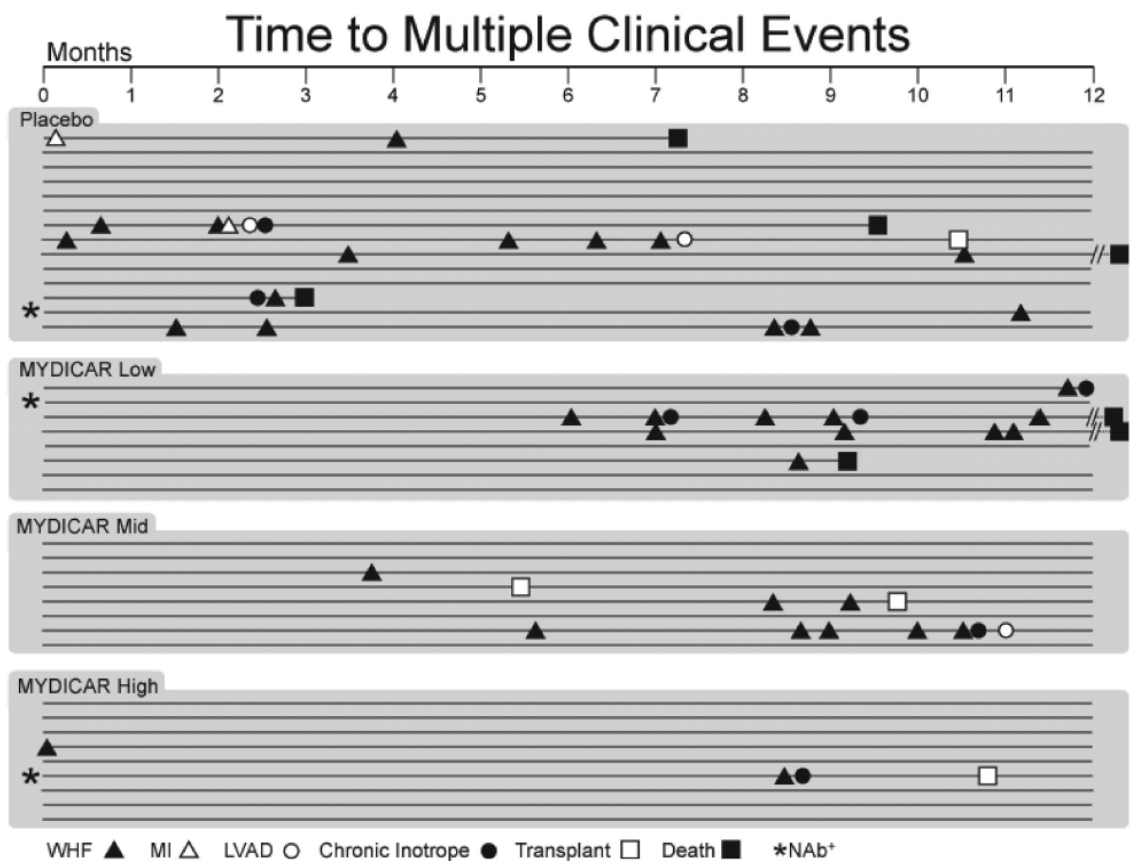
Figure 8. Clinical success of MYDICAR intervention for HF. Patients receiving the highest dose of the SERCA gene therapy rAAV vector (MYDICAR) saw significant improvements in clinical outcomes such as hospitalization and mortality. Clinical events are worsening heart failure (WHF), myocardial infarction (MI), and need for a left-ventricular assist device (LVAD), heart transplant, or prescription of a chronic inotrope. From [109].

therapy intervention (MYDICAR) for use in humans. A phase I clinical trial demonstrated that MYDICAR is safe [112], and a phase II clinical study showed great

success in preventing hospitalization and death of patients receiving the SERCA treatment (**Figure 8**) [109]. Phase III clinical trials are expected to begin soon and if approved, this gene therapy product would be the first significant novel therapy for HF in decades.

1.6.4. PLB Mutant Competition

PLB mutant competition is a strategy to activate SERCA by replacing native PLB with mutant PLB that is less inhibitory but retains high binding affinity for SERCA. Mutant PLB would compete for SERCA binding and displace native PLB, activating SERCA. This method has primarily been pursued by the Thomas and Veglia labs and is the subject of Chapter 3 of this thesis.

1.6.5. Small-Molecule Calcium Cycling Activators

Small-molecule SERCA activators have been sought since the 1980s [113, 114]. While large-scale compound screens at drug companies such as Merck proved unsuccessful, one SERCA-activating compound was identified in an Italian lab and was investigated in a human clinical trial. This drug, called Istaroxime, is claimed to be an ideal drug candidate because it inhibited the Na/K-ATPase in addition to activating SERCA [115, 116]. Inhibition of the Na/K-ATPase is a mechanism to increase intracellular $[Ca^{2+}]$, but other drugs such as digoxin that operate with this same mechanism only improve contractility in the short term and do not improve mortality [117]. However, Istaroxime has shown promise in clinical trials [118, 119].

More recently, the search for small-molecule SERCA activators has been undertaken primarily by the Thomas lab in collaboration with Celladon, Inc. These approaches are the subject of Chapters 4 and 5. Chapter 4 details a high-throughput drug

screen to identify compounds that disrupt FRET between labeled SERCA and PLB in a reconstituted membrane system. Several compounds were identified and some of them increased SERCA ATPase activity and improved contractile parameters of isolated myocytes, but none of the compounds was specific to the SERCA-PLB interaction. The assay presented in Chapter 5 measures the effect of activating and inhibiting compounds on intramolecular FRET between domains on the cytoplasmic headpiece of SERCA. A pilot-scale screen was conducted on a small compound library and several SERCA inhibitors were identified.

Chapter 2 – Fluorescence Spectroscopy and Microscopy

2.1. Principles of Fluorescence

2.1.1. Fluorescence Theory

All forms of spectroscopy study the interaction of matter with radiated energy. Molecules with electrons excited by radiated energy can relax by several different pathways, most commonly by vibrational motion or expending the energy as heat. Some
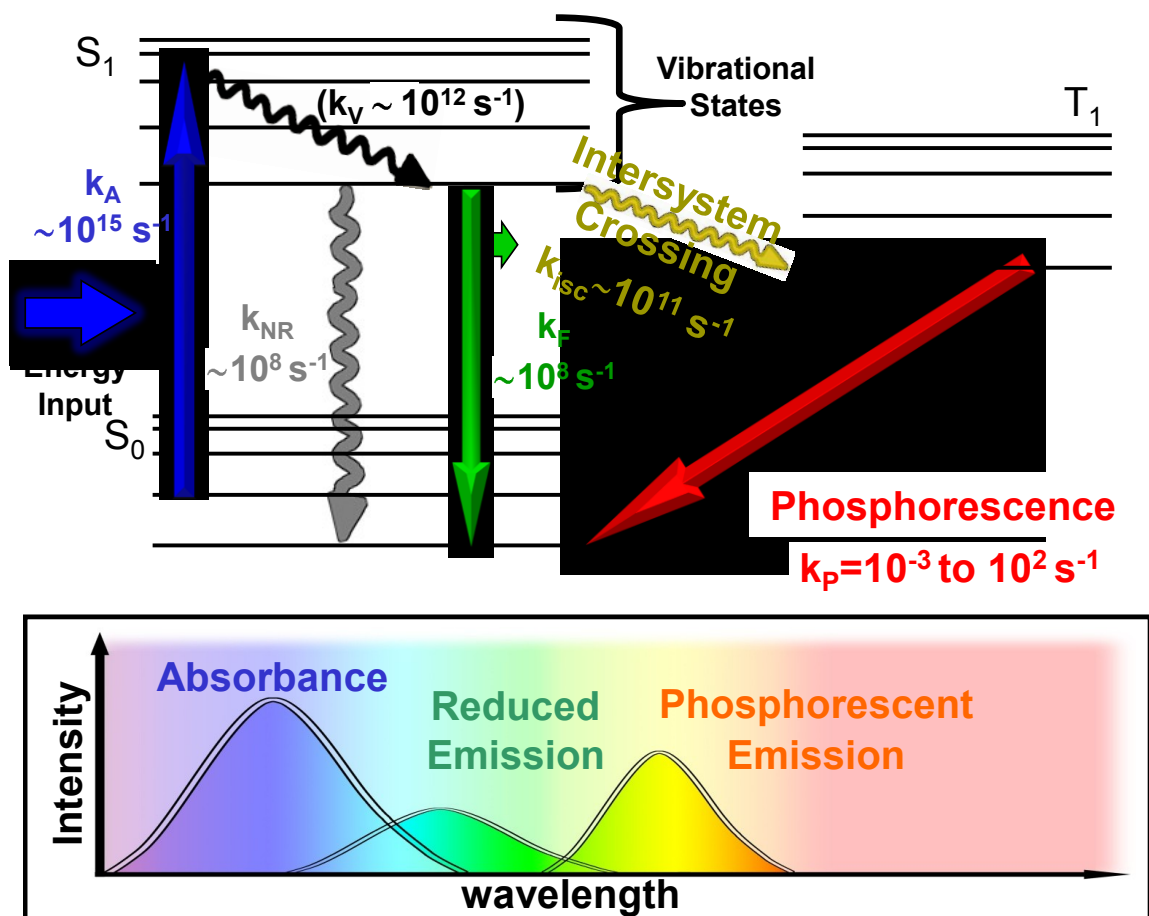
Figure 9. Jablonski diagram showing possible transitions between electronic and vibrational energy states. An electron can absorb energy (blue arrow) to become excited (S_1), relaxing back to the ground state (S_0) by fluorescence emission (green arrow), intersystem crossing followed by phosphorescence emission (red arrow), or non-radiatively (curvy arrows).

molecules, however, are capable of emitting this absorbed energy as a photon (light) in a process called luminescence. The Jablonski diagram (**Figure 9**) depicts many relaxation pathways, including two luminescent (light-emitting) pathways: fluorescence and phosphorescence. An electron is excited from the low energy singlet state (S_0) to a higher-energy excited state (S_1) when the energy gap of the transition is matched by the energy of the photon. The excited luminescent molecule can emit a photon from the singlet excited state and relax back to the ground state, or undergo intersystem crossing to an excited triplet state. Emission from the singlet state is termed fluorescence, and it occurs on the nanosecond timescale ($k_F \sim 10^7$-10^{10} s^{-1}). Relaxation from the triplet state is called phosphorescence, and this quantum mechanically forbidden transition is much slower, on a ms-min time scale. An excited molecule can undergo additional relaxation processes such as internal conversion (releasing thermal energy) or collisional quenching. All of these non-radiative processes return an excited electron to the ground energy state without emitting a photon. The probability that an excited molecule will emit a photon is the quantum yield, given by **Equation 1**, where k_F is the fluorescence rate constant and k_{NR} is the non-radiative rate constant.

$$\phi_F = \frac{k_F}{(k_F + k_{NR})}. \qquad \textbf{Equation 1}$$

Excited fluorescent molecules generally undergo some vibrational relaxation before emitting a photon, so the energy of the emitted is photon is less than that of the photon that was absorbed ($E = h\nu$). This lower-energy photon has a lower oscillatory frequency (ν) and longer wavelength ($\lambda = c/\nu$), making the emitted light shifted toward the red end of the visible spectrum in a phenomenon known as a 'Stokes shift', named

26

after the Irish physicist and fluorescence pioneer George Stokes. Quenching processes that affect the probability of photon emission can be manipulated and observed experimentally to examine the environment of a fluorophore, and the fluorescence resonance energy transfer (FRET) method is discussed throughout this thesis.

2.1.2. Fluorescence Resonance Energy Transfer

FRET is one of the most common uses of fluorescence in biology, serving a wide variety of experimental aims from observing intermolecular binding to measuring intramolecular distances and structural dynamics. FRET occurs when an excited
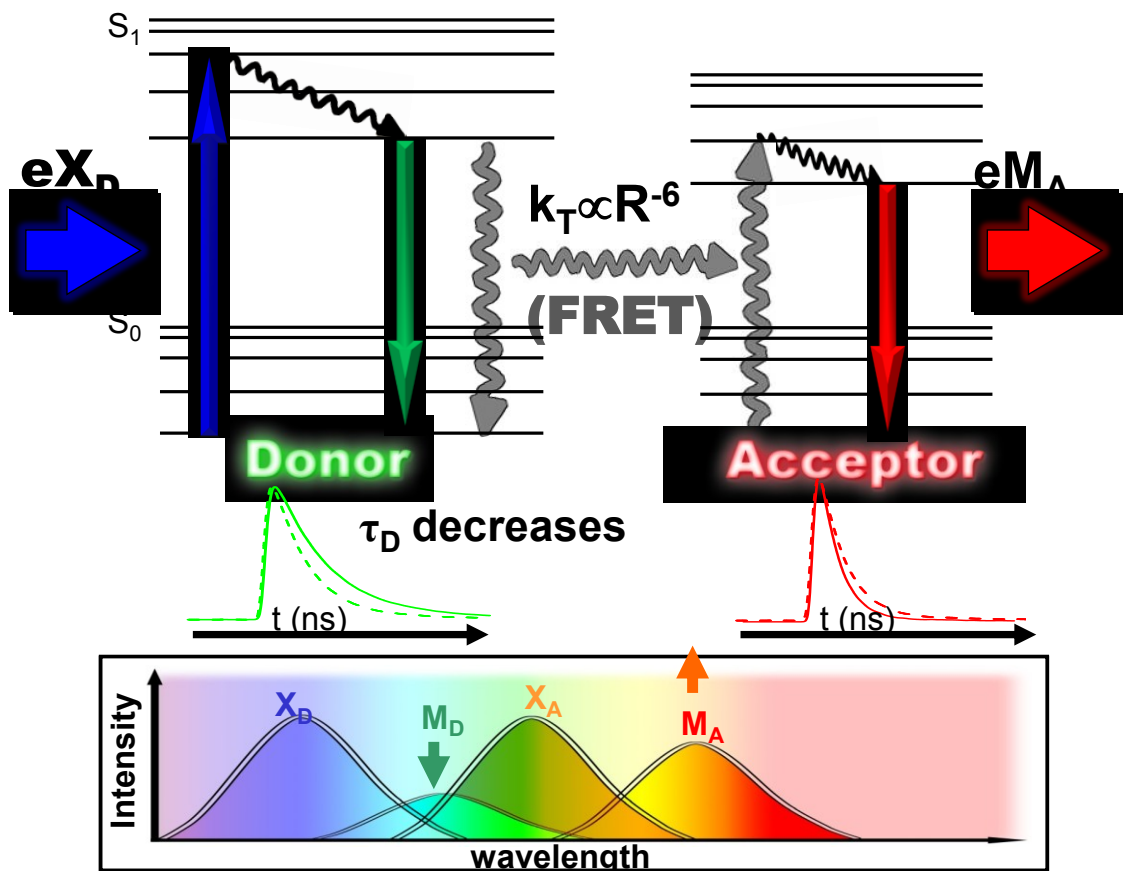
Figure 10. Jablonski diagram depicting FRET. An excited donor molecule relaxes by transferring energy to an acceptor molecule, which is excited and emits a photon. Donor emission intensity is decreased and the lifetime shortened by FRET, while acceptor emission intensity is enhanced and the lifetime is lengthened.

fluorescent molecule interacts with and excites another fluorescent molecule. This non-radiative energy transfer can occur with another molecule of the same fluorophore (homoFRET), or a different molecule (heteroFRET), as long as the energy gap of donor relaxation matches that of acceptor excitation. On a fluorescence spectrum that plots fluorescence excitation or emission intensity as a function of wavelength (and thus energy), the emission of the donor (M_D) must overlap with the excitation of the acceptor (X_A) **Figure 10**.

FRET is very sensitive to the distance between donor and acceptor molecules, so it is commonly used to quantitatively measure distances between labeled proteins or other biological molecules that can be specifically labeled. The probability that FRET will occur is equal to the reduction of fluorescence intensity in the presence of an acceptor (F_{DA}) relative to the intensity of the donor alone (F_D) and is given by the energy transfer efficiency (E),

$$E = 1 - \frac{F_{DA}}{F_D}$$

Equation 2

which can also be described by

$$E = \frac{R_0^{\ 6}}{R_0^{\ 6} + R^{\ 6}}$$

Equation 3

where R is the distance between donor and acceptor molecules and R_0 is the Förster distance, which is a function of several probe-specific and environmental factors that affect energy transfer probability. When R is the same as R_0, 50% of the excitation energy of the donor is transferred to the acceptor. E increases towards 1 as the probes

28

become closer ($R<R_0$), and goes to 0 when the probes are farther apart ($R>R_0$). R_0 is defined as

$$R_0 = 9{,}790 \left[J(\lambda) \kappa^2 \eta^{-4} \phi_D \right]^{1/6}$$

Equation 4

where κ^2 is the orientation factor, η is the index of refraction of the solvent, ϕ_D is the quantum yield of the donor, and $J(\lambda)$ is the donor-acceptor overlap integral. The value of the orientation factor describing the relative orientation of the donor and acceptor dipoles can vary from 0 to 4 for static systems, but random orientation ($\kappa^2 = 2/3$) is often assumed. Similarly the index of refraction for aqueous solutions is generally assumed to be 1.4. A donor with a higher quantum yield emits more photons, so FRET can be observed with greater sensitivity than with a lower yield donor. The overlap integral $J(\lambda)$ is high when there is significant overlap between donor emission (F_D) and acceptor excitation (ε_A), increasing the probability that the energy gap will match and energy transfer will occur (**Figure 10**). The overlap integral is defined by

$$J(\lambda) = \frac{\int F_D(\lambda)\, \varepsilon_A(\lambda)\, \lambda^4\, d\lambda}{\int F_D(\lambda)\, d\lambda}$$

Equation 5

Using the right FRET pairs, distance measurements can be made from approximately 2-10 nm.

The efficiency of energy transfer can also be defined by the rate of fluorescent decay (k_D) and the rate of energy transfer (k_T) as

$$E = \frac{k_T}{(k_T + k_D)}$$

Equation 6

and the rate of energy transfer is dependent on both the interprobe distance and the donor lifetime (τ_D) according to

$$k_T = \frac{1}{\tau_D}\left(\frac{R_0}{R}\right)^6 \qquad \textbf{Equation 7}$$

Equation 3 can be rearranged to

$$E = \frac{1}{[1 + (R/R_0)^6]} \qquad \textbf{Equation 8}$$

where it can be seen that E is most sensitive to distance changes when $R = R_0$ (**Figure 11**), and reasonably sensitive distance measurements can be made from
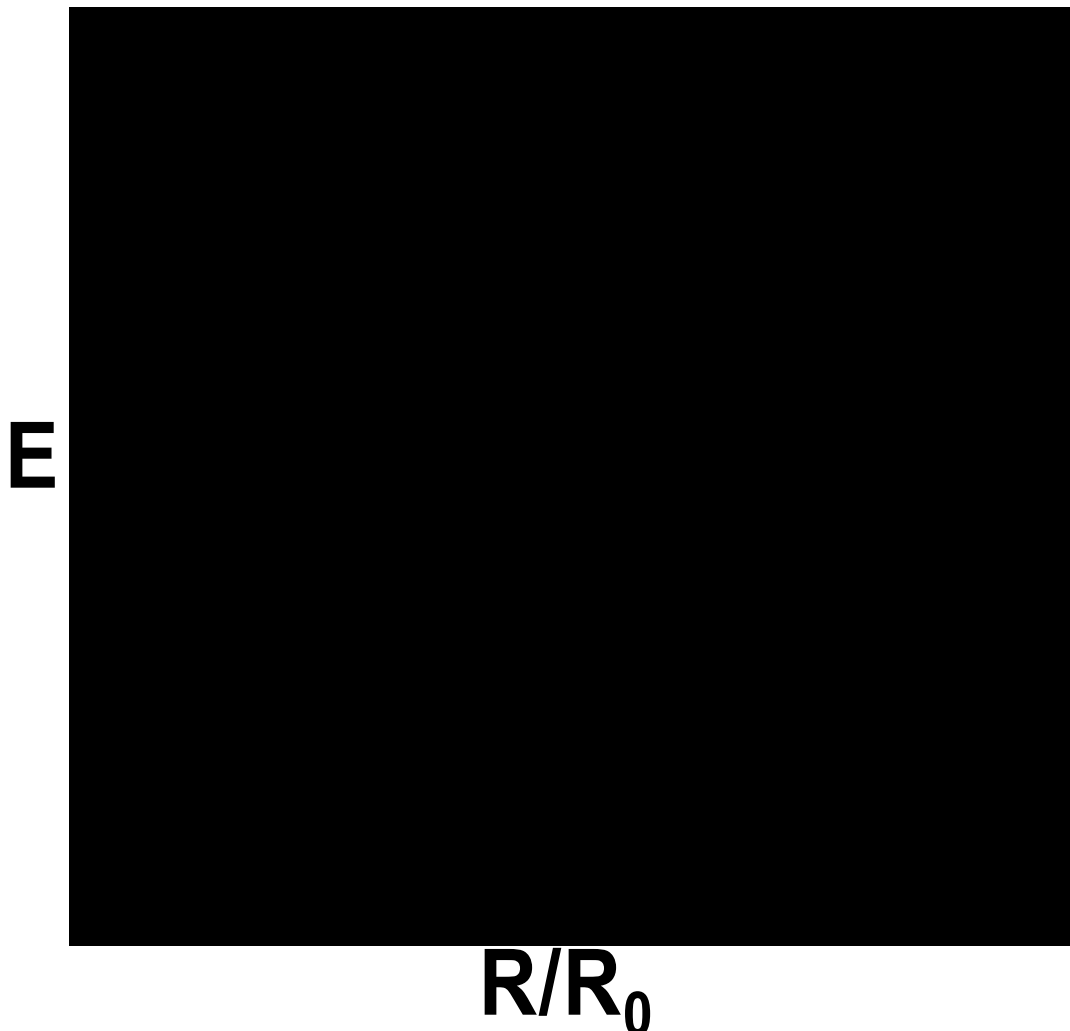
Figure 11. Universal FRET plot. Depicts the dependence of energy transfer on donor-acceptor distance (R). FRET efficiency (E) is most sensitive to changes in distance when $R = R_0$.

approximately $E = 0.1$ to $E = 0.9$.

2.1.3. Time-resolved fluorescence and FRET

Measurements of fluorescence intensity can be useful in simple systems, but several assumptions must be made to extract useful information. Among the most important assumptions is that all of the fluorescent molecules behave the same way, and that all donors are the same distance from an acceptor. In most in vitro biological systems it is difficult to achieve complete labeling, so while some donors may be in close proximity to an acceptor, other molecules in identical complexes will not see an acceptor. Furthermore, conformational heterogeneity cannot be observed by measurements of total fluorescence intensity. These problems can largely be overcome by measuring fluorescence lifetimes.

The time-dependence of fluorescence relaxation is described by a typical Boltzmann distribution of excited molecules in the simplest scenario, and the fraction of excited molecules decays according to a single exponential:

$$F_D(t) = \exp(-t/\tau) \qquad \textbf{Equation 9}$$

When a fluorescent molecule is near a FRET acceptor, the change in its fluorescence lifetime is dependent on that rate of energy transfer according to

$$\frac{1}{\tau_{DA}} = \frac{1}{\tau_D} + k_T(r) \qquad \textbf{Equation 10}$$
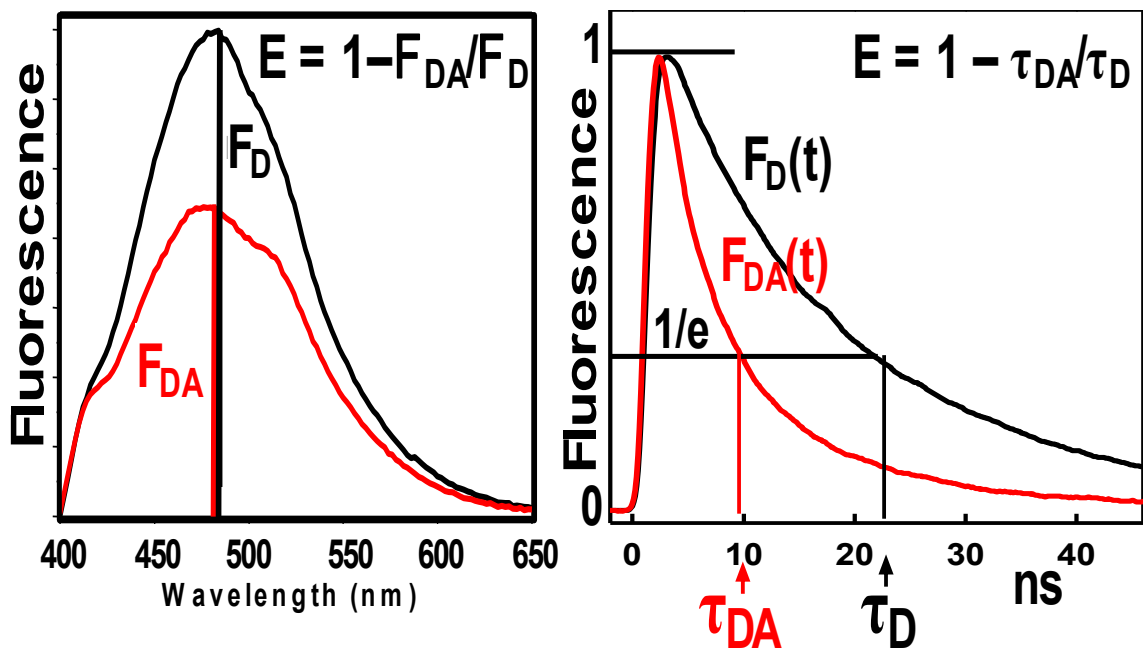
Figure 12. Effects of FRET on fluorescence intensity and lifetime. Fractional decrease in fluorescence intensity (left) and lifetime (right) is proportional to the rate of energy transfer (E).

and the fluorescence decay can be calculated as in **Equation 9** by substituting τ_{DA} for τ_D. The resulting fluorescence decay lifetime is decreased by the same fraction as the intensity, equivalent to the FRET efficiency E (**Figure 12**). A key advantage of time-dependent fluorescence measurements is that they can be resolved into multiple lifetimes by fitting the observed fluorescence decay to multiple exponentials,

$$F_D(t) = \sum_{i=1}^{n} A_i \exp(-t/\tau_i) , \qquad \textbf{Equation 11}$$

Each lifetime in a multiexponential fit represents a different population of fluorescent molecules. In a sample with mixed donor only and donor+acceptor populations, two lifetimes would be detected and they could be used to calculate FRET ($E = 1-\tau_{DA}/\tau_D$), and a distance between donor and acceptor can be extracted by rearranging **Equation 3**.
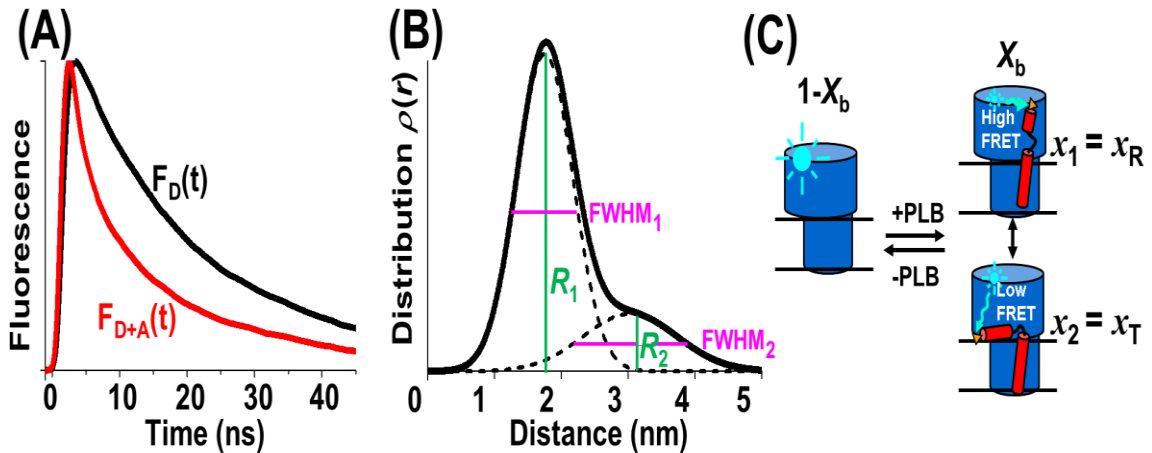
Figure 13. Multiple-distance resolution of time-resolved FRET. (**A**) Time-resolved fluorescence spectra of donor-labeled SERCA alone (F_D) and in the presence of acceptor-labeled PLB (F_{DA}).(**B**) FRET distributions calculated from multiexponential fits of fluorescence decays. (**C**) PLB binds to SERCA in both R and T state conformations, giving rise to the two distinct distances in (**B**). Adapted from Li *et al.* [120]

Time-resolved fluorescence measurements can also resolve conformational heterogeneity. Li *et al.* measured FRET between fluorescently labeled SERCA and PLB in a reconstituted membrane system similar to that described in Chapter 4. The time-resolved fluorescence decays fit to multiple lifetimes (**Figure 13A**), and the authors were able to fit those lifetimes to two separate distance distributions (**Figure 13B**), representing the SERCA-PLB complex in distinct conformations (**Figure 13C**).

2.1.4. Fluorescent Proteins and Probes

Most measurements of biological fluorescence employ either chemically conjugated fluorescent probes or genetically encoded fluorescent proteins. Fluorescent dyes vary greatly in size (200-1000 Da) but are significantly smaller than fluorescent proteins (~27 kDa). Probes can also be conjugated with a wide variety of chemical linkers, and they can be used to site-specifically label proteins engineered to have only one reactive amino acid, most often a cysteine or lysine residue. An advantage of genetically encoded fluorescent tags is that the protein can be expressed and evaluated in

a living cell environment. These tags are most often used to assess subcellular localization of a protein or to monitor gene expression, but they can also be used to measure FRET. Many new labeling methods are currently being developed to address the limitations of in-cell labeling methods so that proteins in living cells can be labeled with small probes rather than relatively large proteins [121-124], but these methods are not utilized in this work. Chapter 4 of this thesis discusses in vitro experiments that employed chemically conjugated proteins while the experiments in Chapters 3 and 5 were based on genetically engineered fusion proteins expressed in living cells. The following is a general description of fluorescent proteins and probes, and specific labeling and fusion construct generation methods are discussed in Chapters 3-5.

Chemically Conjugated Fluorescent Probes

The best fluorescent probes are small, bright, resistant to photobleaching, and reactive only at specifically engineered functional groups. Many small molecule probes use specific chemically reactive groups to bind to specific amino acids. Iodoacetamide and maleimide groups react specifically with cysteine residues, and esters and isothiocyanate groups are used to target the amine group of lysine residues. Labeling specificity depends on the reactivity of the cysteine or lysine residues in a protein. In some cases, a specific cysteine or lysine can be labeled in the presence of other residues that may not be reactive because they are buried in the protein or in a hydrophobic pocket, while in other cases all but one reactive residue must be removed from the protein via directed mutagenesis.

SERCA is a cysteine-rich enzyme with 24 cysteine residues in the SERCA1a skeletal muscle isoform, but it can be specifically labeled by IAEDANS (5-((((2-

Probes to label SERCA and PLB
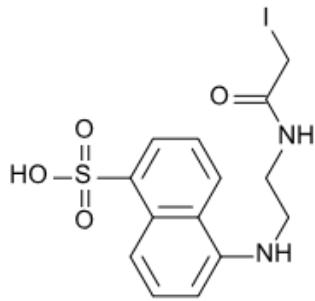
IAEDANS
MW = 434 Da
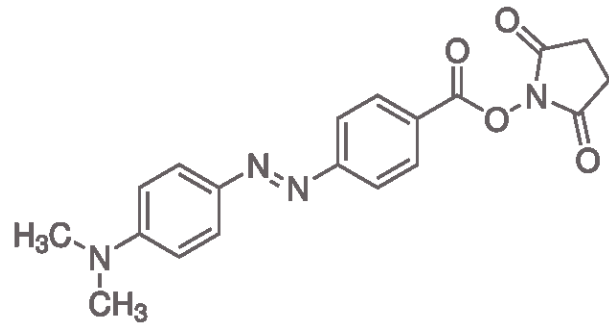
DABCYL
MW = 269 Da

Labeling Reactions

Iodoacetamide + Cysteine
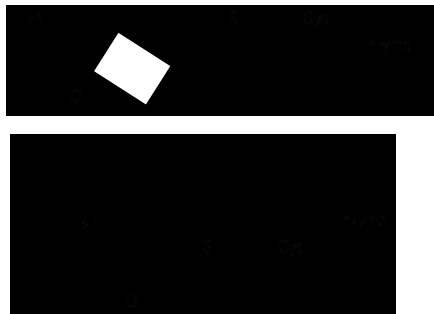
Succinimidyl Ester + Lysine
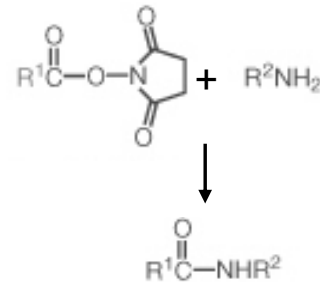
Figure 14. IAEDANS and DABCYL probes used to label SERCA and PLB. Both probes react specifically with a native residue in the target; cys674 in SERCA and Lys3 in PLB.

iodoacetyl)amino)ethyl)amino) naphthalene-1-sulfonic acid) at cys674 (**Figure 14**). This native cys674 residue allows one to label SERCA isolated from animal skeletal muscle specifically without the need for mutagenesis or recombinant expression. PLB is small enough that it can be chemically synthesized with reactive residues at any location, and

35

the three native cysteines are usually removed to prevent PLB oligomerization. Experiments in Chapter 4 were done with IAEDANS-labeled SERCA1a and PLB labeled at the native Lys3 residue with a probe that contains a succinimidyl ester functional group, DABCYL (4-((4-(dimethylamino)phenyl)benzoic acid succinimidyl ester) (**Figure 14**). DABCYL can only be used as a FRET acceptor because it does not emit photons, making it a 'dark' acceptor.

Fluorescent Proteins

The discovery of fluorescent proteins and their use as fusion tags brought about a
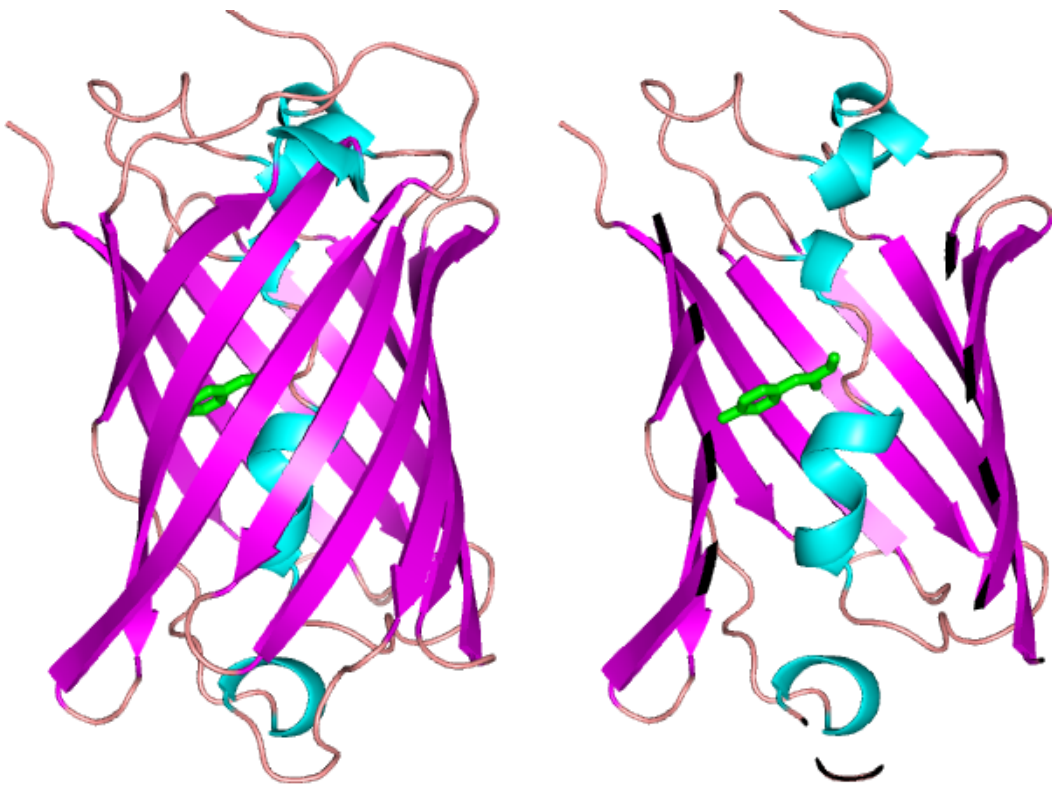
Figure 15. GFP structure. GFP (PDB 1GFL) is a β-barrel with the chromophore in the center formed by the cyclization of three amino acids in the central helix. Images generated in PyMol.

true revolution in molecular and cellular biology. The discovery and cloning of the green

fluorescent protein (GFP) found in the jellyfish *Aequorea victoria* allowed the generation of fluorescent fusion proteins (FFPs) with any protein that can be expressed recombinantly, in nearly any cell type [125]. Roger Tsien has pioneered the development of new fluorescent proteins derived from GFP and other proteins found mainly in marine life, resulting in a 2008 Nobel Prize shared with Martin Chalfie and Osamu Shimomura for discovery and development of GFP. The GFP originally isolated was a 238 amino acid, 27 kDa protein that formed a β-barrel structure with the fluorescent properties deriving from a chromophore in the center of the barrel (**Figure 15**) [126]. The chromophore, formed by side chains from a central helix and several hydrogen-bonded amino acids, is protected from the environment by the barrel structure [127]. Mutations to the amino acids involved in generating the chromophore frequently perturb the excitation or emission spectra of the protein and are commonly used to develop new fluorescent proteins [128].

GFP derivatives are improved and diversified in a variety of ways. Wild-type GFP has two excitation peaks nearly 100 nm apart, but a single amino acid change can eliminate one of these peaks, making it easier to specifically excite GFP in the presence of other fluorophores. Many naturally occurring fluorescent proteins dimerize with relatively high affinity, and mutations can be introduced to prevent oligomerization. Mutation of a few amino acids can change the excitation/emission spectra of the GFP to generate colors spanning the majority of the visible spectrum, and new fluorescent proteins and colors are being developed rapidly [128]. Improvements to GFP derivatives in the past several years have allowed FFPs to be used to measure FRET in living cells in

37

addition to subcellular localization and as a marker for gene expression. These FRET

assays are often qualitative, seeking to determine whether two proteins interact at all,

rather than determining precise distances. The assays presented in Chapters 3 and 5 both

measure FRET quantitatively using FFPs, but they do so by different methods.

In Chapter 3, SERCA and PLB are expressed in human embryonic kidney (HEK)

cells as fusion proteins to cyan and yellow fluorescent proteins (CFP and YFP),
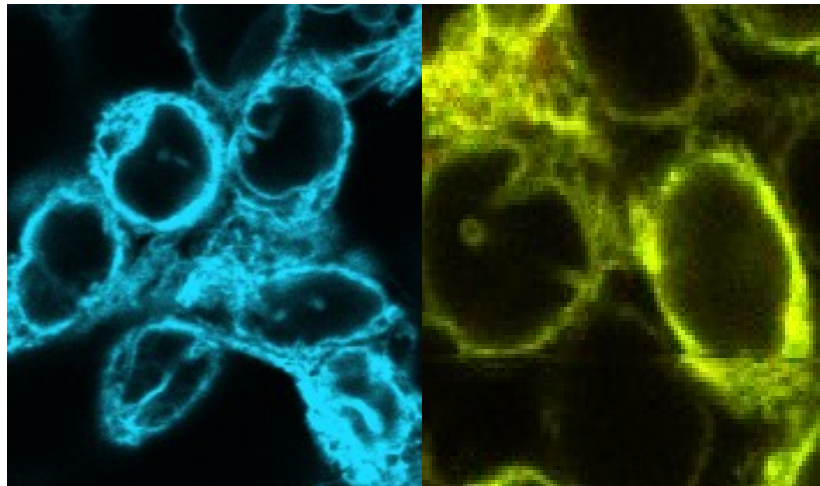
Figure 16. Expression of CFP-SERCA and YFP-PLB in a stable HEK cell line. All of the stable cells are fluorescent and fluorescence appears localized to ER (reticulated and outside the nucleus).

respectively (**Figure 16**). FRET between CFP and YFP is measured by photobleaching to

determine the extent of interaction between SERCA and PLB in an intensity-based assay.

The FRET level is then monitored when unlabeled mutant PLB is added to quantify the

ability of the mutant PLB to compete with the wild-type PLB. Decreased FRET indicates

that some of the labeled PLB has been displaced.

FRET assays in Chapter 5 differ in two significant ways: 1) both fluorescent

proteins are attached to SERCA to measure intramolecular interactions, and 2)

fluorescent lifetimes were measured instead of total fluorescence intensity, generating a

38

much more precise measurement in a fraction of the time required for photobleaching. These experiments also used GFP as a donor instead of CFP, and red fluorescence protein (RFP) as an acceptor, because there is less optical interference from cells at the longer wavelengths used to excite GFP.

2.2. Fluorescence Instrumentation

2.2.1. Steady-state FRET

The results of steady-state FRET experiments are discussed in Chapters 3 and 4 of this thesis. FRET in Chapter 3 was calculated by a photobleaching method. Cells expressing CFP-SERCA and YFP-PLB (**Figure 16**) were imaged on a Nikon microscope using a Cascade II CCD camera that records fluorescence intensity. Fluorescence intensity was recorder before (F_{DA}) and after photobleaching the acceptor, leaving only donor fluorescence (F_D). FRET was calculated according to **Equation 2.**

Experiments in Chapter 4 were done by acquiring full fluorescence spectra and calculating E as in **Figure 12**. Fluorescence intensity spectra were acquired using a Gemini EM spectrofluorimeter microplate reader from Molecular Devices. This instrument has a Xenon flash lamp and dual monochromators to select excitation and emission wavelengths. AEDANS-SERCA was excited at 350 nm, and donor emission was recorded from 420-600 nm with 2 nm increments. Buffer background was subtracted from the experimental emission spectra and FRET was calculated according to **Equation 2**.

2.2.2. Time-resolved fluorescence lifetime plate reader

Time-resolved FRET experiments in Chapter 5 were performed using a fluorescence lifetime plate reader developed by Fluorescence Innovations Inc. in collaboration with the Thomas lab (**Figure 17**). The plate reader uses laser excitation and an ultrafast
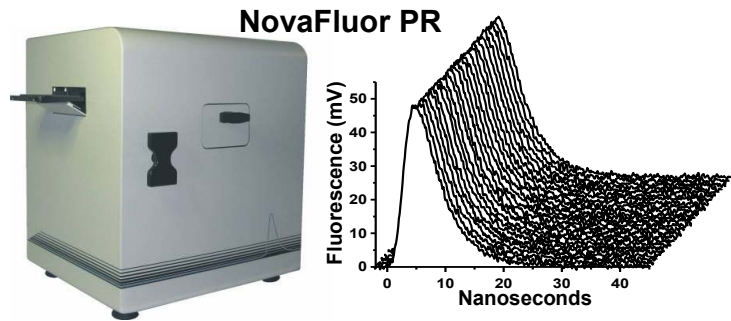
Figure 17. Fluorescence Lifetime Plate Reader. NovaFluorPR (left) scans a 96- or 384-well plate in 2.5 minutes, yielding waveforms with S/N≥100 (right).

digitizer to record fluorescence decays every 0.1 ms (**Figure 17**). A full 384-well plate can be read and analyzed in minutes. GFP was excited by 473 nm laser light and emission was filtered using a 520/35 nm Semrock filter.

Chapter 3 – Phospholamban Mutants Compete with Wild Type for SERCA Binding in Living Cells

Phospholamban Mutants Compete with Wild Type for SERCA Binding in Living Cells

Simon J. Gruber, Suzanne Haydon, and David D. Thomas[*]

Department of Biochemistry, Molecular Biology and Biophysics, University of

Minnesota Medical School, Minneapolis, Minnesota 55455

We have used fluorescent fusion proteins stably expressed in HEK cells to detect directly the interaction between the sarcoplasmic reticulum Ca-ATPase (SERCA) and phospholamban (PLB) in living cells, in order to design PLB mutants for gene therapy. Ca^{2+} cycling in muscle cells depends strongly on SERCA. Heart failure (HF), which contributes to 12% of US deaths, typically exhibits decreased SERCA activity, and several potential therapies for HF aim to increase SERCA activity. We are investigating the use of LOF-PLB mutants (PLB_M) as gene therapy vectors to increase SERCA activity. Active SERCA1a and WT-PLB, tagged at their N termini with fluorescent proteins (CFP and YFP), were coexpressed in stable HEK cell lines, and fluorescence resonance energy transfer (FRET) was used to detect their interaction directly.

Phosphorylation of PLB, induced by forskolin, caused an increase in FRET from CFP-SERCA to YFP-PLB, indicating that SERCA inhibition can be relieved without dissociation of the complex. This suggests that a LOF mutant might bind to SERCA with sufficient affinity to complete effectively with WT-PLB, thus relieving SERCA inhibition. Therefore, we transiently expressed a series of PLB_M in the CFP-SERCA/YFP-PLB cell line, and found decreased FRET, implying competition between PLB_M and WT-PLB for binding to SERCA. These results establish this FRET assay as a rapid and quantitative means of screening PLB_M for optimization of gene therapy to activate SERCA, as needed for gene therapy in HF.

3.1. Introduction

The sarcoplasmic reticulum (SR) Ca-ATPase (SERCA) is an integral membrane protein that pumps Ca^{2+} from the cytosol into the SR lumen in muscle cells, thus maintaining low cytosolic $[Ca^{2+}]$ in resting myocytes and potentiating contraction. In cardiac muscle, SERCA is inhibited at submicromolar $[Ca^{2+}]$ by the single-pass transmembrane protein phospholamban (PLB), which can be phosphorylated to relieve SERCA inhibition [129]. Because SERCA activity or expression is reduced in many instances of heart failure (HF) [3, 130], SERCA activation is a widely pursued goal for development of new therapies [130]. A gene therapy approach using rAAV to overexpress SERCA2a in heart tissue recently concluded phase II clinical trials with promising results [109], and small-molecule SERCA activators are also being sought [131]. PLB-based approaches involve overexpression of a pseudophosphorylated PLB (S16E) [132] or a protein phosphatase I inhibitor to increase the phosphorylation of PLB [133]. Here we explore expression of loss-of-function PLB mutants (PLB_M) to displace WT-PLB and activate SERCA.
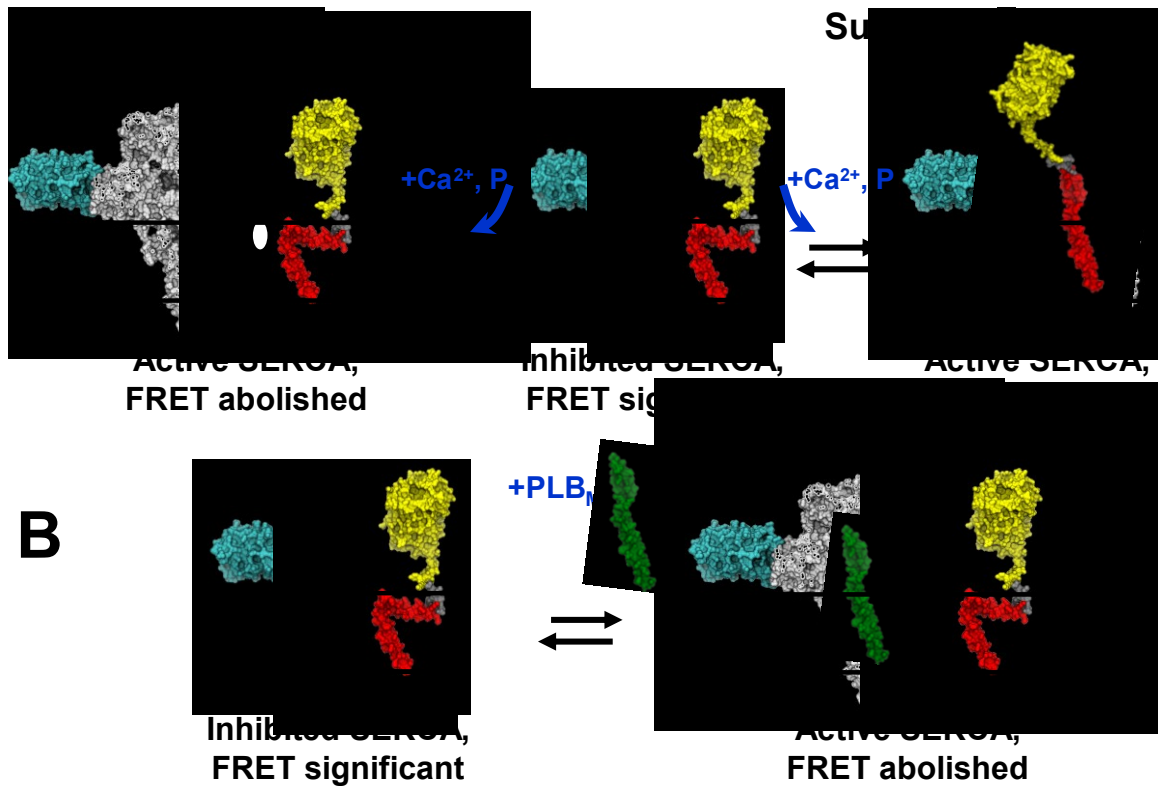
Figure 18. SERCA-PLB inhibition relief schemes. (**A**) Alternative mechanisms for relief of SERCA inhibition can be distinguished by FRET from CFP-SERCA to YFP-PLB. (**B**) Proposed gene therapy approach, based on Subunit Model, is testable by FRET.

Clear understanding of the mechanism by which PLB inhibits SERCA (**Figure 18A**) is critical to designing an effective therapy. In the conventional model, supported by crosslinking and immunoprecipitation [61, 74], SERCA inhibition can only be relieved by dissociation of PLB ("Dissociation Model," **Figure 18A** left), but recent spectroscopic studies suggest that PLB remains bound to SERCA even after activation by PLB phosphorylation or Ca^{2+} ("Subunit Model", **Figure 18A** right) [46, 64, 134, 135]. If this model is valid, an alternative therapeutic approach is suggested – a loss-of-function PLB mutant (PLB_M), introduced by gene therapy, could relieve SERCA inhibition if it binds tightly to SERCA, thus competing with endogenous PLB (**Figure 18B**). Evidence favoring this hypothesis in a reconstituted membrane system was recently published [65].

In the present study we have used fluorescent fusion proteins to detect directly the SERCA-PLB interaction in living cells. We used fluorescence microscopy to determine whether phosphorylation of YFP-PLB dissociates it from CFP-SERCA (**Figure 18A**), and to measure the ability of several PLB_M to compete with YFP-PLB for CFP-SERCA binding (**Figure 18B**).

3.2. Methods

3.2.1 Generation of Stable Cell Lines Expressing Fluorescent Fusion Proteins

ECFP and EYFP mammalian vectors (Clonetech), containing the monomeric A206K mutation, were fused to the N-terminus of rabbit SERCA1a and canine PLB respectively. HEK293 cells (ATCC) were cultured in Dulbecco's Modified Eagle Medium (DMEM) without phenol red (Gibco/Invitrogen), supplemented with 10% fetal bovine serum (Atlanta Biologicals), at 37º C and 10% CO_2. Cells were transiently transfected using Lipofectamine (Invitrogen), and stable cell lines were generated by G418 (Sigma) selection. Surviving clones expressing CFP-SERCA and YFP-PLB were further selected by fluorescence expression seen via fluorescence microscopy. The goal was to obtain measurable CFP fluorescence with a substantial excess of YFP over CFP.

3.2.2. Transient Expression of non-fluorescent PLB_M for Competition Measurements

Mutations in WT-PLB cDNA (resulting in PLB_M in plasmid pRH132) were made using the QuickChange XLII mutagenesis kit (Agilent). PLB_M were expressed in stable CFP-SERCA/YFP-PLB cell lines using 293fectin (Invitrogen). The amount of PLB_M DNA used, volume of 293fectin, and time after transfection to maximize competition were all optimized so that PLB_M expression was within 20% of that observed for the stable expression of YFP-PLB. Final conditions in a six-well plate required 1.25 pmol

DNA with 9 μL 293fectin, and photobleaching measurements were acquired 48h after transfection.

3.2.3. Western Blots to Quantify PLB and SERCA Content

Cells were pelleted and homogenized 48h after transient transfection with PLB_M DNA or after 5 min. incubation in 40μM forskolin [136]. Cell homogenates were run on 4-20% Tris-HCl gels (Criterion, Biorad) at 5 μg total homogenate protein along with standard curves of PLB (synthetic, WT or phosphorylated) and rabbit light SR [137], transferred to Immobilon-FL membranes (Millipore), and blocked for 1 hour in 1x TBS/casein (Bio-rad). Primary antibodies for unphosphorylated PLB (Ab2D12, Abcam), PLB phosphorylated at S16 (Ab285, Merck), SERCA1 (IIH11, Abcam), or GFP variants (1GFP63, Abcam) were visualized using IR secondary antibodies (goat-anti-mouse or goat-anti-rabbit) from LI-COR Biosciences. Blots were scanned on the Odyssey (LI-COR Biosciences). Concentrations of PLB (phosphorylated and unphosphorylated forms) and PLB_M were determined with high accuracy using synthetic standards run on the same blots as the cell homogenates [138, 139]. The slopes of standard curves were calculated from summed monomer and pentamer band intensities of three load concentrations for each standard (0.2, 0.4, and 0.8 pmoles), using LI-COR Odyssey software and median, one-pixel background subtraction. Band intensities for both monomer and pentamer of YFP-PLB in cell homogenates were summed, and concentrations of both YFP-uPLB (C_U) and YFP-pPLB (C_P) were calculated by solving simultaneous equations, using the standard slopes [138, 139]. X_P (the fraction of phosphorylated YFP-PLB) was then calculated by $X_P = C_P/(C_U + C_P)$ [138, 139]. A GFP antibody was used to label duplicate blots of the cell homogenates and indicated that total [YFP-PLB] was unaffected by

incubation with forskolin. Blots with the SERCA antibody showed that all samples used in phosphorylation experiments had essentially the same CFP-SERCA expression levels (36 ± 5 nmol SERCA/g total protein). The molar ratio of YFP-PLB to SERCA was found to be 7.8 ± 0.9, and the transient expression of PLB_M was consistently observed to be similar (7.1 ± 1.2).

3.2.4. Fluorescence Resonance Energy Transfer (FRET) Measurements in Live HEK Cells

Acceptor-selective photobleaching of cells co-expressing CFP-SERCA and YFP-PLB was done essentially as described previously [140] on an Eclipse TE200 microscope (Nikon Instruments), using CFP (excitation 430nm/24, emission 470nm/24) and YFP (excitation 500nm/20, emission 535nm/30) filters in automated filter wheels (Ludl) driven by MetaMorph software (Molecular Devices). Images were acquired using a 40x dry objective (0.55 numerical aperture), an X-Cite metal-halide lamp (EXFO), and a Cascade II CCD camera (Photometrics). A 10-ms exposure time was used in both channels with no neutral density filters, or a 100-ms exposure time was used with two neutral density filters, to reduce CFP photobleaching over the course of the experiment. Images at both emission wavelengths were then acquired at 20-second intervals before and after the start of 20-second exposures to high intensity light at YFP-specific excitation wavelengths. Photobleaching intervals were continued until YFP intensity was reduced to less than 5% of its starting value. The fractional decrease of fluorescence emission intensity of the donor (CFP-SERCA) caused by the presence of an acceptor (YFP-WT-PLB) is defined as the FRET efficiency $E = 1 - (F_{DA}/F_D)$, where F_{DA} and F_D are the fluorescence intensities in the presence and absence of acceptor, respectively. F_{DA}

47

was measured as the CFP intensity prior to the start of the YFP photobleach. F_D was determined by the y-axis intercept of the linear fit to a data plot of YFP intensity (on x-axis) to CFP intensity (y-axis) over the course of the photobleach for each cell, to account for any CFP photobleaching and incomplete YFP photobleaching [140]. FRET values were calculated for all cells in each experimental condition and averaged together to determine $FRET_{ave}$. To eliminate any changes in $FRET_{ave}$ due to differences in YFP-PLB expression levels, only cells with YFP intensities common to all experimental conditions were included in the $FRET_{ave}$ calculation.

3.3. Results

3.3.1. PLB Phosphorylation

We expressed CFP-SERCA and YFP-PLB stably in HEK cells (at a molar ratio of 7.8 PLB/SERCA, to ensure saturation), then measured FRET using acceptor-selective
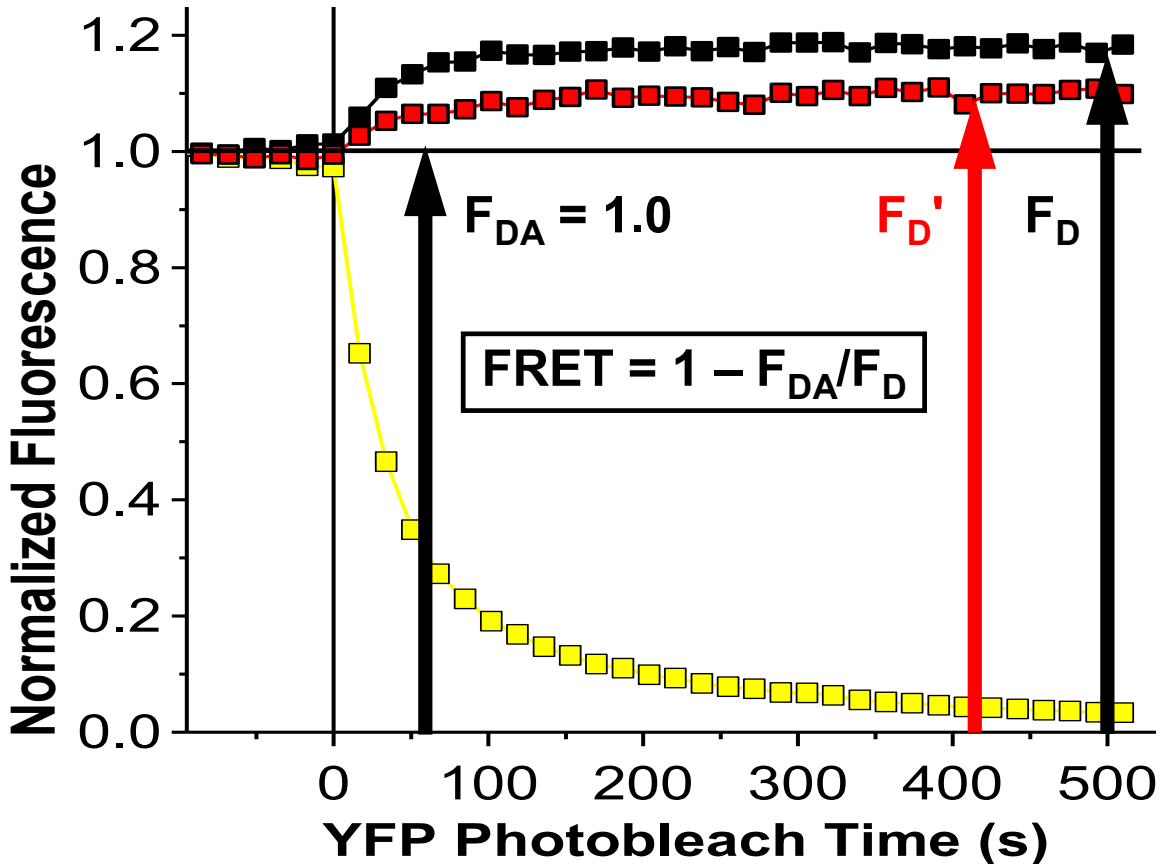
Figure 19. **FRET from CFP-SERCA to YFP-PLB in live HEK cells**. Normalized fluorescence was measured for YFP (yellow) or CFP (black or red). YFP acceptors were selectively photobleached, and FRET was calculated as shown. Black: control. Red: FRET is reduced after transient expression of PLB_M.

photobleaching (**Figure 19**). The control FRET value of the parent cell line was 15.4 ±

1.2%, measured repeatedly and on different days over several weeks. This stable cell line

was critical to evaluating perturbations due to PLB phosphorylation or competition with

PLB_M. FRET was calculated for every cell and averaged together based on initial YFP

intensity.

49

FRET between CFP-SERCA and YFP-PLB increased significantly when PLB

phosphorylation was induced by incubating the cells in forskolin (fsk), which activates
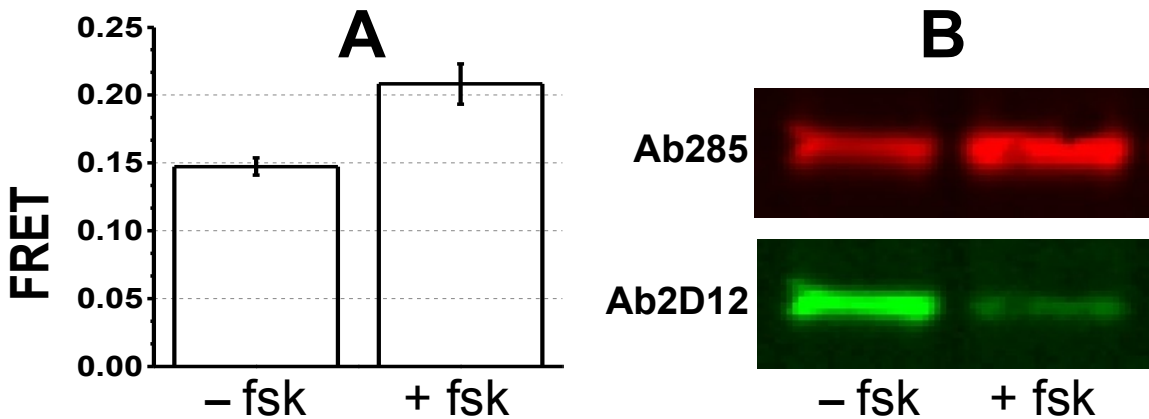
Figure 20. **Effect of PLB phosphorylation on SERCA-PLB FRET in live cells**. (**A**) FRET in live cells, before and after 5 min incubation in 40 μM forskolin (fsk), increases from $0.15 \pm .01$ to 0.21 ± 0.02 (SEM, n = 8, p < 0.01). (**B**) Immunoblot of cell homogenates from (**A**) shows increased YFP-PLB phosphorylation, by increased Ab285 (red, specific for pPLB) and decreased Ab2D12 (green, specific for uPLB). Quantitative densitometry, using purified uPLB and pPLB standards [138], shows that phosphorylation increased from $51 \pm 4\%$ to $87 \pm 5\%$ in PLB monomer (shown) and pentamer bands.

the PKA pathway at adenylyl cyclase (**Figure 20A**). Immunoblots from the same cells,

using antibodies specific for phosphorylated and unphosphorylated PLB, verify that

phosphorylation of YFP-PLB increased substantially (from 51% to 87%) after forskolin

treatment (**Figure 20B**). Increased FRET indicates increased SERCA-PLB association or

a shorter donor-acceptor distance within the SERCA-PLB complex. If the Dissociation

Model of SERCA regulation were valid, we would expect a decrease in FRET (**Figure

18A**, left). Thus this data clearly supports the Subunit Model (**Figure 18A**, right), in

which phosphorylation changes the structure of the SERCA-PLB complex but does not

dissociate it.

FRET measurements were used to calculate the distance between CFP and YFP

before and after induction of PLB phosphorylation. Since FRET is a linear combination

of the values for unphosphorylated (U) and phosphorylated (P) PLB, FRET = X_U*FRET_U + X_P*FRET_P, where X_P (= 1-X_U) is the fraction of PLB that is phosphorylated. Solving two simultaneous equations (before and after fsk), we find that the FRET values for the bound SERCA-PLB complex in the absence and presence of phosphorylation are $FRET_U$ = 0.07 ± .02 and $FRET_P$ = 0.23 ± 0.04. Since YFP-PLB is in large excess over CFP-SERCA, and since phosphorylation actually increases FRET, we assume that all CFP donors are participating in FRET. Assuming a single interprobe distance R in each case, $R = (1/FRET-1)^{-1/6}*4.92$ nm, giving $R = 7.7 ± 0.4$ nm (unphosphorylated) and $6.0 ± 0.2$ nm (phosphorylated) [96]. Thus phosphorylation of PLB causes a change in the structure of the SERCA-PLB complex that decreases the CFP-YFP distance by $\Delta R = 1.7 ± 0.6$ nm ($p < 0.01$, $n = 8$), consistent with the Subunit Model in **Figure 18A** (right).

3.3.2. PLB_M Competition

In contrast to the increased FRET induced by PLB phosphorylation, FRET
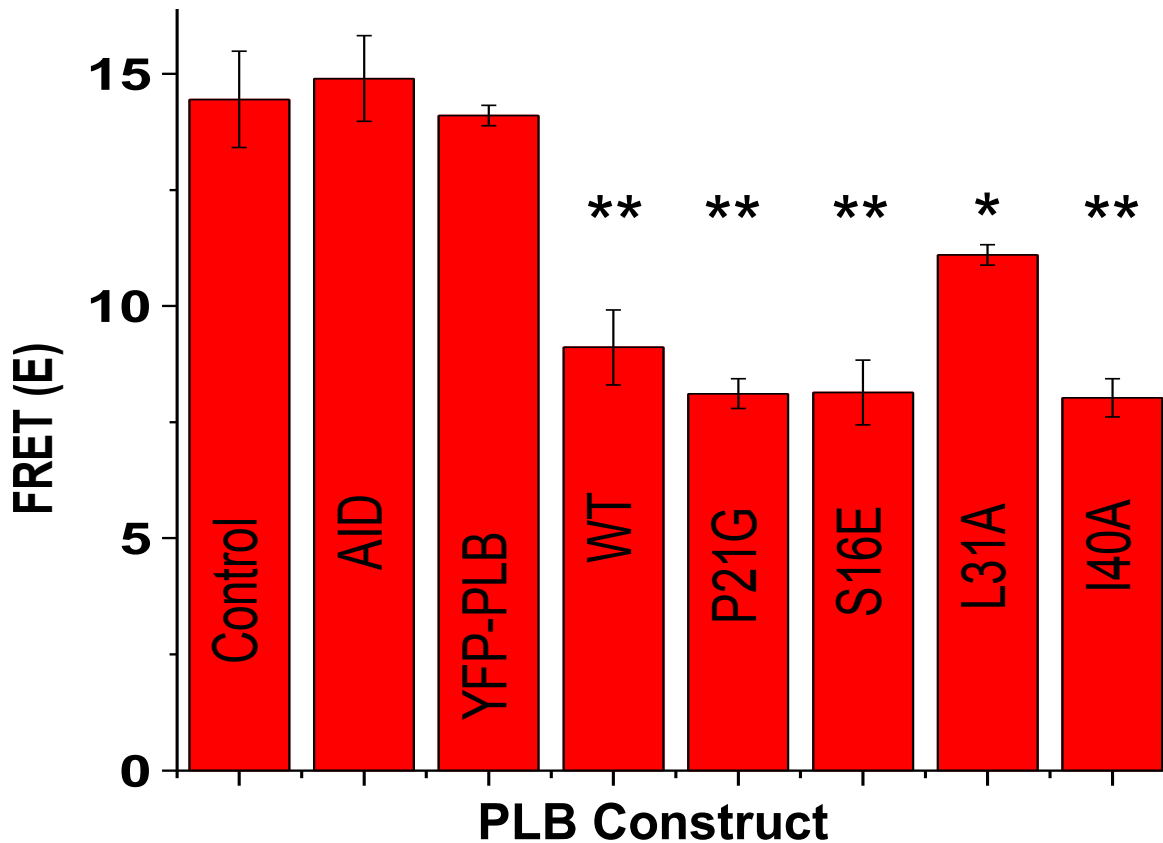
Figure 21. FRET competition in live cells. Decreased FRET indicates that unlabeled PLB_M constructs compete effectively with YFP-PLB for binding to CFP-SERCA. $n \geq 3$ for each PLB_M, significant difference from control is indicated by ** ($p < 0.001$) and * ($p < 0.01$).

between CFP-SERCA and YFP-PLB decreased significantly when unlabeled PLB_M was

added (**Figure 19, Figure 21**). FRET measurements, following transient transfection of

unlabeled PLB_M into the stable CFP-SERCA/YFP-PLB HEK cell line, showed that all

PLB_M studied here compete effectively with YFP-PLB for SERCA binding, and several

reduced FRET by approximately half (**Figure 21**). Expression levels of YFP-PLB and

PLB_M were similar, so a 50% decrease in FRET indicates that PLB_M has a SERCA

affinity similar to that of YFP-PLB. Further addition of YFP-PLB or a cytosolic protein

(activation-induced deaminase, AID, used as a control) did not affect FRET (**Figure 21**), indicating that CFP-SERCA is saturated with YFP-PLB at the start of each competition experiment. The data in **Figure 21** were obtained from PLB variants based on the human sequence. Essentially the same results were obtained when these same mutations (WT, P21G, and S16E) were studied on the background of the monomeric AFA-PLB mutant (not shown).

Several PLB_M compete effectively with YFP-PLB, with a potency (affinity) equal to or greater than that of unlabeled WT-PLB (**Figure 21**). The pseudo-phosphorylated mutant S16E, which rescues HF phenotypes in animal models when introduced via rAAV [132], is a potent competitor, reducing CFP-YFP FRET by 45%. Two other LOF PLB_M, P21G and L31A, also showed competition; this is important, since these mutants, unlike S16E, can still be phosphorylated by PKA at S16 and are thus preferable as gene therapy candidates. I40A, a superinhibitory (GOF) mutant of PLB [141], showed similar competitive potency as WT and several LOF mutants (**Figure 21**).

In the competition experiments, we assume that the effect of unlabeled PLB_M is to decrease the fraction of CFP-SERCA that is bound to YFP-PLB:

$$FRET' = X_B * FRET,$$

where FRET and FRET′ are values observed before and after transient expression of unlabeled PLB_M, and X_B is the mole fraction of CFP-SERCA that remains bound to YFP-PLB after PLB_M expression. Since the levels of YFP-PLB and PLB_M are very similar, this means that, to a good approximation,

$$K_A(PLB_M)/K_A(PLB) = FRET/FRET' - 1,$$

53

where K_A is the affinity ($1/K_D$) of the PLB variant for CFP-SERCA. Since most of the PLB_M tested, as well as WT-PLB, decreased FRET by about half (FRET/FRET′ = 2) (Fig. 4), each has about the same SERCA affinity as YFP-PLB. The exception is L31A, which gave FRET/FRET′ = 0.7, so its SERCA affinity is about half that of the others.

3.4. Discussion

We showed previously that the SERCA-PLB interaction can be measured by FRET in living cells transiently expressing fluorescent fusion proteins CFP-SERCA and YFP-PLB [142]. The present study establishes a stable cell line to make precise FRET measurements over time (**Figure 19**), making it possible to compare the effects of numerous perturbations, such as PLB phosphorylation (**Figure 20**) or the introduction of unlabeled PLB_M to compete for SERCA binding (**Figure 19, Figure 21**). We used this assay to resolve several controversies regarding SERCA/PLB regulation. We found that FRET between SERCA and PLB actually increases upon phosphorylation (**Figure 20**), clearly contradicting the Dissociation Model in favor of the Subunit Model (**Figure 18A**). Since PLB inhibition can be relieved by phosphorylation without decreasing SERCA affinity, a loss-of-function mutation might do the same (**Figure 18B**). This hypothesis was confirmed by the competition experiments, in which all mutants tested showed competition with WT-PLB for SERCA binding (**Figure 19, Figure 21**).

This system offers the potential for probing the fundamental regulatory mechanism of the SERCA-PLB system in living cells [42, 142], but our main motivation is therapeutic development. This direct and rapid competition assay in HEK cells

provides a platform for evaluating further PLB_M for gene therapy treatment of HF to activate SERCA (**Figure 18**). The effectiveness of S16E, the pseudophosphorylated PLB_M, to compete significantly for SERCA binding in HEK cells (**Figure 21**) helps explain its success as a gene therapy tool in animal models of HF [132]. Introduction of S16E-PLB into the human heart could cause chronic inotropic stimulation and is otherwise unregulated, so it is not optimal for gene therapy [143]. Better PLB_M must be developed, with intact phosphorylation sites.

L31A-PLB is a well-known LOF mutant [65], but it still competes with WT-PLB, albeit less effectively than S16E-PLB (**Figure 21**), in agreement with recent FRET experiments on purified proteins [65]. The P21G mutant, designed from magnetic resonance-based structural analysis [68], provides encouraging evidence that a LOF PLB_M with an intact phosphorylation site can be just as effective as S16E (**Figure 21**). Most of the PLB_M tested show similar SERCA affinity as WT-PLB, but none shows significantly tighter binding (**Figure 21**). We are currently developing double mutants, combining LOF mutations with other mutations that increase SERCA affinity [68]. We envision an assortment of mutants to fine-tune SERCA activity to treat distinct HF syndromes. Our FRET competition assay in live cells provides a rapid and inexpensive method for screening potential therapeutic PLB_M mutants before they are tested in animals or humans. This FRET assay also has the potential for high-throughput screening of small molecules as potential HF drugs to activate SERCA [65, 144].

Acknowledgements

Chapter 4 – High-Throughput FRET Assay Yields Allosteric SERCA Activators

Reprinted from:

High-Throughput FRET Assay Yields Allosteric SERCA Activators

Razvan L. Cornea[1], Simon J. Gruber[1], Elizabeth L. Lockamy[1], Joseph M. Muretta[1],

Dongzhu Jin[2], Jiqiu Chen[2], Russell Dahl[3], Tamas Bartfai[4], Krisztina M. Zsebo[3], Gregory

D. Gillispie[1,5], and David D. Thomas[1]

[1]Department of Biochemistry, Molecular Biology and Biophysics, University of

Minnesota, Minneapolis, MN 55455, USA.

[2]Cardiovascular Research Center, Mount Sinai School of Medicine, New York, NY

10029, USA.

[3]Celladon Corporation, San Diego, CA 92130, USA.

[4]Harold Dorris Neurological Institute, Department of Molecular and Integrative

Neurosciences, The Scripps Research Institute, La Jolla, CA 92037.

[5]Fluorescence Innovations, Inc., Minneapolis, MN 55455, USA.

Using fluorescence resonance energy transfer (FRET), we performed a high-throughput screen (HTS) in a reconstituted membrane system, seeking compounds that reverse inhibition of sarcoplasmic reticulum Ca-ATPase (SERCA) by its cardiac regulator, phospholamban (PLB). Such compounds have long been sought to correct aberrant Ca^{2+} regulation in heart failure. Donor-SERCA was reconstituted in phospholipid membranes with or without acceptor-PLB, and FRET was measured in a steady-state fluorescence microplate reader. A 20,000-compound library was tested in duplicate. Compounds that decreased FRET by more than three standard deviations were considered hits. From 43 hits (0.2%), 31 (72%) were found to be false positives upon more thorough FRET testing. The remaining 12 hits were tested in assays of Ca-ATPase activity, and six of these activated SERCA significantly, by as much as 60%, and several also enhanced cardiomyocyte contractility. These compounds directly activated SERCA from heart and other tissues. These results validate our FRET approach and set the stage for medicinal chemistry and pre-clinical testing. We were concerned about the high rate of false positives, resulting from the low precision of steady-state fluorescence. Preliminary studies with a novel fluorescence lifetime plate reader show 20-fold higher precision. This instrument can dramatically increase the quality of future HTS.

4.1. Introduction

The sarcoplasmic reticulum calcium ATPase (SERCA) is responsible for clearing Ca^{2+} from the sarcoplasm, leading to muscle relaxation. In heart, and particularly in the ventricular myocardium, SERCA2a is under tight inhibitory regulation by phospholamban (PLB), a small (52-residue) single-pass transmembrane protein that is co-expressed with SERCA in the sarcoplasmic reticulum (SR). PLB decreases the apparent Ca^{2+} affinity of SERCA, thus inhibiting Ca^{2+} pumping at diastolic (submicromolar) concentrations of intracellular $[Ca^{2+}]$ [145]. The transmembrane domain of PLB is responsible for the inhibition of SERCA [67], which is relieved by systolic (micromolar) $[Ca^{2+}]$ or when PLB is phosphorylated at residues 16 and/or 17 in the cytoplasmic domain [129]. This enables the myocardium to tap into a Ca^{2+} pumping reserve necessary for the fight-or-flight response.

SERCA activity decreases significantly in heart failure (HF), resulting in incomplete and slower relaxation after each heart beat, contributing to the altered calcium homeostasis that is a hallmark of HF [146]. The ratio of PLB to SERCA is increased in HF, thus resulting in increased SERCA inhibition. Rescuing SERCA activity in the heart has been achieved via gene therapy, overexpressing SERCA2a or expressing non-inhibitory PLB mutants [147]. SERCA activation has been shown to be harmless in normal animals and to improve muscle function in animal models of several types of heart disease, as well as muscular dystrophy [147]. The SERCA2a gene therapy treatment has been shown to be effective for human HF patients in phase II clinical trials [148]. These results clearly validate SERCA activation as a target for HF therapy. However, given the inherent complexity of gene therapy, we are pursuing an alternative approach –

the direct activation of SERCA by small-molecule drugs – which would enable acute hospital intervention in HF, as well as chronic use in case of reduced cardiac activity.

Industrial and academic researchers have searched intensively but unsuccessfully
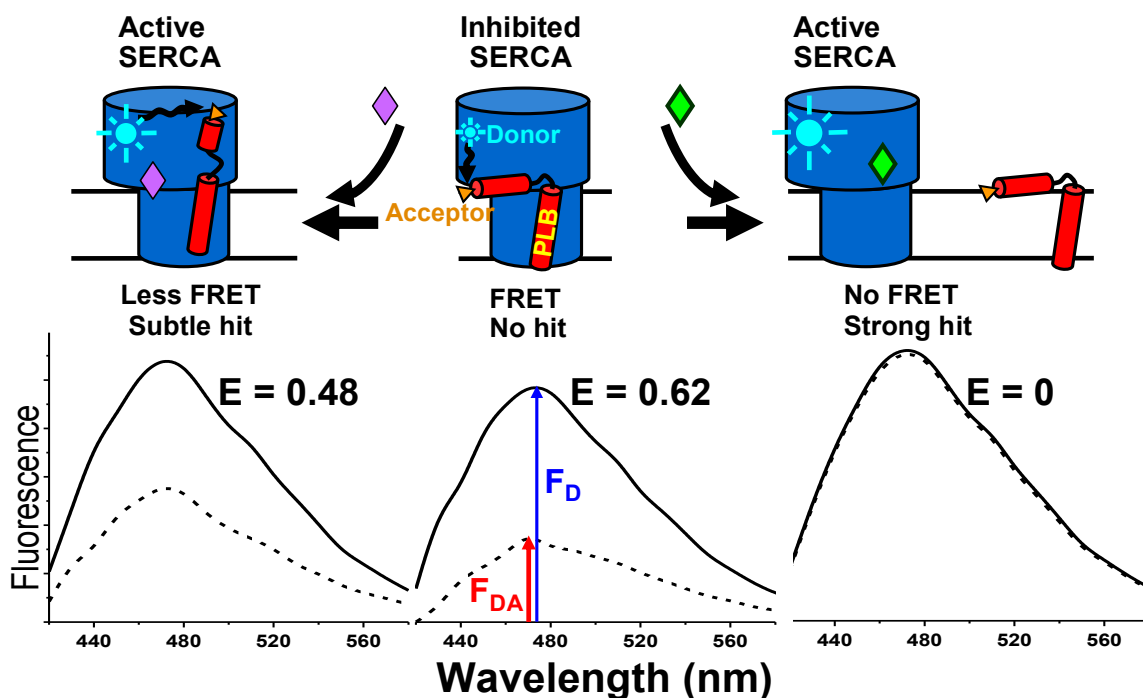
Figure 22. FRET assay for disruption of the inhibitory SERCA-PLB interaction. Top: schematic diagram illustrating possible effects of compounds on the SERCA-PLB complex. Bottom: fluorescence intensity spectra that would result (solid curve is donor-only control, F_D, dashed curve is donor-acceptor complex, F_{DA}). FRET efficiency is given by $E = 1 - F_{DA}/F_D$. Center: Most compounds have no effect, so the SERCA-bound donor remains quenched by FRET to the PLB-bound acceptor, giving high E value (no hit). Right: a compound that completely dissociates the complex would completely eliminate FRET, giving $E = 0$ (strong hit). Left: a compound that causes a structural rearrangement within the SERCA-PLB complex would cause a more subtle change in FRET.

for compounds that dissociate PLB from SERCA to relieve inhibition of Ca^{2+} transport specifically in the heart and improve the prognosis in HF patients [114]. Based on our basic research on the SERCA-PLB system, it is likely that prior efforts failed due primarily to the lack of a robust HTS assay for inhibitors of the SERCA-PLB interactions. Previous attempts to study this system used cumbersome functional assays

60

that required several minutes each [114]. We use that kind of functional assay for our secondary screen, as discussed below, but successful HTS requires a primary assay that (a) detects directly a signal that is strongly correlated with function, preferably at molecular level, and (b) is truly high-throughput, so that thousands of compounds can be tested in a day. We have approached both requirements using fluorescence resonance energy transfer (FRET). We developed an assay to measure the SERCA-PLB interaction directly with FRET, using purified SERCA and PLB labeled with fluorescent dyes in reconstituted membranes (**Figure 22**) [64]. In this assay, an excited donor on SERCA transfers energy to a nearby acceptor on PLB, thus decreasing the donor's fluorescence intensity (**Figure 22**). Using this assay, we discovered that relief of SERCA inhibition does *not* require dissociation of the SERCA-PLB complex (**Figure 22**, right), as proposed by others [73]. Instead, a subtle allosteric structural change of the SERCA-PLB complex, without dissociation, is sufficient to relieve inhibition. (**Figure 22**, left) [46, 64, 149]. Thus the FRET signal should detect any structural change within SERCA that alters the distance from the SERCA-bound donor to the acceptor on PLB.

Fortunately, due to the R^{-6} distance dependence of FRET, it can detect subtle structural changes resulting from protein-protein interactions and/or conformational changes. In addition, a precise FRET measurement can be done in less than a second, offering the clear potential for a high-throughput assay. Here we report results from a high-throughput screen (HTS) we have conducted using our SERCA-PLB FRET assay (**Figure 22**) [64], modified for a fluorescence microplate reader. We screened a small-molecule library for compounds that disrupt the physical interaction between donor-

labeled SERCA and acceptor-labeled PLB, aiming to increase the Ca^{2+} transport activity of SERCA by disinhibiting the enzyme. It was expected that most compounds would not change the FRET efficiency E (**Figure 22**, center). If the SERCA-PLB complex is dissociated, FRET should be completely eliminated (**Figure 22**, right). But if a more subtle structural change occurred, without dissociation (**Figure 22**, left), there would be smaller change in FRET. This screen was specifically targeted at the SERCA-PLB interface with two main goals: (a) reversing inhibition of SERCA by PLB and (b) thus specifically targeting SERCA in the heart.

4.2. Materials and Methods

The 20,000-compound DIVERSet™ library of molecules of below 600 molecular weight was obtained from ChemBridge (San Diego, CA). The screen was conducted in NUNC 242764 384-well black-wall/clear-bottom microplates (Nalge Nunc International, Rochester, NY); CappAero™ 16-channel pipettes were from Capp A/S (Odense, Denmark). The Gemini EM microplate fluorimeter and Aquamax DW4 liquid dispenser were purchased from Molecular Devices (Sunnyvale, CA). Fluorophores 5-((((2-iodoacetyl)amino)ethyl)amino)naphthalene-1-sulfonic acid (IAEDANS) and 4-((4-(dimethylamino)phenyl)azo)benzoic acid, succinimidyl ester (DABCYL) were purchased from Invitrogen.

4.2.1. Isolation of sarcoplasmic reticulum vesicles

Skeletal muscle SR membrane vesicles were isolated from longissimus dorsi obtained from New Zealand white rabbits, as previously described [64]. Cardiac SR membrane vesicles were isolated from ventricular myocardium obtained from fresh pig hearts [150].

4.2.2. SERCA preparation and labeling

SERCA was purified by Reactive-Red™ (Sigma) affinity chromatography from skeletal SR using a procedure described previously [64], and was stored at -80 °C until further usage. Purified SERCA was labeled with IAEDANS, a small fluorescent probe that reacts at Cys-674 in the P-domain, as described previously [64]. Samples of AEDANS-SERCA were flash-frozen and stored in the dark at -80°C until further usage.

4.2.3. PLB synthesis and labeling

PLB (canine sequence) was assembled on Fmoc-Leu-PEG-PS resin by Fmoc chemistry using a PE Biosystems Pioneer™ peptide synthesis system, as previously reported [64]. The *N*-terminal amino group of unlabeled PLB was acetylated using acetic anhydride. For FRET, the non-fluorescent acceptor DABCYL was reacted at Lys-3 of WT-PLB (denoted DABCYL-PLB). The composition and concentration of synthetic PLBs were confirmed by MALDI-TOF and amino acid analysis, and samples were stored in methanol at -20°C.

4.2.4. Co-reconstitution of SERCA and PLB

Samples were prepared fresh daily, scaling up our previous method [64], to 2 mg reconstituted AEDANS-SERCA (donor-only sample), and 2 mg AEDANS-SERCA co-reconstituted with 530 μg DABCYL-PLB (to obtain a donor+acceptor sample with a molar PLB/SERCA = 5, close to that found in the normal heart)[151]. The molar ratio of lipid/SERCA was 700. These amounts are sufficient for five "donor-only" and five "donor+acceptor" 384-well plates, plus one quality-control test plate.

4.2.5. Plates, plate preparation

The NUNC plates were chosen for their relatively small and uniform intrinsic fluorescence signal in the 420–600 nm wavelength range. The DIVERSet™ library was

diluted in dimethyl sulfoxide (DMSO) and reformatted for the screen in these plates at the University of Minnesota High-Throughput Biological Analysis Facility. Columns 1 and 24 of each plate were reserved for no-compound controls (20/plate) and buffer blanks (12/plate); these wells contained the same volume of DMSO as the wells containing library compounds. Columns 2-23 contained library compounds in duplicate. These plates were sealed and stored at -20°C until used in the screen. On the day they were used in the screen, the assay plates were equilibrated to room temperature (25°C), then spun 5 min at 1000 x g in an Eppendorf 5810R centrifuge equipped with an A-4-81 rotor and microplate adaptor-buckets. Sample containing 90 nM AEDANS-SERCA (78 μL) was applied to the assay plate over the 2 μL of test-compound using an Aquamax DW4 liquid dispenser (Molecular Devices, Sunnyvale, CA) to obtain a final compound concentration of 10 μM. Before reading, assay plates were incubated for 20 minutes at room temperature.

4.2.6. Fluorescence data acquisition

Typically, in HTS assays using fluorescence intensity, a single-wavelength measurement is recorded for each well. In this screen, the relatively low brightness of AEDANS-SERCA and high probability of spectral distortion (e.g., due to test-compound fluorescence), particularly at wavelengths shorter than 500 nm, led us to acquire full fluorescence intensity spectra for each well. This increased amount of information aided in determining whether a reading was reliable, or skewed by compound fluorescence or by other factors contaminating the AEDANS-SERCA spectrum. Plates were read in a Gemini EM microplate fluorometer (Molecular Devices, Sunnyvale, CA) with excitation

at 355 nm from a Xenon flash lamp (1 J/flash), and a 420 nm long-pass emission filter. Fluorescence emission spectra were recorded from 420 to 600 nm, with 10 nm step size.

Fluorescence lifetime measurements were conducted in a prototype of the NovaFluor plate reader (Fluorescence Innovations, Bozeman, MT), which uses direct waveform recording (DWR) to provide the rate of data acquisition necessary for HTS [152]. Fluorescence was excited 355 nm using a 10 kHz passively Q-switched microchip laser (JDS Uniphase). Fluorescence emission was focused into a photomultiplier tube module (Hamamatsu) and digitized with 0.2 ns resolution. This instrument can scan a 384-well plate in less than 2 minutes, yielding waveforms with S/N=100 in each well for samples containing 90 nM AEDANS-SERCA. This rate of data acquisition at high S/N is at least 100 times faster than achievable by other fluorescence lifetime plate readers.

4.2.7. HTS Data analysis

Fluorescence spectra were corrected by subtracting the signal corresponding to buffer controls within the plate. Compounds that distorted the fluorescence spectrum were excluded from the hit selection. Donor-only and donor-acceptor controls (i.e., containing no library compound, only the corresponding 2 µL volume of DMSO) were used to determine standard deviation (SD) within the plate. The FRET efficiency E was calculated according to:

$$E = 1 - (F_{DA}/F_D),$$ **Equation 12**

where F_D is the fluorescence intensity of the donor-only sample, which is decreased to F_{DA} by the acceptor in the donor-acceptor sample. Assay quality was determined based on controls on each plate, as indexed by the z′ parameter [153]:

$$z' = 1 - 3(\sigma_D + \sigma_{DA})/(\mu_D -$$

<div align="right">**Equation 13**</div>

$$\mu_{DA}),$$

where σ_D and σ_{DA} are the SDs of the control F_D and F_{DA}, respectively; μ_D and μ_{DA} are the means of the control F_D and F_{DA}, respectively. A compound was considered a hit if it decreased E by more than three times the SD of the no-compound controls.

4.2.8 Secondary Functional Assays
Ca-ATPase activity.

The reconstituted samples used in HTS were characterized as a function of pCa using an NADH-linked, enzyme-coupled ATPase assay adapted for 96-well microplates (**Figure 23**) [65]. Each well contained 2 µg (skeletal) or 7 µg (cardiac) of SR vesicles (adjusted for the different SERCA contents of skeletal and
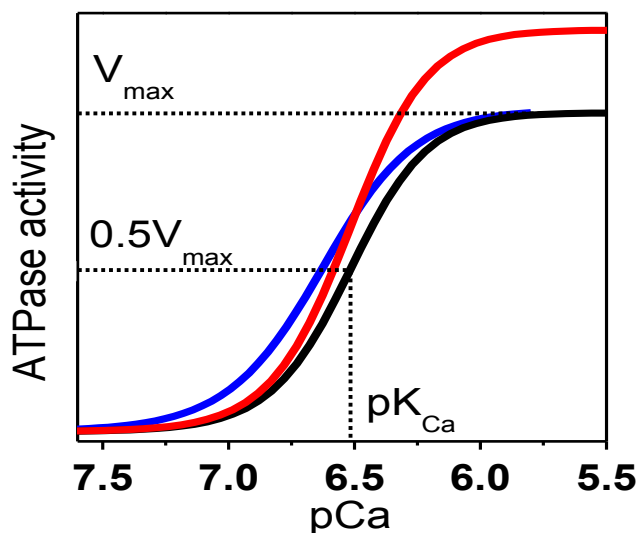
Figure 23. Functional effects of a hit. Desirable compounds may act on the Ca^{2+} dependence of SERCA's ATPase activity (black) to increase its apparent Ca^{2+} affinity (pK_{Ca}, blue) or to increase the maximum rate (V_{max}, red), or a combination of both (not shown). Curves represent fits of **Equation 14)** to typical Ca-ATPase data.

cardiac SR), 50 mM MOPS (pH 7.0), 100 mM KCl, 5 mM $MgCl_2$, 1 mM EGTA, 0.2 mM NADH, 1mM phosphoenol pyruvate, 5 IU of pyruvate kinase, 5 IU of lactate dehydrogenase, 3.5 µg/ml of the calcium ionophore A23187, and $CaCl_2$ added to set free $[Ca^{2+}]$ to the desired values. The assay was started upon the addition of ATP at a final concentration of 5 mM, and read in a SpectraMax Plus microplate spectrophotometer.

The Ca-ATPase assays were conducted over a range of $[Ca^{2+}]$, and the ATPase activities were fitted using the Hill function:

$$V = V_{max}/[1 + 10^{-n\,(pK_{Ca} - pCa)}],$$ **Equation 14**

where V is the initial ATPase rate, V_{max} is the ATPase at saturating $[Ca^{2+}]$, n is the Hill coefficient, and pK_{Ca} is the apparent Ca^{2+} dissociation constant. The assay provides a confirmation of the functional integrity of SERCA reconstituted in the absence of PLB (**Figure 23**, **blue**), and the right-shift in the calcium curve when co-reconstituted with PLB (**Figure 23**, **black**) was diagnostic of the correct functional coupling within the SERCA-PLB complex. We used this method as our primary orthogonal assay to determine whether a hit compound, identified by the FRET screen, activated SERCA function. A compound that reverses the inhibitory effect of PLB on SERCA (e.g., by completely dissociating the complex) should shift the Ca-curve to the left (**Figure 23**, black to blue), thus resulting in an increased rate of Ca^{2+} transport at nM $[Ca^{2+}]$ (as in diastole). However, activation can also be achieved by increasing V_{max} (**Figure 23,** black to red).

Cardiomyocyte assays.

Adult male Sprague-Dawley rats weighing 250-300g were obtained from Charles River Laboratories and used for the assessment of myocyte contractility. Cardiac myocytes were obtained by enzymatic isolation as described previously [154]. Left ventricular myocytes were suspended in a buffer containing 10 mM HEPES (pH 7.4), 131 mM NaCl, 4 mM KCl, 2 mM $MgCl_2$, 1 mM $CaCl_2$, 10 mM glucose. Cells were

incubated with either test compound dissolved in DMSO, or DMSO vehicle only, for at least 10 minutes before the measurements of cellular contractility. Myocyte contractility was measured using the IonOptix video-based edge detection system (IonOptix Corporation Milton, MA) [155]. Sarcomere length was monitored at 25°C in field-stimulated myocytes at 1 Hz, with 4 ms pulse duration, 30 V using a STIM-AT thermostated stimulator.

Measurement of $[Ca^{2+}]_i$ transients was carried out as described previously [156]. Myocytes were loaded with the membrane-permeant fluorescent Ca^{2+} indicator fura-2 AM (Invitrogen). After myocyte incubation with the indicator for 15 min at 25° C, fluorescence imaging was conducted using the IonOptix photomultiplier system, with excitation from a 75 W halogen lamp for 0.5 s at 360 nm, then at 380 nm for the duration of the recording protocol. Emission was recorded at 500 nm (40 nm bandwidth). Cells were observed using an inverted microscope, through an Olympus Fluor x40 oil objective. We measured multiple, randomly chosen myocytes treated with test compound or DMSO vehicle.

4.3. Results

4.3.1. HTS performance.

Tests were conducted with control samples to determine the precision of our assay. The relatively weak IAEDANS fluorescence spectrum is prone to distortion by test-compound fluorescence or by other factors contributing to sample irregularity (e.g., bubbles, particulates, variations in plate background). This could make the FRET measurement imprecise, thus negatively impacting the screen quality. Therefore, we devised methods to minimize spectral distortions during data acquisition, and to identify

distorted spectra during data analysis. Use of a non-fluorescent acceptor (DABCYL) facilitates distortion detection and correction because it allows using the entire donor fluorescence spectrum for FRET calculations. In preliminary assessments of the assay quality, we found that spectral distortions were less at longer wavelengths of the IAEDANS spectrum (>500 nm). For AEDANS-SERCA samples, we found that the coefficient of variance (CV = σ/μ x 100%) was significantly higher at 470 nm (10%) than at 520 nm (6%). We measured approximately the same CV for the donor-only sample and for samples in which FRET efficiency E was about 0.5. To predict assay quality, we calculated the factor z' based on CV and signal window (ΔE), with **Equation 13)** rewritten as:

$$z' = 1 - 3CV(2 - \Delta E)/\Delta E, \qquad \textbf{Equation 15}$$

Based on the measured CV, and on the average FRET efficiency of the 5DAB-PLB/AEDANS-SERCA samples (E = 0.57±0.09), we predicted z' parameters of 0.25±0.22 and 0.54±0.11 for readings at 470 and 520 nm, respectively (**Figure 24A**). Therefore, the screen was preliminarily deemed at least "doable" (with readings at 470 nm), and "excellent" (with readings at 520 nm), if complete inhibition of FRET serves as the condition for hit selection.

69
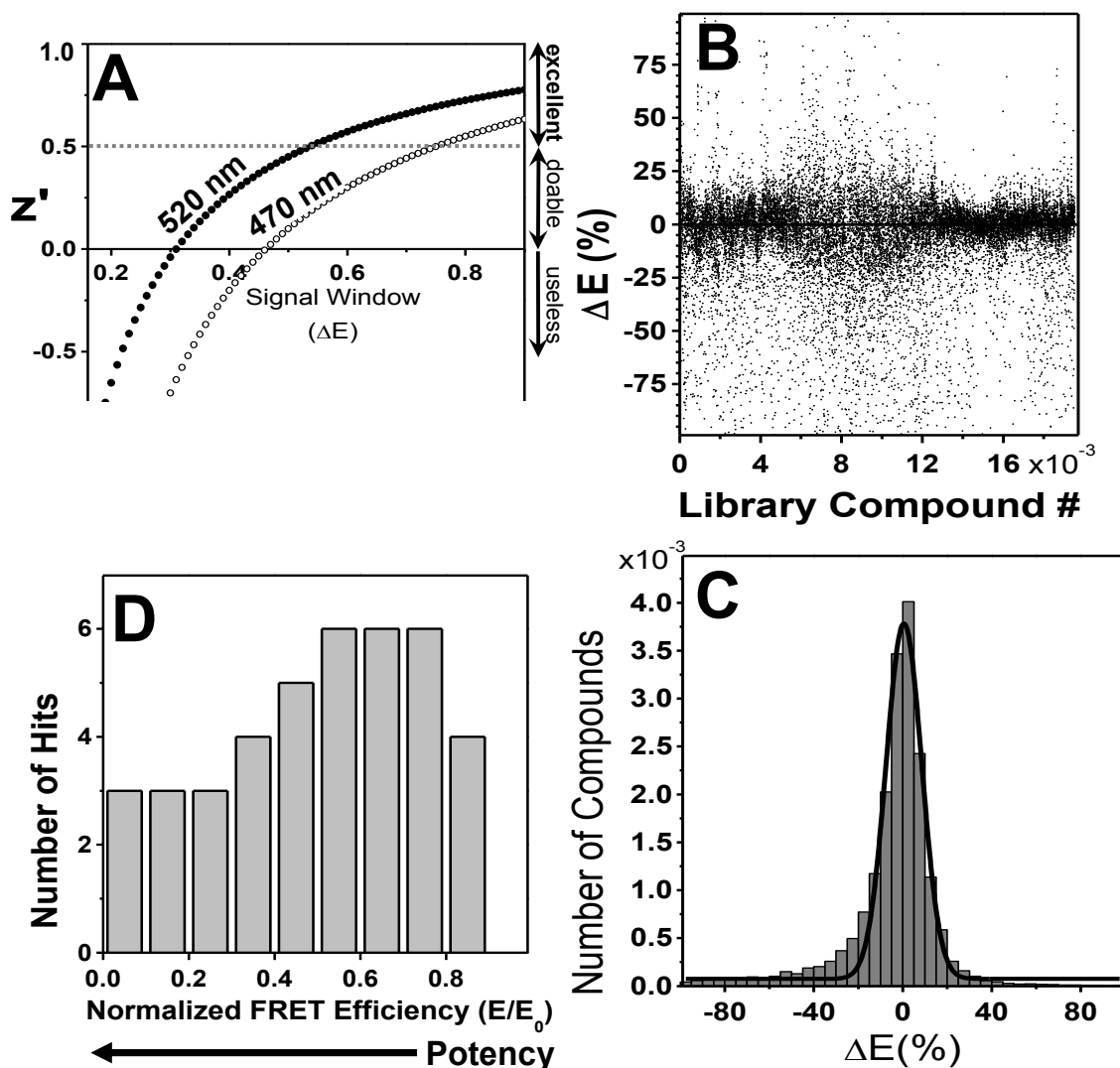
Figure 24. High-throughput screen results. Compounds were screened, in duplicate, at a concentration of 10 μM (in DMSO). (**A**) Assay quality (z') depends on the signal window (change in FRET efficiency, ΔE, as defined in **Equation 12)**, and CV according to **Equation 15). (B**) Compound effects on ΔE show a distribution that is fitted by a Gaussian (**C**), giving the average effect, $\mu = 0.5\pm0.3\%$, and the global SD, $\sigma = 8\%$. (**D**) Distribution of hits. E_0 is the mean value of the energy transfer efficiency E observed in the absence of added compound.

The library was screened in 110 duplicate plates, and the apparent effect of compounds on the FRET efficiency, Δ*E*, is- shown for all compounds in **Figure 24B**, with positive and negative Δ*E* values indicating increase or decrease, respectively, relative to the *E* of controls. Our goal was to identify compounds that significantly

70

decrease the FRET efficiency. The distribution of ΔE can be reasonably fitted by a Gaussian, centered at approximately the control value, $\mu = 0.5\% \pm 0.3\%$, with a global SD, $\sigma = 8\%$ (**Figure 24C**). To decrease the probability of false hits, all compounds were screened in duplicate on the same plate. Z' was calculated for each plate based on the no-compound controls (20/plate). For the actual screen, the average z' value was 0.4 ± 0.2.

A slight asymmetry in the distribution is observed (**Figure 24C**), with negative ΔE values somewhat more numerous than positive values. This is due to compounds that have a fluorescence spectrum comparable in intensity over the same wavelength range as the spectrum of AEDANS-SERCA. Such compounds increase the total fluorescence, and thus will appear to decrease FRET. The compounds distorting AEDANS-SERCA spectra (donor-only) were identified based on their effect on the donor-only spectrum, and were eliminated from consideration during the hit selection process.

Only data from plates with $z' \geq 0$ were analyzed for hits. Although a significant number of compounds increased ΔE beyond the 3σ threshold (**Figure 24B**), most of these values appear to result from irregularities in the fluorescence spectra, so the corresponding compounds were filtered out. Our final set of hits consisted of 43 compounds, about a 0.2% hit rate (which is considered low for most screens, but is typical for screens of protein-protein interaction), which we ranked based on the observed E value relative to controls (E_0, no compound). (**Figure 24D**). However, when these 43 preliminary hits were rescreened exhaustively ($n \geq 10$) at 10 μM concentration, only 12 (28%) were found to cause a significant decrease in FRET (beyond the 3σ threshold). These 12 compounds were selected for secondary functional screens.

71

4.3.2. Ca-ATPase activity in purified SR.

The functional effects of the hit compounds were first measured *in vitro* using Ca-ATPase assays, which were carried out in skeletal SR (SERCA1 only) and cardiac SR
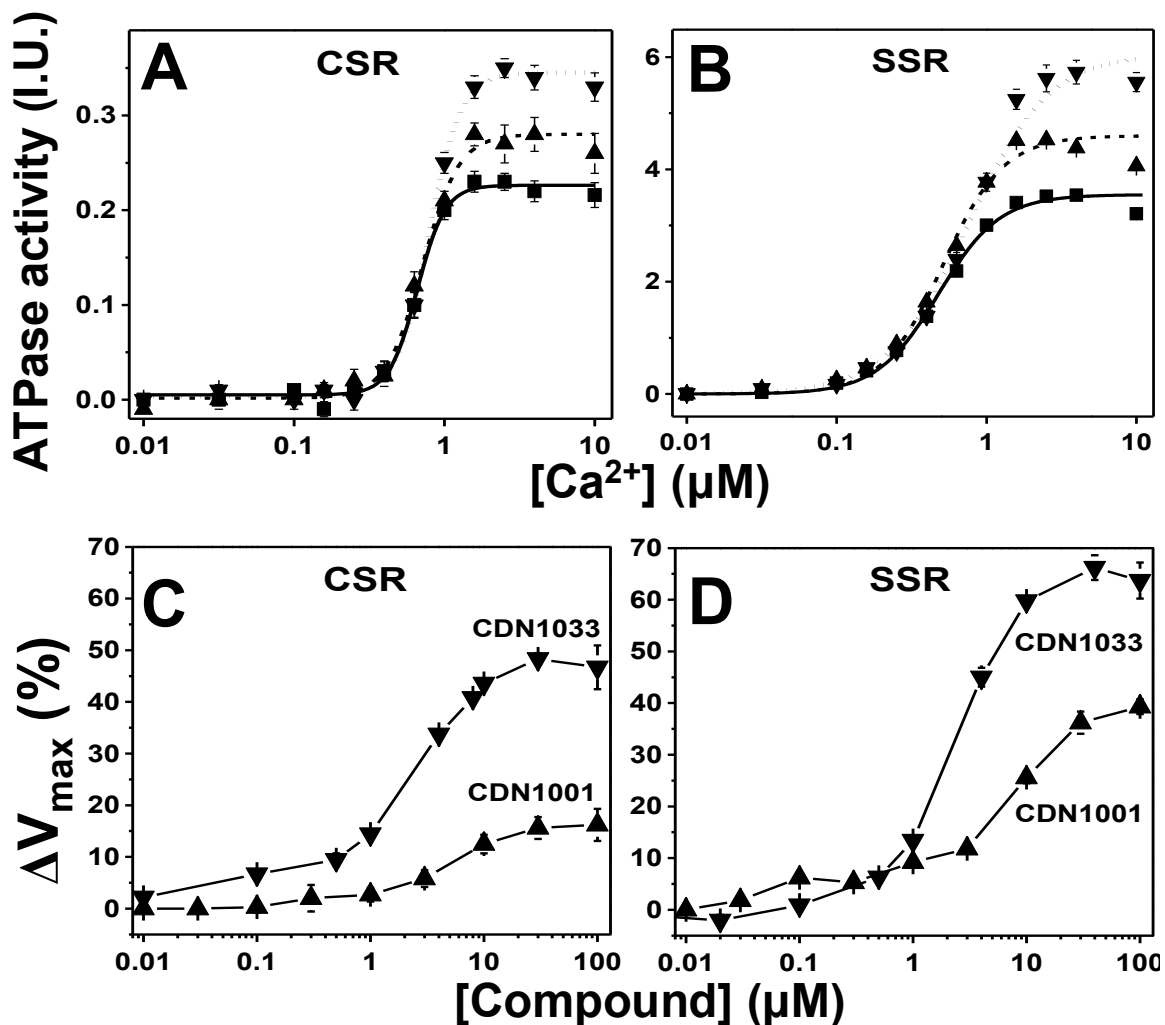
Figure 25. ATPase assays. ATPase activity was measured after 20 min incubation in the presence of either CDN1001 (up-triangles) or CDN1033 (down triangles) or DMSO control (squares). Top (**A,B**): Ca-dependence in the presence and absence of 10 μM compound. Bottom (**C,D**): Dose-response curves for V_{max} (limiting activity at high Ca). Left (**A,C**): Cardiac SR, containing SERCA2a and PLB. Right (**B,D**): Skeletal SR, containing SERCA1a and no PLB. Mean ± S.E. (n≥ 3).

(SERCA2a and PLB) (**Figure 25**). We were searching for either of the effects expected

to be useful in the treatment of HF, which are illustrated in (**Figure 23**). Based on the

design of the assay, *i.e.*, for detection of disruptions of the SERCA-PLB interaction, we

expected that the main effect of the hits would be a left shift in the Ca-curves, as depicted in **Figure 23** (blue vs. black curve), corresponding to an increase in the apparent Ca-affinity of SERCA due to dissociation from PLB. Surprisingly, when we measured the effects of 10 μM hit compound on the Ca-dependence of SERCA's ATPase activity, we found that none of the tested compounds caused a significant shift in the apparent Ca affinity. However, 6 of the 12 compounds tested at 10 μM increased V_{max} by at least 10% in both cardiac and skeletal SR (red vs. black curve in **Figure 23**). Results from the two most effective of these compounds are shown in **Figure 25**. CDN 1033 increased V_{max} by about 50% in cardiac SR and 65% in skeletal SR. None of the compounds had effects that were specific for cardiac SR. In fact, in several cases, the V_{max} increase was greater in skeletal SR (where SERCA1a is expressed in the absence of PLB) than in cardiac SR (where SERCA2a is coexpressed with PLB) (**Figure 25**). Therefore, these results show that the hit compounds identified by our screen act directly on SERCA, and that their action is not dependent on the SERCA-PLB interaction or on a specific SERCA isoform. The significant differences in compound potencies observed for skeletal and cardiac SR could be due to intrinsic differences in the SERCA isoforms or to the presence of PLB in cardiac SR. Further assays on purified SERCA isoforms will be needed to distinguish these possibilities. All six hit compounds were subjected to a battery of other tests to examine their selectivity for SERCA, assessing their effects on numerous other ion pumps and channels (e.g., Na/K-ATPase, L-type Ca channel, ryanodine receptor), and no significant functional effects were observed. Thus these compounds are the first reported small-molecule activators that are specific for SERCA. Results from the dose-response of

73

V_{max} indicate EC_{50} in the micromolar range for both CDN1001 and CDN1033 for both cardiac and skeletal SR (**Figure 25C,D**). The physical properties of CDN1001 and CDN1033 – molecular weights less than 400, log P values less than 4 and polar surface areas of less than 100 – suggest they would be viable lead candidates for optimization toward clinical applications. Medicinal chemistry efforts are in progress to increase the affinities of these compounds for SERCA by generating compound libraries inspired by the structures of the hits.

4.3.3. Cardiomyocyte assays.

Myocyte contractility assays were performed in order to determine whether the hit
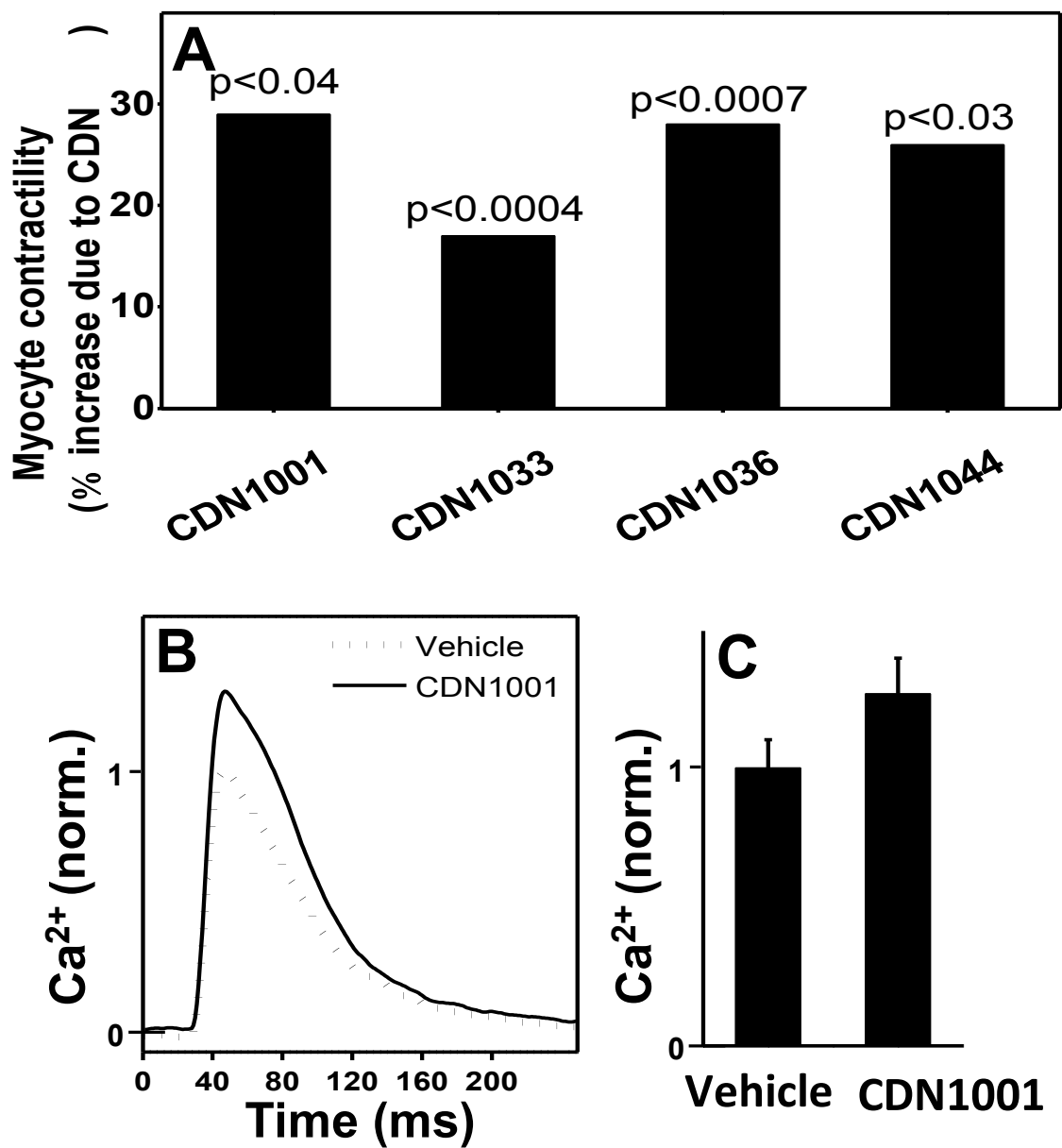
Figure 26. Effects of hit compounds on cardiomyocyte contractility and Ca^{2+} transients. (A) Effects of compounds (10 μM) on the amplitude of sarcomere length oscillations (n=20, p-values indicated). Values are normalized to the control for each experiment, which was typically a sarcomere length change of 5 to 10 %. Standard deviations were (left to right) 11%, 3%, 5% and 9%. **(B)** Ca^{2+} transients measured by fura-2, normalized to vehicle control, as affected by 10 μM CDN1001. **(C)** Mean value of transients recorded as in B (n = 20, p ≤ 0.01).

compounds that were confirmed by the ATPase assays have effects on cells isolated from the tissue meant to be targeted by the drug that will be eventually developed based on these compounds. We used myocytes isolated from rat left ventricular myocardium. The sarcomere length of field-stimulated (1 Hz) myocytes was monitored over time, measuring both length and Ca^{2+} transients (**Figure 26**). Four compounds significantly increased contractility, as measured by sarcomere shortening (**Figure 26A**). The effect of CDN1001 in enhancing the amplitude of Ca^{2+} transients (**Figure 26B,C**) is consistent with its effect on myocyte contractility (**Figure 26A**), as well as on the Ca-ATPase activity of isolated cardiac SR (**Figure 25**).

4.3.4. Fluorescence lifetime plate reader.

At the start of the present HTS campaign, steady-state fluorescence intensity detection was the available technology in fluorescence microplate readers. A major factor limiting effectiveness of HTS is inadequate precision provided by conventional, steady-state fluorescence plate readers, resulting in too many false positives (wasting subsequent resources) and false negatives (missing potential hits) [157]. The precision of steady-state fluorescence intensity detection is highly dependent on the amount (concentration) of fluorophore in the well, which depends primarily on the precision of sample dispensing. These are the major factors that affected the quality of our HTS assay, as discussed above in Results (**Figure 24**).
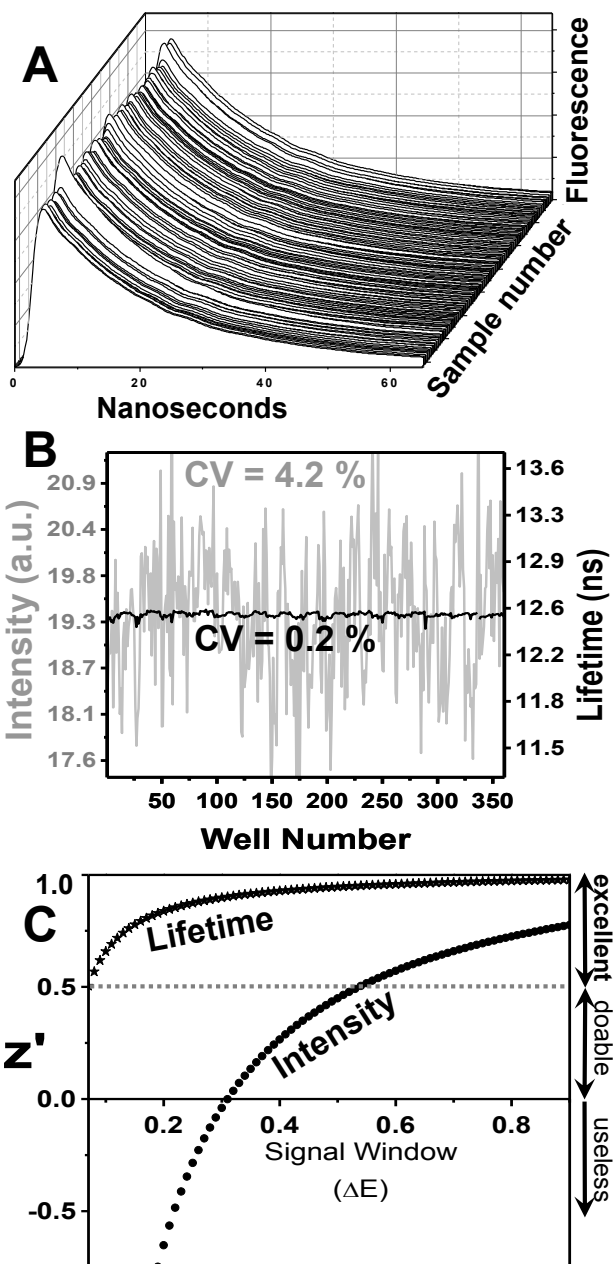
Figure 27. Screening with fluorescence lifetime plate-reader. (A) FLT decays of IAEDANS-SERCA samples in a 384-well plate. **(B)** Plots of intensity (gray, integrated area) and lifetime (black), with coefficient of variance (CV, indicating the well-to-well variability) indicated. **(C)** Z′ (**Equation 15**) vs signal window, based on the CV values in B.

Fluorescence lifetime (FLT) detection, resolving the nanosecond emission kinetics following a laser pulse, provides a signal (time-resolved waveform shape) that is not affected by fluorophore concentration, so FLT offers great potential for increasing precision in HTS. Nevertheless, most fluorescence experiments, including FRET, are currently detected by intensity, primarily because the conventional FLT method, single-photon counting (SPC), is slow, requiring many seconds for a single measurement that yields adequate S/N (≥100) for high resolution and precision. We have recently solved this problem by using a fluorescence lifetime plate reader (Fluorescence Innovations, Minneapolis, MN) that uses direct waveform recording (DWR) [152] to acquire accurate and precise subnanosecond-resolved fluorescence waveforms several times per millisecond. This unprecedented combination of speed and precision makes it possible to scan a 384-well plate in less than 2 min, acquiring high-quality fluorescence lifetime decays (S/N ≥ 100) of control samples containing 90 nM AEDANS-SERCA, as used in the original screen (**Figure 27A**). When intensity is measured, we observe the well-to-well variability typical of fluorescence intensity plate-readers (CV = 4.2%, **Figure 27B**, gray). This is similar to the value we observed with the intensity plate-reader (Molecular Devices Gemini) used in the original screen (**Figure 24A**). However, when the mean fluorescence lifetime (calculated from the first moment of each decay) is measured, there is a dramatic increase in precision by a factor of 20 (CV 0.2%). To overcome this difference in precision, it would be necessary to run 400 intensity measurements for each lifetime measurement. This improvement in precision is directly reflected in the predicted HTS assay quality, with $z' > 0.5$ for changes in FRET efficiency as small as 0.07 (**Figure**

27C). This sharp improvement in assay quality provides the sensitivity necessary to detect the subtle conformational changes we expect to be caused by most compounds that act as allosteric activators of SERCA and other drug targets [66, 158, 159].

4.4. Discussion

Deficient removal of Ca^{2+} from the cytoplasm of myocytes into the sarcoplasmic reticulum reservoir has been associated in human heart failure (HF) with reduced expression and activity of SERCA2a [160, 161]. To correct this situation, the rate of Ca^{2+} removal from the cytoplasm of failing cardiomyocytes must be enhanced. To achieve this goal, Hajjar and coworkers have validated a therapeutic approach (in HF animal models) consisting of SERCA over-expression in heart, where it restores normal Ca^{2+} cycling and cellular metabolism, leading to significant improvement in cardiac function [112, 148, 162, 163]. Indeed, the clear effectiveness and safety of AAV-SERCA gene therapy have recently been demonstrated in a phase 2 clinical trial for patients with advanced heart failure [148]. Although very promising, the gene therapy approach has limitations that leave a large percentage of the heart patient population outside its applicability [112]. Therefore, alternative means – pharmacological – of activating Ca^{2+} transport by SERCA should be identified.

To find compounds that activate SERCA, we conducted an HTS campaign using our proprietary high-throughput FRET assay, in which we detect energy transfer between a donor on affinity-purified SERCA and an acceptor on synthetic PLB. FRET is a popular spectroscopic method used for HTS of peptidase inhibitors and activators. However, in those assays the peptide substrate is derivatized to carry both the donor and the acceptor. The use of FRET to identify modulators of protein-protein interactions, as we have done in this study, is more rarely used.

The donor-acceptor pair (IAEDANS-DABCYL) has a relatively short R_0 (32 Å) [64], providing sensitivity to inter-probe distance-changes in a range that is expected to occur within the SERCA-PLB complex (16—48 Å). To our knowledge, this is the first high-throughput screen for modulators of protein-protein interactions of a reconstituted complex of membrane proteins. This approach was dictated by our initial goal -- to develop an HTS assay that monitors the SERCA-PLB interaction interface, in order to find compounds that disrupt the regulatory interaction between the two proteins, or completely dissociate the complex. We found a very low hit rate (0.2% of the compounds screened), and 72% of these turned out to be false positives. On the remaining 12 hits, we conducted secondary assays on the Ca-ATPase activity of SR membranes purified from cardiac and skeletal muscle. Half of these compounds were found to activate SERCA by at least 10%, but the effects were not specific for cardiac SERCA. These findings suggest that the compounds act directly on SERCA, probably via an allosteric mechanism to activate SERCA's Ca-ATPase activity. These mechanistic details will be determined in future studies.

The compounds that activated SERCA in isolated SR samples were then tested on isolated cardiomyocytes to determine whether they can enhance cardiac contractility. About 50% of the hits significantly increased the amplitude of sarcomere shortening, which is an index of cardiomyocyte contractility. CDN1001 was studied in more detail, and we found that enhancement of sarcomere shortening by this compound was accompanied by a similar increase in the amplitude of the $[Ca^{2+}]$ transient, and both intracellular effects are similar in size with the effect of CDN1001 on SERCA V_{max}. In

light of these encouraging results with cardiac myocytes, CDN1001 has been further tested for effects on full heart and on animals. The results are quite encouraging but will be reported in a different manuscript. Medicinal chemistry design and synthesis of CDN1033 analogs have led to a series of drug-like allosteric SERCA agonists that show potential to reduce ER stress. These studies will be the focus of a different report.

Pharmaceutical companies have searched intensively for low molecular weight, systemically administered compounds that could relieve SERCA inhibition, improve Ca^{2+} homeostasis, and thus improve the prognosis in HF patients [113, 114]. They have failed for two principal reasons: (a) inadequate understanding of the structure-function correlations in the SERCA-PLB complex, and (b) lack of an effective assay for detecting the SERCA structural changes. Our efforts thus far have led to the discovery of first-in-class small-molecule allosteric modulators of SERCA. This finding is significant because the only previously reported small molecule SERCA activator, istaroxime [164], is a molecule with several weaknesses precluding its clinical development, including polypharmacology, or lack of specificity (specifically, Na^{+},K^{+}-ATPase inhibition), narrow therapeutic index, and reported toxicity [165].

Although the principle of our FRET HTS assay has been validated by secondary functional assays, showing that some FRET-detected compounds are potent SERCA activators, we were disappointed by the high rate of false positives: 72% of the apparent hits from the initial FRET screen did not have a significant effect on FRET following repeated trials. This high rate of false positives is clearly due to the modest precision of the intensity-based screen, and this lack of precision probably also implies a high rate of

false negatives – compounds having effects on FRET that are not detected, i.e., hits that are missed. This high rate of false negatives greatly increases the size of the library that must be screened in order to obtain a given number of valid hits. Therefore, we have improved the signal-to-noise ratio of the assay by using the fluorescence lifetime plate-reader. The data with this instrument in **Figure 27** show clearly that fluorescence lifetime detection produces 20 times better precision on identical samples, changing the z' value to >0.5 (i.e., excellent) even for very small changes in FRET ($\Delta E > 0.07$).

We have carried out the first HTS campaign using reconstituted membrane proteins and a novel FRET assay that measured directly the interaction of SERCA and PLB. We identified several promising leads from a 20,000-compound library. None of these compounds was specific for SERCA in cardiac SR, or for the SERCA-PLB interaction (as originally hoped), but several compounds in the primary FRET screen were found to activate SERCA selectively (i.e., without activating other ATPases or Ca^{2+} channels) in the micromolar concentration range. These are the first reports of such SERCA-specific activators. This success is particularly remarkable because of SERCA's reputation as a "difficult drug target." It is a difficult target in part because it is an integral membrane protein in complex with an integral membrane protein inhibitor (PLB), but mainly because the goal is enzyme activation. Drugs that activate enzymes are rare. The task of activating an enzyme is much more exacting than inhibiting it, most likely requiring subtle allosteric structural modulation, which places great demands on the quality of the HTS assay. For future HTS campaigns to identify allosteric activators, the fluorescence lifetime plate-reader technology may be crucial, due to its dramatic

83

improvement in precision and assay quality (**Figure 27**). The compounds discovered in this and future SERCA-screening campaigns represent a promising new approach for treating heart failure, since ongoing gene therapy trials have already validated SERCA activation as an effective therapeutic strategy [148]. Evidence increasingly supports the proposal that activation of SERCA can be effective in treating other conditions, such as cancer [166] and diabetes [100] (SERCA2b) or muscular dystrophy [86, 167] (SERCA1a). Thus compounds discovered in this screen are likely to have diverse therapeutic applications.

Acknowledgments

Chapter 5 – Discovery of enzyme modulators via high-throughput time-resolved FRET in living cells

Discovery of enzyme modulators via high-throughput time-resolved FRET in living cells

Simon J. Gruber[1], Razvan L. Cornea[1], Ji Li[1], Kurt C. Peterson[2], Tory M. Schaaf[1],

Gregory D. Gillispie[1,2], Russell Dahl[3], Krisztina M. Zsebo[4], Seth L. Robia[5], and David

D. Thomas[1]

[1]Department of Biochemistry, Molecular Biology and Biophysics, University of

Minnesota, Minneapolis, MN 55455

[2]Fluorescence Innovations Inc., Minneapolis, MN 55455

[3]Department of Pharmaceutical Sciences, Rosalind Franklin University, Chicago, IL

60064, USA.

[4]Celladon Corporation, San Diego, CA 92130, USA.

[5]Department of Cell and Molecular Physiology, Loyola University Chicago, Maywood,

IL 60153

We have used a "2-color" SERCA (sarco/endo-plasmic reticulum calcium

ATPase) biosensor and a unique high-throughput fluorescence lifetime plate-reader

(FLT-PR) to develop a high-precision live-cell assay designed to screen for small

molecules that perturb SERCA structure. A SERCA construct, in which red fluorescent

protein (RFP) was fused to the N terminus and green fluorescent protein (GFP) to an

interior loop, was stably expressed in an HEK cell line that grows in monolayer or

suspension. Fluorescence resonance energy transfer (FRET) from GFP to RFP was measured in the FLT-PR, which increases precision 30-fold over intensity-based plate-readers without sacrificing throughput. FRET was highly sensitive to known SERCA modulators. We screened a small chemical library and identified ten compounds that significantly affected 2-color SERCA FLT. Three of these compounds reproducibly lowered FRET and inhibited SERCA in a dose-dependent manner. This assay is ready for large-scale HTS campaigns, and is adaptable to many other targets.

5.1 Introduction

Muscle contraction and relaxation are primarily controlled by calcium transport proteins [1]. The ryanodine receptor initiates contractions by releasing micromolar levels of Ca^{2+} from the sarcoplasmic reticulum (SR), and relaxation is achieved when the sarcoplasmic reticulum Ca-ATPase (SERCA) pumps Ca^{2+} back into the SR against a 3-log $[Ca^{2+}]$ gradient. In cardiac muscle, the SERCA2a isoform is regulated by the inhibitory transmembrane protein phospholamban, which inhibits Ca^{2+} transport only at low diastolic $[Ca^{2+}]$. SERCA is maximally active at high, systolic $[Ca^{2+}]$ or when PLB is phosphorylated at S16 or T17 by PKA or CaMKII, respectively. PKA phosphorylation of PLB is a key part of the β-adrenergic response pathway activated when cardiac reserves must be accessed [168].

Decreased Ca^{2+}-transport activity associated with many forms of heart failure (HF) is often due to decreased SERCA2a expression or activity [168], so several recent efforts to combat heart failure aim to increase SERCA activity either by increasing SERCA expression [109] or by reducing PLB inhibition [168, 169]. Overexpression of
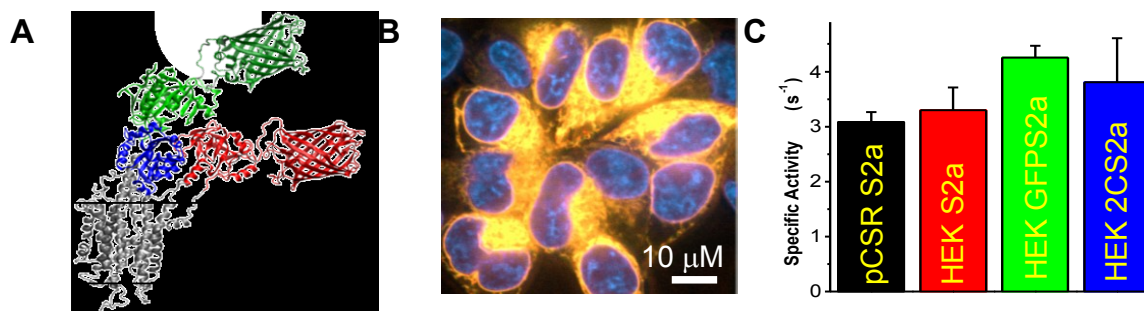
Figure 28. 2-Color SERCA. (**A**) Computational model of GFP and RFP modeled on the crystal structure of SERCA1a (PDB 1IWO). (**B**) Confocal imaging of RFP and GFP (merged) fluorescence with DAPI nuclear stain shows 2-color SERCA localized in intracellular ER membranes. (**C**) ATPase activity data for pig cardiac SR (black), and stable cell lines expressing unlabeled SERCA2a (red), GFP-SERCA2a (green), and 2-color-SERCA2a (blue).

SERCA2a via rAAV gene therapy has been effective in both animal models of HF and human clinical trials [109]. However, the complexities of gene therapy call for a parallel effort to develop small-molecule activators of SERCA [170].

Screens for small-molecule SERCA activators have previously focused on directly measuring ATPase activity, which is a low-throughput, low-precision approach [171, 172]. We recently reported a FRET-based assay for high-throughput screening of the SERCA-PLB complex in reconstituted membranes [170]. This HTS assay was designed to detect changes in FRET as an indicator of structural changes caused by compounds that bind to, and structurally alter, the SERCA-PLB complex. A pilot screen was carried out using this method with steady-state (intensity) detection of fluorescence, hits were resolved, some of which turned out to be SERCA activators [173]. This outcome validated our approach, but also revealed that fluorescence lifetime (FLT) detection provides a much higher precision than steady-state detection, thus having the potential to substantially lower the rate of false positives (hits that cannot be confirmed when re-measured).

Here, we used a recently developed GFP/RFP "2-color" SERCA2a (2CS) construct as FRET probe (**Figure 13A**) [41], and an FLT plate reader (FLT-PR) to screen, in live cells, for small molecules that affect SERCA structure. 2CS is active and properly localized to intracellular membranes when stably expressed in HEK cells (**Figure 13B, C**). GFP-RFP FRET was shown to be sensitive to both [Ca^{2+}] and thapsigargin (TG), a potent SERCA inhibitor, making it an ideal tool to screen for small molecule effectors of SERCA [41]. We evaluated 2CS FRET in intact live cells in the presence of a variety of previously identified SERCA activators and inhibitors [173], and found that live-cell 2CS FRET is sensitive to SERCA effectors in a dose-responsive manner. We then performed a pilot screen of the 1280-compound <u>L</u>ibrary <u>o</u>f <u>P</u>harmacologically <u>A</u>ctive <u>C</u>ompounds (denoted LOPAC; Sigma-Aldrich) using the live-cell 2CS FRET assay. This screen yielded a few hits, i.e., compounds that significantly changed FRET. Secondary assays, measuring the Ca-ATPase activity, revealed that several hits from the FRET assay also altered SERCA function. This in-cell FRET assay represents a novel, highly sensitive tool to detect both activators and inhibitors of SERCA. The high-precision afforded by direct wave recording technology implemented in the Fluorescence Innovations fluorescence lifetime plate reader (FLT-PR) prototype enables in-cell high-throughput screening.(HTS) using 2CS.

5.2. Materials and Methods

5.2.1. Molecular biology, cell culture, and localization

TagRFP was fused to the N-terminus of canine SERCA2a. This fusion position is in the A-domain of the pump. EGFP was fused as an intrasequence tag before residue 509 in the N-domain. The structural model presented in **Figure 13A** corresponds to the

isoform SERCA1a, which is 84% homologous to SERCA2a. Hou et al. evaluated several intrasequence fusion positions chosen using E1/E2 x-ray crystal structures of SERCA1a to identify unstructured loops and predict large relative distance changes from E1 to E2 without affecting SERCA function [41]. The 509 site was chosen because it produced FRET sensitive to SERCA structural state and actively transported Ca^{2+}.

Cells were transiently transfected using 293fectin (Invitrogen), and stable cell lines were generated by G418 (Sigma) selection. Surviving clones expressing GFP-SERCA2a or 2CS were further selected by fluorescence microscopy and flow cytometry. Cell lines with the smallest population of non-expressing cells were selected and have been grown continuously while stably expressing 2CS or GFP-SERCA2a for over a year.

Fluorescence microscopy of HEK-GnTI$^-$ cells (ATCC, Manassas, VA) expressing 2CS was performed in glass-bottom chambered coverslips (Matek Corporation, Ashland, MA) several weeks after establishing a stable cell line. Confocal microscopy was performed using a Zeiss cell observer SD spinning disk confocal microscope equipped with a 0.55 N.A. 63 X oil immersion objective. Cells were stained 20 min before imaging with Hoechst 33342 NucBlue counterstain (Invitrogen) Excitation was accomplished with laser illumination at 405 nm for NucBlue, 488 nm for GFP, and 561 nm for RFP.

5.2.2. Homogenization of Cells for Activity Assays.

Cells were homogenized as previously described [136]. Briefly, cells were pelleted by spinning at 500g and washed 3X with PBS. Pellets were resuspended in 1-2 mL homogenization buffer (0.5 mM $MgCl_2$, 10 mM Tris-HCl, pH 7.5, 4°C) and homogenized with 30 strokes in a Potter-Elvehjem homogenizer. Sucrose buffer (500mM sucrose, 100mM MOPS, pH 7.0, 4°C) was added at a 1:1 ratio and homogenate was

assayed for protein concentration (BCA kit from Thermo Scientific, Rockford, IL) before flash freezing and storing at -80°C.

5.2.3. Cardiac SR and skeletal SR preparation.

Cardiac sarcoplasmic reticulum (SR) vesicles were prepared from the ventricular tissue of swine hearts by adapting a previous method [174]. The swine heart was placed in a solution (10 mM NaHCO$_3$, 10mM Tris-HCl, 0.1 mg/mL Aprotinin, 0.1 mg/mL Leupeptin, 80 mM Benzamidine, 100 mM PMSF, 0.1 mg/mL Pepstatin A, pH 7.2, 4°C) immediately after being sacrificed, and kept on ice. All following procedures were performed at 4°C. The atria, fat and connective tissue were removed from the heart. The ventricular muscles were minced into 1 cm^3 pieces and homogenized in 500 mL of SR buffer (100 mM KCl, 20 mM MOPS, pH 7.0, 4°C) using a blender (Waring, Torrington, CT). The homogenates were centrifuged at 5000 rpm (Sorvall, GSA rotor) for 20 minutes. The pellets were collected and treated with homogenization and centrifugation like before. Two supernatants were combined, filtered through 6 layers of cheesecloth, and spun at 8500 rpm (Sorvall, GSA rotor) for 20 min. The supernatant was filtered through 6 layers of cheesecloth. KCl was added to the filtrate to a final 600 mM, and stirred for 15 minutes. The filtrated was spun at 12000 rpm for 1 hour. The pellet was homogenized in 100 mL sucrose buffer (0.1 M sucrose, 1 mM NaN3, 20 mM MOPS, pH 7.0 4°C), and spun at 30000 rpm (Beckman Ti45 rotor) for 45 minutes. The pellet was homogenized in 15 mL sucrose buffer with a Potter-Elvehjem homogenizer. Total SERCA by weight in these vesicles was 30 ± 5% as determined by densitometry analysis of SDS-PAGE. Rabbit light skeletal SR vesicles were prepared using a method previously reported [175]. Rabbit muscles were harvested from the hind leg of New

Zealand White rabbits and purified using a sucrose gradient. The result light skeletal SR contains 80% SERCA.

5.2.4. Enzymatic activity of 2CS and compound effects on pig cardiac SR

An enzyme-coupled, NADH-linked ATPase assay was used to measure SERCA ATPase activity [176] in 96-well microplates. Each well contained 50 mM MOPS (pH 7.0), 100 mM KCl, 5 mM MgCl$_2$, 1 mM EGTA, 0.2 mM NADH, 1 mM phosphoenol pyruvate, 10 IU/mL of pyruvate kinase, 10 IU/mL of lactate dehydrogenase, 3.5 µg/mL of the calcium ionophore A23187, and CaCl$_2$ added to set free [Ca^{2+}] to the desired values [64]. 2.5 µg of cardiac SR or 25 µg of HEK cell homogenate were used in each well to correct for the difference in SERCA content. The assay was started upon the addition of ATP at a final concentration of 5 mM and read in a SpectraMax Plus microplate spectrophotometer (Molecular Devices, Sunnyvale, CA), bring the total volume to 200 µL. Results were normalized to SERCA content determined from immunoblotting.

Effects of known activators and LOPAC hits on SERCA ATPase activity was evaluated in pig cardiac SR. Compounds were dissolved in DMSO, and adjusted to 40 times the concentrations used in the final assay wells. 4 µL prediluted compounds were added to each well to keep the final [DMSO] at 2% (v/v).

5.2.5. Western blot to quantify SERCA content

Cell homogenates and cardiac SR were electrophoresed on 4-20% Tris-HCl gels (Criterion, Biorad) at 5 µg total protein, transferred to Immobilon-FL membranes (Millipore), and blocked by dipping in methanol and air drying. Membrane was incubated with SERCA2a primary antibody diluted 1:1000 (2A7-A1, Abcam) for 3 h, washed, and

visualized by 1 h incubation with goat-anti-mouse 800 nm IR secondary antibody (LI-COR Biosciences). Blots were quantified on the Odyssey scanner (LI-COR Biosciences).

5.2.6. Compound plating and fluorescence lifetime measurements in plate reader

LOPAC compounds were generously provided by Dr. Courtney Aldrich, associate director of the University of Minnesota Center for Drug Design. The 96-well plate format LOPAC library were reformatted into four 384-well polystyrene mother plates (Corning, Corning, NY) using a Biomek FX liquid handler (Beckman Coulter, Brea, CA), and diluted to 500 μM using DMSO. Column 1, 22, 23 and 24 were loaded with DMSO for in-plate no-compound controls. The LOPAC compounds were distributed in column 2 through 21. Each plate contains 64 wells of DMSO controls, and 320 wells of compounds from the LOPAC library. Black well, high-quality-glass bottom Greiner 384-well microplates (PN 781892) were selected as the assay plates for their optical clarity, low autofluorescence, and low inter-well cross-talks. 1 μL compounds were transferred from the mother plates into assay plates using a Mosquito HV liquid handler (TTP Labtech Ltd, UK). The plates were sealed and stored at -20 °C until use. On the day of screening, the plates were equilibrated to room temperature (25 °C). Stable GFP-SERCA2a (donor only control) or 2CS cells were lifted from a 225 cm^2 flask by incubating with TrypLE (Invitrogen) for 5 min. Cells were collected and pelleted for 5 min at 500g and resuspended in 10mL PBS, then analyzed on a Countess cell counter (Invitrogen) and diluted to 1x10^6 cells/mL. 49 μL Cells were plated on top of the compounds by a FlexDrop IV reagent dispenser (PerkinElmer, Waltham, MA). Assay plates were spun for 1 min at *200 g* and allowed to incubate at RT for 20 min before reading on a NovaFluor fluorescence lifetime plate reader (Fluorescence Innovations Inc., Minneapolis, MN).

GFP fluorescence was excited with a 473 nm microchip laser from Concepts Research Corporation (Belgium, WI) and emission was filtered with 490 nm long pass and 520/35 nm band pass filters from Semrock (Rochester, NY).

5.2.7. HTS data analysis

Time-resolved fluorescence waveforms for each well were fitted to single-exponential decays using NovaFluor analysis software. Each plate contained 64 control wells with only DMSO, and a hit was defined as a compound that changed the 2CS donor lifetime by more than three times the standard deviation (SD) relative to the controls. Fluorescent compounds that caused the intensity of both untransfected HEK cells and 2CS cells to be outside the range of the 64 controls on a plate were excluded from the hits as likely false positives.

5.3. Results

5.3.1. Ca-ATPase Activity of 2CS.

We have previously reported that a 2CS construct with an N-terminal cerulean and internal yellow fluorescent protein actively transports Ca^{2+} and has Ca^{2+}-dependent ATPase activity [41]. Here, we show that SERCA ATPase activity is not significantly affected by the RFP or GFP probes (**Figure 13C**). Both unlabeled SERCA2a and 2CS stably expressed in HEK cells have Ca^{2+}-dependent ATPase specific activity comparable to pig cardiac SR, which expresses SERCA2a at a high level (20-30% of total protein).

5.3.2. GFP-RFP FRET in FLT Plate Reader
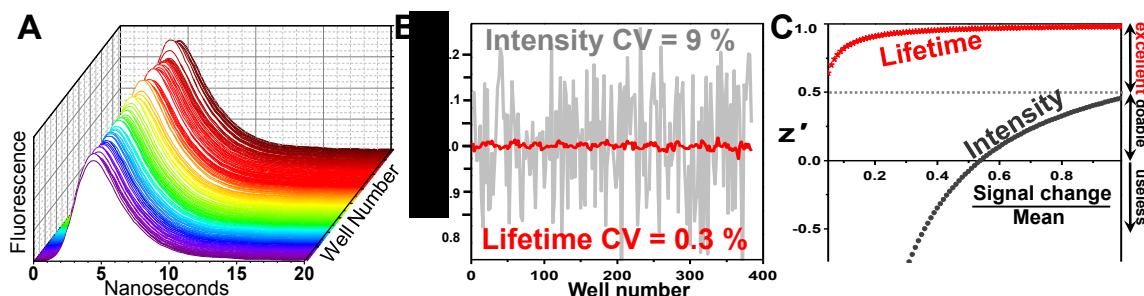
Figure 29. FLT-PR performance. (**A**) Waveforms from a high-throughput FRET assay performed in FLT-PR, on live cells expressing 2-color SERCA (identical control samples, no compounds added). (**B**) Lifetime measurement yields a 30x decrease in CV compared with intensity detection. (**C**) Dramatically improved assay is ideally suited to detect small structural changes.

The advent of the FLT-PR allowed us to rapidly obtain precise fluorescence waveforms from 96- or 384-well plates in under two minutes per plate (**Figure 29A**). We previously showed that this plate reader could measure lifetimes in the same amount of time that a traditional plate reader measures intensity, but with a much better coefficient of variation (CV) [173]. This was true to an even greater extent for cells in a 384-well plate stably expressing GFP-SERCA2a or 2CS (**Figure 29B**). This precision means that a very small change in lifetime will be detected reliably and is ideal for a high-throughput screen (**Figure 29C**). We were initially concerned about optical interference from concentrated cell solutions (up to ~2.5 x 10^6 cells/mL), but found that both GFP-SERCA and 2CS stable cell lines were ≥30X more fluorescent in the plate reader than untransfected cells at the same concentration. In contrast, our traditional intensity mode fluorescence plate reader barely distinguishes GFP fluorescence from the background with S/N <1. Cell density was optimized to minimize CV, and we found that a wide range of densities gave the same lifetime with high precision for both donor and donor-acceptor cells. $1x10^6$ cells/mL gave CV values of 0.2-0.4% consistently for the GFP lifetime in both cell lines and this concentration was used for further experiments,

however, we were able to obtain CVs as low as 0.34% with $<5x10^4$ cells/mL (data not shown). This level of precision allows us to reliably detect changes in lifetime on the order of tens of picoseconds (**Figure 29C**). The donor-only lifetime on separate days was consistently 2.5 ± 0.1 ns and the 2CS lifetime was 2.2 ± 0.1 ns, giving a basal FRET efficiency (E) of 0.12 ± 0.05.

We previously developed a screen based on FRET between dabcyl-labeled PLB and AEDANS-SERCA and found several SERCA activators that show promise as preclinical treatments for heart failure or diabetes. We tested the most potent SERCA activators and found that they both reduce FRET between GFP and RFP in 2CS. CDN 1134 and CDN 1163 represent two distinct classes of SERCA activators. CDN 1134 increases the apparent Ca^{2+} affinity of SERCA (K_{Ca}) in the presence or absence of PLB, while CDN 1163 increases the maximal turnover rate of the enzyme (V_{max}). Both compounds reduced FRET in a dose-dependent manner. CDN 1134 exhibited the same concentration dependence for both activity and FRET assays (**Figure 30A**), and CDN 1163 also showed FRET changes at concentrations similar to those needed to activate V_{max} (**Figure 30B**). We also found a strong dose-dependent response from the SERCA inhibitor cyclopiazonic acid (CPA). CPA clearly displayed similar concentration dependence for both activity and FRET assays (**Figure 30C**). The FRET titration was fitted to a binding curve that gave an apparent K_d of 42 nM, which is on the low end of a wide range of reported K_d values [177].
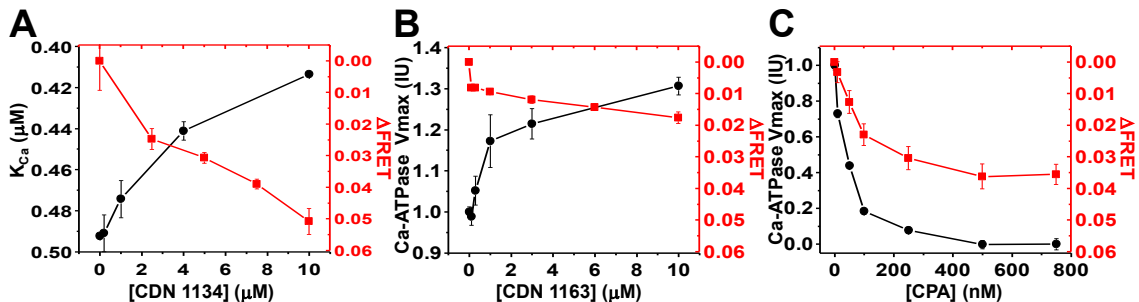
Figure 30. Effects of known activators and inhibitors on 2CS FRET. Small molecule SERCA activators developed from our previous SERCA-PLB fluorescence intensity screen both reduce FRET (**A** and **B**), and the inhibitor CPA also reduces FRET in a dose-dependent manner (**C**).

5.3.3. LOPAC Library Screen

The 1280 compound LOPAC library arranged in 384 well plates provided to us as a gift by Dr. Courtney Aldrich (at the U of MN Center for Drug Design). Each plate was scanned in the FLT plate reader and compounds that caused the 2CS GFP lifetime to be outside the 3SD window from the mean were identified as hits. Assays on hit compounds were repeated to determine whether they were true hits, and we found that seven of the hits were false positives. A 3SD cutoff predicts ~four random false positives for a screen of this size. We also eliminated compounds that caused fluorescence
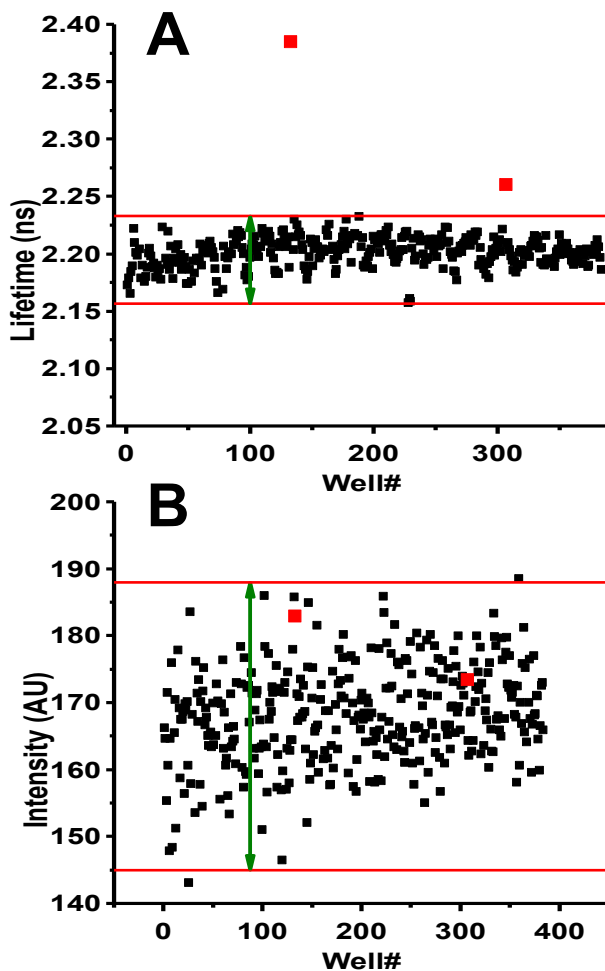
Figure 31. Lifetime and intensity plate profile. Results from one of the four 384-well plates containing the 1280 compound LOPAC library. Lifetime fitting of waveforms (**A**) identifies two hits (red symbols) that are SERCA effectors (TG and XCT 790), both of which are missed by intensity-based screening (**B**). Red bars delimit the 3SD hit selection window.

96
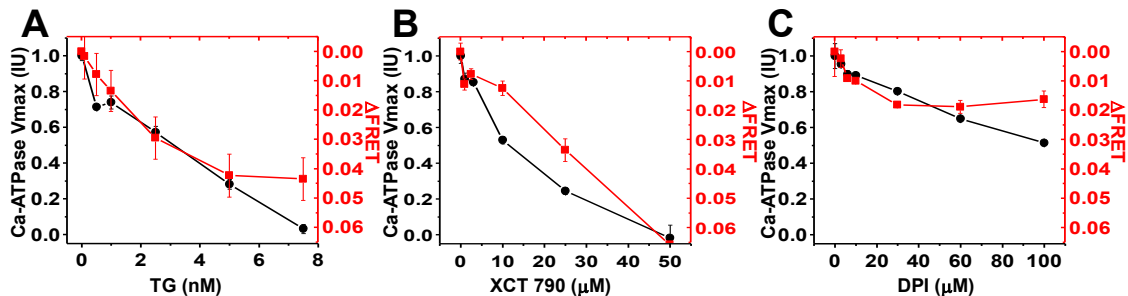
Figure 32. FRET and functional effects of LOPAC compounds identified in the screen. All three compounds reduce FRET and inhibit ATPase activity in a dose-response manner with similar dose dependence. TG (**A**) and XCT 790 (**B**) completely inhibit ATPase activity at the highest concentrations tested, while DPI inhibits <50% of ATPase activity at 100 mM (**C**).

intensity to be outside the range of the 64 DMSO controls on each plate, and this was 7.1% of the library. **Figure 31** shows results from one of the LOPAC plates that contained two of the three reproducible hits. Both hits are clearly distinct from the other compounds and controls on the plate when the single-lifetime fits of the fluorescence decays are analyzed (**Figure 31A**). The hits are not distinguishable from the other compounds or controls when analyzed in peak intensity mode (**Figure 31B**). Intensity mode analysis has a much greater window to identify hits due to the much greater CV, and many false positives would be detected before either of the two true hits would be identified.

The three reproducible hits were thapsigargin (TG, Sigma Cat. No. T 9033), diphenyline iodonium chloride (DPI, Sigma Cat. No. D 2926), and XCT 790 (Sigma Cat. No. X 4752). TG is a well-known SERCA inhibitor that we did not know was present in the library [177], and DIC has also been shown to inhibit SERCA Ca^{2+} transport activity [178]. The third compound, XCT 790, is a well known antagonist of the estrogen-like receptor α [179], but has not been previously studied as an effector of SERCA activity.

97

TG was the most potent FRET effector in both the LOPAC screen and subsequent dose-response assays, reducing FRET by ~33% (E = 0.12 vs 0.08) at only 7.5 nM, when ATPase activity is nearly ablated (**Figure 32A**). This result is consistent with previous steady-state FRET results of 2CS that showed TG promoting a more open, low-FRET headpiece conformation [41].

XCT 790 was also a strong FRET effector, reducing FRET by ~42% (E = 0.12 vs 0.07) while inhibiting ATPase activity with a similar concentration dependence (**Figure 32B**). XCT 790 is a yellow color when dissolved in DMSO but it did not contribute any fluorescence intensity to plate reader measurements and had no effect on the lifetime of GFP-SERCA2a alone.

The third hit, DPI, was the weakest FRET effector, maximally reducing FRET from 0.12 to 0.10, ~18%. However, the FRET change was extremely reproducible and the concentration dependence of DPI was again similar to that of ATPase inhibition (**Figure 32C**). The ATPase dependence is very similar to a previous report showing 18% inhibition of Ca^{2+} uptake into microsomes with 30 μM DPI and 32% inhibition at 100 μM DPI [178].

5.4. Discussion

SERCA activation is a sought-after therapeutic goal to treat a wide variety of diseases including HF, muscular dystrophy, and diabetes. Many approaches have been taken to achieve the desired aim of increasing SERCA activity and reducing cytosolic $[Ca^{2+}]$. In this respect, gene therapy to overexpress SERCA2a in the heart is quite effective as a means to enhance Ca-transport capacity. . Phase II clinical trials showed

improvement in hemodynamic parameters as well as quality of life when patients were treated with an adeno-associated viral vector that expresses SERCA2a in the heart [109]. These results show that normalizing Ca^{2+} cycling in failing hearts mitigates disease symptoms and improves muscle function. However, only about 50% of the HF patients qualify for the gene therapy approach due to the prevalence of AAV neutralizing antibodies in the general population. Small-molecule SERCA activators are designed to restore Ca^{2+} cycling by activating existing SERCA pumps in the SR, and is expected to provide a more mainstream pharmacological therapy for HF patients without the limitations currently associated with gene therapy.

We have previously conducted a FRET-based high-throughput screen to detect small molecules that disrupt the interaction between SERCA and PLB [173]. Several compounds were identified in that screen and many proved to be SERCA activators, but all of them activated SERCA alone and none were specific to the SERCA-PLB interaction. Those compounds were most likely allosteric SERCA activators that directly perturbed the structure of SERCA and altered SERCA-PLB FRET as a result. Here we have searched exclusively for compounds that directly affect SERCA by placing both probes on different domains of the SERCA headpiece.

Crystal structures of SERCA1a show large rearrangements of the cytoplasmic headpiece during the enzymatic cycle with large (~3 nm) changes in distance between the N and A domain, making them ideal locations for FRET probes to find functional effectors. Previous studies showed that this fusion protein actively pumps Ca^{2+}, is properly localized to intracellular membranes, and FRET is sensitive to both TG

inhibition and Ca^{2+} activation [41]. Here we have confirmed the result that TG promotes a more open SERCA headpiece and that stably expressed 2CS in HEK cells is sensitive to allosteric regulators, thus suitable to use in screens for small molecules that perturb SERCA structure.

Using the fluorescence lifetime plate reader, we have developed the first high-throughput fluorescence lifetime assay in living cells. The precision of the lifetime measurement (CV = 0.3%) allowed us to detect very small changes in FRET between GFP and RFP, and we showed that this FRET signal is sensitive to both activators and inhibitors of SERCA function. Most compounds tested showed similar concentration dependence for FRET and ATPase assays, indicating a tight link between structural and functional perturbations.

Our pilot-scale screen of the LOPAC library did not uncover any new activators but we did identify two known inhibitors and a new inhibitor, XCT 790. All three hits, TG, DPI and XCT 790, showed similar FRET and ATPase concentration dependence, supporting a strong connection between the measured structural perturbations and enzyme function. DPI is also interesting because it was identified in a 2006 screen of the LOPAC library as a compound that inhibited growth of the malarial parasite *plasmodium falciparum* [180]. The SERCA-like pump in this parasite is a target for the development of new drugs to treat drug resistant strains of malaria [181]. The IC_{50} for inhibition of parasite growth was submicromolar, while both the ATPase data here and Ca^{2+} uptake assays reported previously agree that there is very little functional inhibition below $10\mu M$ [178]. While DPI may prove to be an effective treatment for drug resistant malaria, the

connection between SERCA inhibition, structural perturbation, and restriction of *plasmodium falciparum* growth remains unclear.

Structures obtained from crystals grown in the presence of TG have shown a compact (closed) headpiece conformation [33], but our data with 2CS suggest that TG opens the headpiece in living cells (Fig. 5), consistent with our previous results [41].

The assay presented here shows promise for large-scale HTS campaigns to identify new SERCA activators or inhibitors. The FLT-PR enables detection of very small changes with high precision, and here we show that the instrument is capable of measuring lifetimes precisely in live cells. Two-color constructs could be made with other SERCA isoforms or different proteins that undergo conformational changes associated with function. Compounds that activate the SERCA1a isoform expressed in skeletal muscle have shown promise in treating muscular dystrophy, and activation of SERCA2b in non-muscle cells slows the progression of diabetes in mice models. The identification of new SERCA activators, whether they are isoform-specific or not, could generate new small molecule drugs that treat several of the most common and costly diseases in the world.

Summary and Future Directions

Summary.

The work presented here represents multiple routes to find novel mechanisms to activate SERCA currently being pursued by the Thomas lab. SERCA activation is a sought-after goal for a variety of muscle and non-muscle diseases, including heart failure, muscular dystrophy, and diabetes. The etiology of these diseases is not always due to SERCA deficiency, but in all cases it has been shown that increased Ca^{2+}-cycling is a viable therapeutic strategy. Gene therapy to increase expression of SERCA in heart failure patients has been very successful, demonstrating the feasibility of our SERCA-based approaches.

The first approach taken as part of this work was to use mutants of PLB that are less inhibitory than wild-type PLB and introduce them via gene therapy to relieve inhibition of SERCA. These mutants would need to displace endogenously expressed PLB, and a FRET-based assay was established using proteins expressed in a human cell line to evaluate competitive potency. PLB_M developed by the Thomas and Veglia labs were shown to be able to compete with wild-type PLB for SERCA binding, and competitive potencies were in line with predictions based on the known properties (e.g. SERCA affinity) of the mutants.

Although gene therapy to express SERCA has been successful in early clinical trials for heart failure, there are a number of drawbacks that make alternative therapies desirable. Small molecule SERCA activators that could be administered orally, avoiding significant clinical intervention or regulatory risk, have been sought for decades. Two new fluorescence-based methods to identify small-molecule activators of SERCA are

discussed in this work. The first assay, undertaken in collaboration with Celladon Inc., identified molecules that disrupted FRET between SERCA and PLB in reconstituted membranes. Several of these compounds were shown to activate SERCA in secondary assays and a few improved the contractility of isolated myocytes. The second assay exploited the structural changes that occur when SERCA pumps Ca^{2+}. Both activators and inhibitors of SERCA function were shown to have significant effects on intramolecular FRET, indicating that the structure-function relationship of SERCA could potentially be used to screen for new activators. A pilot-scale screen of the LOPAC library identified several SERCA inhibitors but no new activators, and this result was not surprising given the small scale of the compound library.

Each of these projects represents progress in a different direction of identifying mechanisms to activate SERCA2a in cardiac tissue. Small-molecule drug screens established with the new FLT-PR are much more promising that previous drug screens that relied on the SERCA-PLB interaction, but nevertheless identified high quality lead compounds for pharmacologic optimization. The technological breakthroughs represented by the FLT-PR are of use to any fluorescence based assay and improve the potential success of both small-molecule drug screens and FRET assays to detect PLB_M disruption of the SERCA-PLB complex.

Future Directions.

All of the projects discussed here remain active in the Thomas lab. PLB_M are being optimized as double mutants that combine a mutation that increases SERCA binding affinity with a mutation that causes a LOF phenotype. These mutants should have improved competitive potency and still allow SERCA to remain active. Additionally,

these in-cell FRET competition experiments will be done with fluorescence lifetimes measurements rather than the steady-state photobleaching experiments presented here. Use of the FLT-PR will allow us to specifically measure the fraction of SERCA bound to a wild-type PLB and the fraction that is free, making it much easier to evaluate what is happening when a PLB_M is introduced.

The compounds that are presented in Chapter 4 as SERCA activating compounds are still under development by Celladon, Inc. Several of the compounds have undergone significant pharmacokinetic and safety studies in animals, and phase I clinical trials to evaluate safety in humans could begin in the near future.

The success of the 2-color-SERCA project has led to many new projects in the lab. One primary goal for future experiments is to identify the mechanism of action of the activators and inhibitors that alter FRET between SERCA cytoplasmic domains. Crystals are being grown in the presence and absence of SERCA activators and inhibitors to help address these questions. We are also extending this approach to new protein complexes with known structure-function relationships. For example, if two proteins are known to interact in a disease state, one could easily screen for compounds that disrupt FRET between the two proteins. The FLT-PR technology that enabled the experiments in Chapter 5 has incredible potential for making rapid, in-cell measurements of protein-protein interactions, and the potential applications are nearly limitless.

A potential application of the FLT-PR to a new disease involved Ataxin 1, a nuclear protein encoded by the SCA1 gene and expressed in neuronal cells. It is normally 816 residues with a polyglutamine repeat tract towards the N-terminus, and the number of

repeats dictates disease phenotype for Spinocerebellar Ataxia Type 1 [182]. A normal number of glutamine repeats is ~30, and >40 repeats causes disease. There is not much structural data for Ataxin 1, but a crystal structure exists of the AXH domain, residues 563-694. The C-terminus beyond the AXH domain is thought to be largely disordered. The protein can undergo many posttranslational modifications; one of particular importance is phosphorylation at S776 [183]. Blocking phosphorylation of S776 prevents Ataxia from developing. Ataxin1 has many interacting partners and possible functions, some of which are perturbed by phosphorylation. One of these proteins, 14-3-3, only interacts with Ataxin 1 when it is phosphorylated, and it has been suggested that blocking phosphorylation of Ataxin 1 prevents disease by limiting interactions with 14-3-3 [184]. The FLT-PR could be used to screen for compounds that disrupt the 14-3-3-Ataxin 1 interaction by labeling each with a FRET donor-acceptor and identifying compounds that significantly reduce FRET. These compounds could be tested in animal models of Ataxia for their ability to improve the disease phenotype.

Another potential drug screening campaign that could focus on a well-established structure-function relationship is to identify activators of cardiac or skeletal myosin. Myosin activation is also a therapeutic goal for heart failure [185], and small-molecule screens for myosin activators have been conducted with some success [186]. Myosin undergoes significant structural changes as it produces force at the sarcomere. Agafonov et al. recently showed that FRET between fluorescent probes placed on the relay helix of myosin is sensitive to ATP, indicating that the structural changes in myosin that take place during its kinetic cycle can be detected reliably with properly placed probes [187].

High-throughput screens could be conducted to identify allosteric effectors of myosin structure in the presence or absence of ATP, followed by secondary assays to evaluate effects on myosin ATPase activity.

New assays developed for the FLT-PR will benefit from the ability to conduct high-throughput screens using genetically engineered fluorescently-tagged proteins expressed in living cells, unprecedented technology optimized in Chapter 5 of this work. The ability to tag proteins with fluorescent proteins or smaller probes is developing rapidly, expanding the potential targets with structure-function correlations that can be exploited for drug discovery. Improved versions of GFP and RFP are already being used by the Thomas lab to increase precision and the distances we can measure accurately. We are also expressing proteins in new cell types including myocytes, making it possible to screen small-molecules in a more physiologically relevant environment than ever before. All of these advances will be actively pursued by the Thomas lab as work continues into this exciting new landscape for drug discovery.

References

1. Bers, D.M. 2002. Cardiac excitation-contraction coupling. *Nature* 415:198-205.
2. Periasamy, M. and A. Kalyanasundaram. 2007. SERCA pump isoforms: their role in calcium transport and disease. *Muscle Nerve* 35:430-42.
3. MacLennan, D.H. and E.G. Kranias. 2003. Phospholamban: a crucial regulator of cardiac contractility. *Nat Rev Mol Cell Biol* 4:566-77.
4. MacLennan, D.H. and T. Toyofuku. 1996. Regulatory interactions between calcium ATPases and phospholamban. *Soc Gen Physiol Ser* 51:89-103.
5. Simmerman, H.K. and L.R. Jones. 1998. Phospholamban: protein structure, mechanism of action, and role in cardiac function. *Physiol Rev* 78:921-47.
6. Tada, M., M. Kadoma, J. Fujii, Y. Kimura, and Y. Kijima. 1989. Molecular structure and function of phospholamban: the regulatory protein of calcium pump in cardiac sarcoplasmic reticulum. *Adv Exp Med Biol* 255:79-89.
7. Hagemann, D. and R.P. Xiao. 2002. Dual site phospholamban phosphorylation and its physiological relevance in the heart. *Trends Cardiovasc Med* 12:51-6.
8. Kuhlbrandt, W. 2004. Biology, structure and mechanism of P-type ATPases. *Nat Rev Mol Cell Biol* 5:282-95.
9. Vandecaetsbeek, I., P. Vangheluwe, L. Raeymaekers, F. Wuytack, and J. Vanoevelen. 2011. The Ca2+ pumps of the endoplasmic reticulum and Golgi apparatus. *Cold Spring Harb Perspect Biol* 3.
10. Vangheluwe, P., L. Raeymaekers, L. Dode, and F. Wuytack. 2005. Modulating sarco(endo)plasmic reticulum Ca2+ ATPase 2 (SERCA2) activity: cell biological implications. *Cell Calcium* 38:291-302.
11. Dally, S., R. Bredoux, E. Corvazier, J.P. Andersen, J.D. Clausen, L. Dode, M. Fanchaouy, P. Gelebart, V. Monceau, F. Del Monte, J.K. Gwathmey, R. Hajjar, C. Chaabane, R. Bobe, A. Raies, and J. Enouf. 2006. Ca2+-ATPases in non-failing and failing heart: evidence for a novel cardiac sarco/endoplasmic reticulum Ca2+-ATPase 2 isoform (SERCA2c). *Biochem J* 395:249-58.
12. Gelebart, P., V. Martin, J. Enouf, and B. Papp. 2003. Identification of a new SERCA2 splice variant regulated during monocytic differentiation. *Biochem Biophys Res Commun* 303:676-84.
13. Dally, S., E. Corvazier, R. Bredoux, R. Bobe, and J. Enouf. 2010. Multiple and diverse coexpression, location, and regulation of additional SERCA2 and SERCA3 isoforms in nonfailing and failing human heart. *J Mol Cell Cardiol* 48:633-44.
14. Clausen, J.D., I. Vandecaetsbeek, F. Wuytack, P. Vangheluwe, and J.P. Andersen. 2012. Distinct roles of the C-terminal 11th transmembrane helix and luminal extension in the partial reactions determining the high Ca2+ affinity of sarco(endo)plasmic reticulum Ca2+-ATPase isoform 2b (SERCA2b). *J Biol Chem* 287:39460-9.
15. Autry, J.M. and L.R. Jones. 1997. Functional Co-expression of the canine cardiac Ca2+ pump and phospholamban in Spodoptera frugiperda (Sf21) cells reveals new insights on ATPase regulation. *J Biol Chem* 272:15872-80.

16.	Hovnanian, A. 2007. SERCA pumps and human diseases. *Subcell Biochem* 45:337-63.

17.	Bobe, R., R. Bredoux, E. Corvazier, C. Lacabaratz-Porret, V. Martin, T. Kovacs, and J. Enouf. 2005. How many Ca(2)+ATPase isoforms are expressed in a cell type? A growing family of membrane proteins illustrated by studies in platelets. *Platelets* 16:133-50.

18.	Aulestia, F.J., P.C. Redondo, A. Rodriguez-Garcia, J.A. Rosado, G.M. Salido, M.T. Alonso, and J. Garcia-Sancho. 2011. Two distinct calcium pools in the endoplasmic reticulum of HEK-293T cells. *Biochem J* 435:227-35.

19.	Dhitavat, J., R.J. Fairclough, A. Hovnanian, and S.M. Burge. 2004. Calcium pumps and keratinocytes: lessons from Darier's disease and Hailey-Hailey disease. *Br J Dermatol* 150:821-8.

20.	MacLennan, D.H. 1970. Purification and properties of an adenosine triphosphatase from sarcoplasmic reticulum. *J Biol Chem* 245:4508-18.

21.	Andersen, J.P. 1995. Functional consequences of alterations to amino acids at the M5S5 boundary of the Ca(2+)-ATPase of sarcoplasmic reticulum. Mutation Tyr763-->Gly uncouples ATP hydrolysis from Ca2+ transport. *J Biol Chem* 270:908-14.

22.	Andersen, J.P. and B. Vilsen. 1994. Amino acids Asn796 and Thr799 of the Ca(2+)-ATPase of sarcoplasmic reticulum bind Ca2+ at different sites. *J Biol Chem* 269:15931-6.

23.	Andersen, J.P., B. Vilsen, E. Leberer, and D.H. MacLennan. 1989. Functional consequences of mutations in the beta-strand sector of the Ca2(+)-ATPase of sarcoplasmic reticulum. *J Biol Chem* 264:21018-23.

24.	Andersen, J.P., B. Vilsen, and D.H. MacLennan. 1992. Functional consequences of alterations to Gly310, Gly770, and Gly801 located in the transmembrane domain of the Ca(2+)-ATPase of sarcoplasmic reticulum. *J Biol Chem* 267:2767-74.

25.	Andersen, J.P. and B. Vilsen. 1995. Structure-function relationships of cation translocation by Ca(2+)- and Na+, K(+)-ATPases studied by site-directed mutagenesis. *FEBS Lett* 359:101-6.

26.	MacLennan, D.H. and N.M. Green. 2000. Structural biology. Pumping ions. *Nature* 405:633-4.

27.	Moller, J.V., P. Nissen, T.L. Sorensen, and M. le Maire. 2005. Transport mechanism of the sarcoplasmic reticulum Ca2+ -ATPase pump. *Curr Opin Struct Biol* 15:387-93.

28.	Futai, M., G.H. Sun-Wada, and Y. Wada. 2004. Proton pumping ATPases and diverse inside-acidic compartments. *Yakugaku Zasshi* 124:243-60.

29.	Bublitz, M., H. Poulsen, J.P. Morth, and P. Nissen. 2010. In and out of the cation pumps: P-type ATPase structure revisited. *Curr Opin Struct Biol* 20:431-9.

30.	Toyoshima, C., M. Nakasako, H. Nomura, and H. Ogawa. 2000. Crystal structure of the calcium pump of sarcoplasmic reticulum at 2.6 A resolution. *Nature* 405:647-55.

31. Dode, L., J.P. Andersen, N. Leslie, J. Dhitavat, B. Vilsen, and A. Hovnanian. 2003. Dissection of the functional differences between sarco(endo)plasmic reticulum Ca2+-ATPase (SERCA) 1 and 2 isoforms and characterization of Darier disease (SERCA2) mutants by steady-state and transient kinetic analyses. *J Biol Chem* 278:47877-89.

32. Vandecaetsbeek, I., M. Trekels, M. De Maeyer, H. Ceulemans, E. Lescrinier, L. Raeymaekers, F. Wuytack, and P. Vangheluwe. 2009. Structural basis for the high Ca2+ affinity of the ubiquitous SERCA2b Ca2+ pump. *Proc Natl Acad Sci U S A* 106:18533-8.

33. Inesi, G., D. Lewis, H. Ma, A. Prasad, and C. Toyoshima. 2006. Concerted conformational effects of Ca2+ and ATP are required for activation of sequential reactions in the Ca2+ ATPase (SERCA) catalytic cycle. *Biochemistry* 45:13769-78.

34. Moller, J.V., G. Lenoir, C. Marchand, C. Montigny, M. le Maire, C. Toyoshima, B.S. Juul, and P. Champeil. 2002. Calcium transport by sarcoplasmic reticulum Ca(2+)-ATPase. Role of the A domain and its C-terminal link with the transmembrane region. *J Biol Chem* 277:38647-59.

35. Abu-Abed, M., T.K. Mal, M. Kainosho, D.H. MacLennan, and M. Ikura. 2002. Characterization of the ATP-binding domain of the sarco(endo)plasmic reticulum Ca(2+)-ATPase: probing nucleotide binding by multidimensional NMR. *Biochemistry* 41:1156-64.

36. Rice, W.J., N.M. Green, and D.H. MacLennan. 1997. Site-directed disulfide mapping of helices M4 and M6 in the Ca2+ binding domain of SERCA1a, the Ca2+ ATPase of fast twitch skeletal muscle sarcoplasmic reticulum. *J Biol Chem* 272:31412-9.

37. Rice, W.J. and D.H. MacLennan. 1996. Scanning mutagenesis reveals a similar pattern of mutation sensitivity in transmembrane sequences M4, M5, and M6, but not in M8, of the Ca2+- ATPase of sarcoplasmic reticulum (SERCA1a). *J Biol Chem* 271:31412-9.

38. MacLennan, D.H., D.M. Clarke, T.W. Loo, and I.S. Skerjanc. 1992. Site-directed mutagenesis of the Ca2+ ATPase of sarcoplasmic reticulum. *Acta Physiol Scand Suppl* 607:141-50.

39. Moller, J.V., C. Olesen, A.M. Winther, and P. Nissen. 2010. The sarcoplasmic Ca2+-ATPase: design of a perfect chemi-osmotic pump. *Q Rev Biophys* 43:501-66.

40. Toyoshima, C., H. Nomura, and Y. Sugita. 2003. Crystal structures of Ca2+-ATPase in various physiological states. *Ann N Y Acad Sci* 986:1-8.

41. Hou, Z., Z. Hu, D.J. Blackwell, T.D. Miller, D.D. Thomas, and S.L. Robia. 2012. 2-Color calcium pump reveals closure of the cytoplasmic headpiece with calcium binding. *PLoS ONE* 7:e40369.

42. Winters, D.L., J.M. Autry, B. Svensson, and D.D. Thomas. 2008. Interdomain fluorescence resonance energy transfer in SERCA probed by cyan-fluorescent protein fused to the actuator domain. *Biochemistry* 47:4246-56.

43. Kranias, E.G. and R.J. Hajjar. 2012. Modulation of Cardiac Contractility by the Phopholamban/SERCA2a Regulatome. *Circ Res* 110:1646-60.

44. Calaghan, S.C., E. White, and J. Colyer. 1998. Co-ordinated changes in cAMP, phosphorylated phospholamban, Ca2+ and contraction following beta-adrenergic stimulation of rat heart. *Pflugers Arch* 436:948-56.

45. Karim, C.B., T.L. Kirby, Z. Zhang, Y. Nesmelov, and D.D. Thomas. 2004. Phospholamban structural dynamics in lipid bilayers probed by a spin label rigidly coupled to the peptide backbone. *Proc Natl Acad Sci U S A* 101:14437-42.

46. Karim, C.B., Z. Zhang, E.C. Howard, K.D. Torgersen, and D.D. Thomas. 2006. Phosphorylation-dependent conformational switch in spin-labeled phospholamban bound to SERCA. *J Mol Biol* 358:1032-40.

47. Traaseth, N.J., K.N. Ha, R. Verardi, L. Shi, J.J. Buffy, L.R. Masterson, and G. Veglia. 2008. Structural and dynamic basis of phospholamban and sarcolipin inhibition of Ca(2+)-ATPase. *Biochemistry* 47:3-13.

48. Traaseth, N.J., D.D. Thomas, and G. Veglia. 2006. Effects of Ser16 phosphorylation on the allosteric transitions of phospholamban/Ca(2+)-ATPase complex. *J Mol Biol* 358:1041-50.

49. Paterlini, M.G. and D.D. Thomas. 2005. The alpha-helical propensity of the cytoplasmic domain of phospholamban: a molecular dynamics simulation of the effect of phosphorylation and mutation. *Biophys J* 88:3243-51.

50. Ha, K.N., L.R. Masterson, Z. Hou, R. Verardi, N. Walsh, G. Veglia, and S.L. Robia. 2011. Lethal Arg9Cys phospholamban mutation hinders Ca2+-ATPase regulation and phosphorylation by protein kinase A. *Proc Natl Acad Sci U S A* 108:2735-40.

51. Verardi, R., L. Shi, N.J. Traaseth, N. Walsh, and G. Veglia. 2011. Structural topology of phospholamban pentamer in lipid bilayers by a hybrid solution and solid-state NMR method. *Proc Natl Acad Sci U S A* 108:9101-6.

52. Cornea, R.L., J.M. Autry, Z. Chen, and L.R. Jones. 2000. Reexamination of the role of the leucine/isoleucine zipper residues of phospholamban in inhibition of the Ca2+ pump of cardiac sarcoplasmic reticulum. *J Biol Chem* 275:41487-94.

53. Becucci, L., A. Cembran, C.B. Karim, D.D. Thomas, R. Guidelli, J. Gao, and G. Veglia. 2009. On the function of pentameric phospholamban: ion channel or storage form? *Biophys J* 96:L60-2.

54. Kovacs, R.J., M.T. Nelson, H.K. Simmerman, and L.R. Jones. 1988. Phospholamban forms Ca2+-selective channels in lipid bilayers. *J Biol Chem* 263:18364-8.

55. Oxenoid, K. and J.J. Chou. 2005. The structure of phospholamban pentamer reveals a channel-like architecture in membranes. *Proc Natl Acad Sci U S A* 102:10870-5.

56. Glaves, J.P., C.A. Trieber, D.K. Ceholski, D.L. Stokes, and H.S. Young. 2011. Phosphorylation and mutation of phospholamban alter physical interactions with the sarcoplasmic reticulum calcium pump. *J Mol Biol* 405:707-23.

57.   Ferrington, D.A., Q. Yao, T.C. Squier, and D.J. Bigelow. 2002. Comparable levels of Ca-ATPase inhibition by phospholamban in slow- twitch skeletal and cardiac sarcoplasmic reticulum. *Biochemistry* 41:13289-96.

58.   Ablorh, N.A., T. Miller, F. Nitu, S.J. Gruber, C. Karim, and D.D. Thomas. 2012. Accurate quantitation of phospholamban phosphorylation by immunoblot. *Anal Biochem* 425:68-75.

59.   Chen, Z., B.L. Akin, and L.R. Jones. 2012. Ca2+ binding to site I of the cardiac Ca2+ pump is sufficient to dissociate phospholamban. *J Biol Chem* 285:3253-60.

60.   Akin, B.L. and L.R. Jones. 2012. Characterizing phospholamban to sarco(endo)plasmic reticulum Ca2+-ATPase 2a (SERCA2a) protein binding interactions in human cardiac sarcoplasmic reticulum vesicles using chemical cross-linking. *J Biol Chem* 287:7582-93.

61.   Asahi, M., E. McKenna, K. Kurzydlowski, M. Tada, and D.H. MacLennan. 2000. Physical interactions between phospholamban and sarco(endo)plasmic reticulum Ca2+-ATPases are dissociated by elevated Ca2+, but not by phospholamban phosphorylation, vanadate, or thapsigargin, and are enhanced by ATP. *J Biol Chem* 275:15034-8.

62.   Li, J., D.J. Bigelow, and T.C. Squier. 2004. Conformational changes within the cytosolic portion of phospholamban upon release of Ca-ATPase inhibition. *Biochemistry* 43:3870-9.

63.   James, Z.M., J.E. McCaffrey, K.D. Torgersen, C.B. Karim, and D.D. Thomas. 2012. Protein-protein interactions in calcium transport regulation probed by saturation transfer electron paramagnetic resonance. *Biophys J* 103:1370-8.

64.   Mueller, B., C.B. Karim, I.V. Negrashov, H. Kutchai, and D.D. Thomas. 2004. Direct detection of phospholamban and sarcoplasmic reticulum Ca-ATPase interaction in membranes using fluorescence resonance energy transfer. *Biochemistry* 43:8754-65.

65.   Lockamy, E.L., R.L. Cornea, C.B. Karim, and D.D. Thomas. 2011. Functional and physical competition between phospholamban and its mutants provides insight into the molecular mechanism of gene therapy for heart failure. *Biochem Biophys Res Commun* 408:388-92.

66.   Li, J., Z.M. James, X. Dong, C.B. Karim, and D.D. Thomas. 2012. Structural and Functional Dynamics of an Integral Membrane Protein Complex Modulated by Lipid Headgroup Charge. *J Mol Biol*.

67.   Karim, C.B., C.G. Marquardt, J.D. Stamm, G. Barany, and D.D. Thomas. 2000. Synthetic null-cysteine phospholamban analogue and the corresponding transmembrane domain inhibit the Ca-ATPase. *Biochemistry* 39:10892-7.

68.   Ha, K.N., N.J. Traaseth, R. Verardi, J. Zamoon, A. Cembran, C.B. Karim, D.D. Thomas, and G. Veglia. 2007. Controlling the inhibition of the sarcoplasmic Ca2+-ATPase by tuning phospholamban structural dynamics. *J Biol Chem* 282:37205-14.

69.   Li, J., C.B. Boschek, Y. Xiong, C.A. Sacksteder, T.C. Squier, and D.J. Bigelow. 2005. Essential role for Pro21 in phospholamban for optimal inhibition of the Ca-ATPase. *Biochemistry* 44:16181-91.

70.   Ha, K.N., M. Gustavsson, and G. Veglia. 2012. Tuning the structural coupling between the transmembrane and cytoplasmic domains of phospholamban to control sarcoplasmic reticulum Ca(2+)-ATPase (SERCA) function. *J Muscle Res Cell Motil* 33:485-92.

71.   Toyoshima, C., M. Asahi, Y. Sugita, R. Khanna, T. Tsuda, and D.H. MacLennan. 2003. Modeling of the inhibitory interaction of phospholamban with the Ca2+ ATPase. *Proc Natl Acad Sci U S A* 100:467-72.

72.   Morita, T., D. Hussain, M. Asahi, T. Tsuda, K. Kurzydlowski, C. Toyoshima, and D.H. Maclennan. 2008. Interaction sites among phospholamban, sarcolipin, and the sarco(endo)plasmic reticulum Ca(2+)-ATPase. *Biochem Biophys Res Commun* 369:188-94.

73.   Chen, Z., B.L. Akin, and L.R. Jones. 2007. Mechanism of reversal of phospholamban inhibition of the cardiac Ca2+-ATPase by protein kinase A and by anti-phospholamban monoclonal antibody 2D12. *J Biol Chem* 282:20968-76.

74.   Chen, Z., B.L. Akin, and L.R. Jones. 2010. Ca2+ binding to site I of the cardiac Ca2+ pump is sufficient to dissociate phospholamban. *J Biol Chem* 285:3253-60.

75.   Chen, Z., B.L. Akin, D.L. Stokes, and L.R. Jones. 2006. Cross-linking of C-terminal residues of phospholamban to the Ca2+ pump of cardiac sarcoplasmic reticulum to probe spatial and functional interactions within the transmembrane domain. *J Biol Chem* 281:14163-72.

76.   Chen, Z., D.L. Stokes, and L.R. Jones. 2005. Role of leucine 31 of phospholamban in structural and functional interactions with the Ca2+ pump of cardiac sarcoplasmic reticulum. *J Biol Chem* 280:10530-9.

77.   del Monte, F., S.E. Harding, U. Schmidt, T. Matsui, Z.B. Kang, G.W. Dec, J.K. Gwathmey, A. Rosenzweig, and R.J. Hajjar. 1999. Restoration of contractile function in isolated cardiomyocytes from failing human hearts by gene transfer of SERCA2a. *Circulation* 100:2308-11.

78.   Gommans, I.M., M.H. Vlak, A. de Haan, and B.G. van Engelen. 2002. Calcium regulation and muscle disease. *J Muscle Res Cell Motil* 23:59-63.

79.   Miyamoto, M.I., F. del Monte, U. Schmidt, T.S. DiSalvo, Z.B. Kang, T. Matsui, J.L. Guerrero, J.K. Gwathmey, A. Rosenzweig, and R.J. Hajjar. 2000. Adenoviral gene transfer of SERCA2a improves left-ventricular function in aortic-banded rats in transition to heart failure. *Proc Natl Acad Sci U S A* 97:793-8.

80.   Hajjar, R.J., K. Zsebo, L. Deckelbaum, C. Thompson, J. Rudy, A. Yaroshinsky, H. Ly, Y. Kawase, K. Wagner, K. Borow, B. Jaski, B. London, B. Greenberg, D.F. Pauly, R. Patten, R. Starling, D. Mancini, and M. Jessup. 2008. Design of a phase 1/2 trial of intracoronary administration of AAV1/SERCA2a in patients with heart failure. *J Card Fail* 14:355-67.

81.   Suckau, L., H. Fechner, E. Chemaly, S. Krohn, L. Hadri, J. Kockskamper, D. Westermann, E. Bisping, H. Ly, X. Wang, Y. Kawase, J. Chen, L. Liang, I. Sipo, R. Vetter, S. Weger, J. Kurreck, V. Erdmann, C. Tschope, B. Pieske, D. Lebeche, H.P. Schultheiss, R.J. Hajjar, and W.C. Poller. 2009. Long-term cardiac-targeted RNA interference for the treatment of heart failure restores cardiac function and reduces pathological hypertrophy. *Circulation* 119:1241-52.

82.   Kranias, E.G. and R.J. Hajjar. 2012. Modulation of cardiac contractility by the phospholamban/SERCA2a regulatome. *Circ Res* 110:1646-60.

83.   Kargacin, M.E. and G.J. Kargacin. 1996. The sarcoplasmic reticulum calcium pump is functionally altered in dystrophic muscle. *Biochim Biophys Acta* 1290:4-8.

84.   Divet, A. and C. Huchet-Cadiou. 2002. Sarcoplasmic reticulum function in slow- and fast-twitch skeletal muscles from mdx mice. *Pflugers Arch* 444:634-43.

85.   Divet, A., A.M. Lompre, and C. Huchet-Cadiou. 2005. Effect of cyclopiazonic acid, an inhibitor of the sarcoplasmic reticulum Ca-ATPase, on skeletal muscles from normal and mdx mice. *Acta Physiol Scand* 184:173-86.

86.   Goonasekera, S.A., C.K. Lam, D.P. Millay, M.A. Sargent, R.J. Hajjar, E.G. Kranias, and J.D. Molkentin. 2011. Mitigation of muscular dystrophy in mice by SERCA overexpression in skeletal muscle. *J Clin Invest* 121:1044-52.

87.   Cain, B.S., D.R. Meldrum, K.S. Joo, J.F. Wang, X. Meng, J.C. Cleveland, Jr., A. Banerjee, and A.H. Harken. 1998. Human SERCA2a levels correlate inversely with age in senescent human myocardium. *J Am Coll Cardiol* 32:458-67.

88.   Babusikova, E., J. Lehotsky, D. Dobrota, P. Racay, and P. Kaplan. 2012. Age-associated changes in Ca(2+)-ATPase and oxidative damage in sarcoplasmic reticulum of rat heart. *Physiol Res* 61:453-60.

89.   Minamisawa, S., Y. Sato, Y. Tatsuguchi, T. Fujino, S. Imamura, Y. Uetsuka, M. Nakazawa, and R. Matsuoka. 2003. Mutation of the phospholamban promoter associated with hypertrophic cardiomyopathy. *Biochem Biophys Res Commun* 304:1-4.

90.   Haghighi, K., G. Chen, Y. Sato, G.C. Fan, S. He, F. Kolokathis, L. Pater, I. Paraskevaidis, W.K. Jones, G.W. Dorn, 2nd, D.T. Kremastinos, and E.G. Kranias. 2008. A human phospholamban promoter polymorphism in dilated cardiomyopathy alters transcriptional regulation by glucocorticoids. *Hum Mutat* 29:640-7.

91.   Medin, M., M. Hermida-Prieto, L. Monserrat, R. Laredo, J.C. Rodriguez-Rey, X. Fernandez, and A. Castro-Beiras. 2007. Mutational screening of phospholamban gene in hypertrophic and idiopathic dilated cardiomyopathy and functional study of the PLN -42 C>G mutation. *Eur J Heart Fail* 9:37-43.

92.   Ceholski, D.K., C.A. Trieber, C.F. Holmes, and H.S. Young. 2012. Lethal, hereditary mutants of phospholamban elude phosphorylation by protein kinase A. *J Biol Chem* 287:26596-605.

93.   Medeiros, A., D.G. Biagi, T.J. Sobreira, P.S. de Oliveira, C.E. Negrao, A.J. Mansur, J.E. Krieger, P.C. Brum, and A.C. Pereira. 2011. Mutations in the human phospholamban gene in patients with heart failure. *Am Heart J* 162:1088-1095 e1.

94.   Haghighi, K., F. Kolokathis, A.O. Gramolini, J.R. Waggoner, L. Pater, R.A. Lynch, G.C. Fan, D. Tsiapras, R.R. Parekh, G.W. Dorn, 2nd, D.H. MacLennan, D.T. Kremastinos, and E.G. Kranias. 2006. A mutation in the human phospholamban gene, deleting arginine 14, results in lethal, hereditary cardiomyopathy. *Proc Natl Acad Sci U S A* 103:1388-93.

95. Haghighi, K., F. Kolokathis, L. Pater, R.A. Lynch, M. Asahi, A.O. Gramolini, G.C. Fan, D. Tsiapras, H.S. Hahn, S. Adamopoulos, S.B. Liggett, G.W. Dorn, 2nd, D.H. MacLennan, D.T. Kremastinos, and E.G. Kranias. 2003. Human phospholamban null results in lethal dilated cardiomyopathy revealing a critical difference between mouse and human. *J Clin Invest* 111:869-76.

96. Kelly, E.M., Z. Hou, J. Bossuyt, D.M. Bers, and S.L. Robia. 2008. Phospholamban oligomerization, quaternary structure, and sarco(endo)plasmic reticulum calcium ATPase binding measured by fluorescence resonance energy transfer in living cells. *J Biol Chem* 283:12202-11.

97. Haghighi, K., T. Pritchard, J. Bossuyt, J.R. Waggoner, Q. Yuan, G.C. Fan, H. Osinska, A. Anjak, J. Rubinstein, J. Robbins, D.M. Bers, and E.G. Kranias. 2012. The human phospholamban Arg14-deletion mutant localizes to plasma membrane and interacts with the Na/K-ATPase. *J Mol Cell Cardiol* 52:773-82.

98. Curtis, J.M., W.S. Hahn, E.K. Long, J.S. Burrill, E.A. Arriaga, and D.A. Bernlohr. 2012. Protein carbonylation and metabolic control systems. *Trends Endocrinol Metab* 23:399-406.

99. Belke, D.D. and W.H. Dillmann. 2004. Altered cardiac calcium handling in diabetes. *Curr Hypertens Rep* 6:424-9.

100. Fu, S., L. Yang, P. Li, O. Hofmann, L. Dicker, W. Hide, X. Lin, S.M. Watkins, A.R. Ivanov, and G.S. Hotamisligil. 2011. Aberrant lipid metabolism disrupts calcium homeostasis causing liver endoplasmic reticulum stress in obesity. *Nature* 473:528-31.

101. Park, S.W., Y. Zhou, J. Lee, and U. Ozcan. 2010. Sarco(endo)plasmic reticulum Ca2+-ATPase 2b is a major regulator of endoplasmic reticulum stress and glucose homeostasis in obesity. *Proc Natl Acad Sci U S A* 107:19320-5.

102. del Monte, F., S.E. Harding, G.W. Dec, J.K. Gwathmey, and R.J. Hajjar. 2002. Targeting phospholamban by gene transfer in human heart failure. *Circulation* 105:904-7.

103. Zhao, X.Y., S.J. Hu, J. Li, Y. Mou, K. Bian, J. Sun, and Z.H. Zhu. 2008. rAAV-asPLB transfer attenuates abnormal sarcoplasmic reticulum Ca2+ -ATPase activity and cardiac dysfunction in rats with myocardial infarction. *Eur J Heart Fail* 10:47-54.

104. Bish, L.T., M.M. Sleeper, C. Reynolds, J. Gazzara, E. Withnall, G.E. Singletary, G. Buchlis, D. Hui, K.A. High, G. Gao, J.M. Wilson, and H.L. Sweeney. 2011. Cardiac gene transfer of short hairpin RNA directed against phospholamban effectively knocks down gene expression but causes cellular toxicity in canines. *Hum Gene Ther* 22:969-77.

105. Chen, G., X. Zhou, S. Florea, J. Qian, W. Cai, Z. Zhang, G.C. Fan, J. Lorenz, R.J. Hajjar, and E.G. Kranias. 2010. Expression of active protein phosphatase 1 inhibitor-1 attenuates chronic beta-agonist-induced cardiac apoptosis. *Basic Res Cardiol* 105:573-81.

106. Fish, K.M., D. Ladage, Y. Kawase, I. Karakikes, D. Jeong, H. Ly, K. Ishikawa, L. Hadri, L. Tilemann, J. Muller-Ehmsen, R.J. Samulski, E.G. Kranias, and R.J. Hajjar. 2013. AAV9.I-1c delivered via direct coronary infusion in a porcine

model of heart failure improves contractility and mitigates adverse remodeling. *Circ Heart Fail* 6:310-7.

107. Iwanaga, Y., M. Hoshijima, Y. Gu, M. Iwatate, T. Dieterle, Y. Ikeda, M.O. Date, J. Chrast, M. Matsuzaki, K.L. Peterson, K.R. Chien, and J. Ross, Jr. 2004. Chronic phospholamban inhibition prevents progressive cardiac dysfunction and pathological remodeling after infarction in rats. *J Clin Invest* 113:727-36.

108. Kaye, D.M., A. Preovolos, T. Marshall, M. Byrne, M. Hoshijima, R. Hajjar, J.A. Mariani, S. Pepe, K.R. Chien, and J.M. Power. 2007. Percutaneous cardiac recirculation-mediated gene transfer of an inhibitory phospholamban peptide reverses advanced heart failure in large animals. *J Am Coll Cardiol* 50:253-60.

109. Jessup, M., B. Greenberg, D. Mancini, T. Cappola, D.F. Pauly, B. Jaski, A. Yaroshinsky, K.M. Zsebo, H. Dittrich, and R.J. Hajjar. 2011. Calcium Upregulation by Percutaneous Administration of Gene Therapy in Cardiac Disease (CUPID): a phase 2 trial of intracoronary gene therapy of sarcoplasmic reticulum Ca2+-ATPase in patients with advanced heart failure. *Circulation* 124:304-13.

110. del Monte, F., D. Lebeche, J.L. Guerrero, T. Tsuji, A.A. Doye, J.K. Gwathmey, and R.J. Hajjar. 2004. Abrogation of ventricular arrhythmias in a model of ischemia and reperfusion by targeting myocardial calcium cycling. *Proc Natl Acad Sci U S A* 101:5622-7.

111. Byrne, M.J., J.M. Power, A. Preovolos, J.A. Mariani, R.J. Hajjar, and D.M. Kaye. 2008. Recirculating cardiac delivery of AAV2/1SERCA2a improves myocardial function in an experimental model of heart failure in large animals. *Gene Ther* 15:1550-7.

112. Jaski, B.E., M.L. Jessup, D.M. Mancini, T.P. Cappola, D.F. Pauly, B. Greenberg, K. Borow, H. Dittrich, K.M. Zsebo, and R.J. Hajjar. 2009. Calcium upregulation by percutaneous administration of gene therapy in cardiac disease (CUPID Trial), a first-in-human phase 1/2 clinical trial. *J Card Fail* 15:171-81.

113. Mayer, E.J., W. Huckle, R.G. Johnson, Jr., and E. McKenna. 2000. Characterization and quantitation of phospholamban and its phosphorylation state using antibodies. *Biochem Biophys Res Commun* 267:40-8.

114. Johnson, R.G., Jr. 1998. Pharmacology of the cardiac sarcoplasmic reticulum calcium ATPase-phospholamban interaction. *Ann N Y Acad Sci* 853:380-92.

115. Micheletti, R., G.G. Mattera, M. Rocchetti, A. Schiavone, M.F. Loi, A. Zaza, R.J. Gagnol, S. De Munari, P. Melloni, P. Carminati, G. Bianchi, and P. Ferrari. 2002. Pharmacological profile of the novel inotropic agent (E,Z)-3-((2-aminoethoxy)imino)androstane-6,17-dione hydrochloride (PST2744). *J Pharmacol Exp Ther* 303:592-600.

116. Rocchetti, M., A. Besana, G. Mostacciuolo, R. Micheletti, P. Ferrari, S. Sarkozi, C. Szegedi, I. Jona, and A. Zaza. 2005. Modulation of sarcoplasmic reticulum function by Na+/K+ pump inhibitors with different toxicity: digoxin and PST2744 [(E,Z)-3-((2-aminoethoxy)imino)androstane-6,17-dione hydrochloride]. *J Pharmacol Exp Ther* 313:207-15.

117. The Digitalis Investigation Group. 1997. The effect of digoxin on mortality and morbidity in patients with heart failure. . *N Engl J Med* 336:525-33.

118. Gheorghiade, M., A.P. Ambrosy, M. Ferrandi, and P. Ferrari. 2011. Combining SERCA2a activation and Na-K ATPase inhibition: a promising new approach to managing acute heart failure syndromes with low cardiac output. *Discov Med* 12:141-51.

119. Shah, S.J., J.E. Blair, G.S. Filippatos, C. Macarie, W. Ruzyllo, J. Korewicki, S.I. Bubenek-Turconi, M. Ceracchi, M. Bianchetti, P. Carminati, D. Kremastinos, J. Grzybowski, G. Valentini, H.N. Sabbah, and M. Gheorghiade. 2009. Effects of istaroxime on diastolic stiffness in acute heart failure syndromes: results from the Hemodynamic, Echocardiographic, and Neurohormonal Effects of Istaroxime, a Novel Intravenous Inotropic and Lusitropic Agent: a Randomized Controlled Trial in Patients Hospitalized with Heart Failure (HORIZON-HF) trial. *Am Heart J* 157:1035-41.

120. Li, J., Z.M. James, X. Dong, C.B. Karim, and D.D. Thomas. 2012. Structural and functional dynamics of an integral membrane protein complex modulated by lipid headgroup charge. *J Mol Biol* 418:379-89.

121. Slavoff, S.A., D.S. Liu, J.D. Cohen, and A.Y. Ting. 2011. Imaging protein-protein interactions inside living cells via interaction-dependent fluorophore ligation. *J Am Chem Soc* 133:19769-76.

122. Lemke, E.A. 2011. Site-specific labeling of proteins for single-molecule FRET measurements using genetically encoded ketone functionalities. *Methods Mol Biol* 751:3-15.

123. Milles, S., S. Tyagi, N. Banterle, C. Koehler, V. VanDelinder, T. Plass, A.P. Neal, and E.A. Lemke. 2012. Click strategies for single-molecule protein fluorescence. *J Am Chem Soc* 134:5187-95.

124. Wombacher, R. and V.W. Cornish. 2011. Chemical tags: applications in live cell fluorescence imaging. *J Biophotonics* 4:391-402.

125. van Roessel, P. and A.H. Brand. 2002. Imaging into the future: visualizing gene expression and protein interactions with fluorescent proteins. *Nat Cell Biol* 4:E15-20.

126. Chalfie, M. 1995. Green fluorescent protein. *Photochem Photobiol* 62:651-6.

127. Prendergast, F.G. 1999. Biophysics of the green fluorescent protein. *Methods Cell Biol* 58:1-18.

128. Pakhomov, A.A. and V.I. Martynov. 2008. GFP family: structural insights into spectral tuning. *Chem Biol* 15:755-64.

129. Simmerman, H.K., J.H. Collins, J.L. Theibert, A.D. Wegener, and L.R. Jones. 1986. Sequence analysis of phospholamban. Identification of phosphorylation sites and two major structural domains. *J Biol Chem* 261:13333-41.

130. Frank, K.F., B. Bolck, K. Brixius, E.G. Kranias, and R.H. Schwinger. 2002. Modulation of SERCA: implications for the failing human heart. *Basic Res Cardiol* 97 Suppl 1:I72-8.

131. Hasenfuss, G. and J.R. Teerlink. 2011. Cardiac inotropes: current agents and future directions. *Eur Heart J* 32:1838-45.

132. Hoshijima, M., Y. Ikeda, Y. Iwanaga, S. Minamisawa, M.O. Date, Y. Gu, M. Iwatate, M. Li, L. Wang, J.M. Wilson, Y. Wang, J. Ross, Jr., and K.R. Chien. 2002. Chronic suppression of heart-failure progression by a pseudophosphorylated mutant of phospholamban via in vivo cardiac rAAV gene delivery. *Nat Med* 8:864-71.

133. Nicolaou, P., R.J. Hajjar, and E.G. Kranias. 2009. Role of protein phosphatase-1 inhibitor-1 in cardiac physiology and pathophysiology. *J Mol Cell Cardiol* 47:365-71.

134. Negash, S., Q. Yao, H. Sun, J. Li, D.J. Bigelow, and T.C. Squier. 2000. Phospholamban remains associated with the Ca2+- and Mg2+-dependent ATPase following phosphorylation by cAMP-dependent protein kinase. *Biochem J* 351:195-205.

135. Bidwell, P., D.J. Blackwell, Z. Hou, A.V. Zima, and S.L. Robia. 2011. Phospholamban binds with differential affinity to calcium pump conformers. *J Biol Chem* 286:35044-50.

136. Maruyama, K. and D.H. MacLennan. 1988. Mutation of aspartic acid-351, lysine-352, and lysine-515 alters the Ca2+ transport activity of the Ca2+-ATPase expressed in COS-1 cells. *Proc Natl Acad Sci U S A* 85:3314-8.

137. Birmachu, W., F.L. Nisswandt, and D.D. Thomas. 1989. Conformational transitions in the calcium adenosinetriphosphatase studied by time-resolved fluorescence resonance energy transfer. *Biochemistry* 28:3940-7.

138. Ablorh, N.A., F. Nitu, K. Engebretsen, D.D. Thomas, and J.S. Holger. 2009. Insulin-dependent rescue from cardiogenic shock is not mediated by phospholamban phosphorylation. *Clin Toxicol (Phila)*:1-7.

139. Ablorh, N.-A., T. Miller, F.R. Nitu, S.J. Gruber, C.B. Karim, and D.D. Thomas. 2012. Accurate quantitation of phospholamban phosphorylation by immunoblot. *Anal Biochem*:accepted.

140. Autry, J.M., J.E. Rubin, S.D. Pietrini, D.L. Winters, S.L. Robia, and D.D. Thomas. 2011. Oligomeric interactions of sarcolipin and the Ca-ATPase. *J Biol Chem* 286:31697-706.

141. Kimura, Y., M. Asahi, K. Kurzydlowski, M. Tada, and D.H. MacLennan. 1998. Phospholamban domain Ib mutations influence functional interactions with the Ca2+-ATPase isoform of cardiac sarcoplasmic reticulum. *J Biol Chem* 273:14238-41.

142. Robia, S.L., K.S. Campbell, E.M. Kelly, Z. Hou, D.L. Winters, and D.D. Thomas. 2007. Forster transfer recovery reveals that phospholamban exchanges slowly from pentamers but rapidly from the SERCA regulatory complex. *Circ Res* 101:1123-9.

143. Crystal, R.G. 2003. Cardiac gene therapy: Pumping the heart. *Gene Therapy* 10:2-3.

144. Muretta, J.M., I.V. Negrashov, A. Kyrychenko, A.S. Ladokhin, D. Kast, G.E. Gillispie, and D.D. Thomas. 2010. High-performance time-resolved fluorescence by direct waveform recording. *Rev Sci Instrum*:in press.

145. Cantilina, T., Y. Sagara, G. Inesi, and L.R. Jones. 1993. Comparative studies of cardiac and skeletal sarcoplasmic reticulum ATPases. Effect of a phospholamban antibody on enzyme activation by Ca2+. *J Biol Chem* 268:17018-25.

146. Kranias, E.G. and D.M. Bers. 2007. Calcium and cardiomyopathies. *Subcell Biochem* 45:523-37.

147. Hadri, L. and R.J. Hajjar. 2011. Calcium cycling proteins and their association with heart failure. *Clin Pharmacol Ther* 90:620-4.

148. Jessup, M., B. Greenberg, D. Mancini, T. Cappola, D.F. Pauly, B. Jaski, A. Yaroshinsky, K.M. Zsebo, H. Dittrich, and R.J. Hajjar. 2011. Calcium Upregulation by Percutaneous Administration of Gene Therapy in Cardiac Disease (CUPID): A Phase 2 Trial of Intracoronary Gene Therapy of Sarcoplasmic Reticulum Ca2+-ATPase in Patients With Advanced Heart Failure. *Circulation*.

149. Gruber, S.J., S. Haydon, and D.D. Thomas. 2012. Phospholamban mutants compete with wild type for SERCA binding in living cells. *Biochem Biophys Res Commun*:epublished.

150. Fruen, B.R., J.M. Bardy, T.M. Byrem, G.M. Strasburg, and C.F. Louis. 2000. Differential Ca(2+) sensitivity of skeletal and cardiac muscle ryanodine receptors in the presence of calmodulin. *Am J Physiol Cell Physiol* 279:C724-33.

151. Ferrington, D., Moewe, P., Yao, Q., and Bigelow, D. 1998. Comparison of the stoichiomtery of phospholamban to SERCA2a in cardiac and skeletal muscle. *Biophys J* 74:356-361.

152. Muretta, J.M., A. Kyrychenko, A.S. Ladokhin, D. Kast, G.E. Gillispie, and D.D. Thomas. 2010. High -performance time-resolved fluorescence by direct waveform recording. *Rev Sci Instrum* 81:103101-1 - 103101-8.

153. Zhang, J.H., T.D. Chung, and K.R. Oldenburg. 1999. A Simple Statistical Parameter for Use in Evaluation and Validation of High Throughput Screening Assays. *J Biomol Screen* 4:67-73.

154. Chemaly, E.R., L. Hadri, S. Zhang, M. Kim, E. Kohlbrenner, J. Sheng, L. Liang, J. Chen, K.R. P, R.J. Hajjar, and D. Lebeche. 2011. Long-term in vivo resistin overexpression induces myocardial dysfunction and remodeling in rats. *J Mol Cell Cardiol* 51:144-55.

155. Jin, H., E.R. Chemaly, A. Lee, C. Kho, L. Hadri, R.J. Hajjar, and F.G. Akar. Mechanoelectrical remodeling and arrhythmias during progression of hypertrophy. *Faseb J* 24:451-63.

156. Zhu, X., O.Y. Bernecker, N.S. Manohar, R.J. Hajjar, J. Hellman, F. Ichinose, H.H. Valdivia, and U. Schmidt. 2005. Increased leakage of sarcoplasmic reticulum Ca2+ contributes to abnormal myocyte Ca2+ handling and shortening in sepsis. *Crit Care Med* 33:598-604.

157. Comley, J. 2010. Fluorescence lifetime finally picking up momentum! *Drug Discovery World*:71-82.

158. Gustavsson, M., N.J. Traaseth, C.B. Karim, E.L. Lockamy, D.D. Thomas, and G. Veglia. 2011. Lipid-Mediated Folding/Unfolding of Phospholamban as a

Regulatory Mechanism for the Sarcoplasmic Reticulum Ca(2+)-ATPase. *J Mol Biol*.

159.   Espinoza-Fonseca, L.M. and D.D. Thomas. 2011. Atomic-level characterization of the activation mechanism of SERCA by calcium. *PLoS One* 6:e26936.

160.   Meyer, M., W. Schillinger, B. Pieske, C. Holubarsch, C. Heilmann, H. Posival, G. Kuwajima, K. Mikoshiba, H. Just, G. Hasenfuss, and et al. 1995. Alterations of sarcoplasmic reticulum proteins in failing human dilated cardiomyopathy. *Circulation* 92:778-84.

161.   Schmidt, U., R.J. Hajjar, C.S. Kim, D. Lebeche, A.A. Doye, and J.K. Gwathmey. 1999. Human heart failure: cAMP stimulation of SR Ca(2+)-ATPase activity and phosphorylation level of phospholamban. *Am J Physiol* 277:H474-80.

162.   Kawase, Y., D. Ladage, and R.J. Hajjar. 2011. Rescuing the failing heart by targeted gene transfer. *J Am Coll Cardiol* 57:1169-80.

163.   Kawase, Y., H.Q. Ly, F. Prunier, D. Lebeche, Y. Shi, H. Jin, L. Hadri, R. Yoneyama, K. Hoshino, Y. Takewa, S. Sakata, R. Peluso, K. Zsebo, J.K. Gwathmey, J.C. Tardif, J.F. Tanguay, and R.J. Hajjar. 2008. Reversal of cardiac dysfunction after long-term expression of SERCA2a by gene transfer in a pre-clinical model of heart failure. *J Am Coll Cardiol* 51:1112-9.

164.   Khan, H., M. Metra, J.E. Blair, M. Vogel, M.E. Harinstein, G.S. Filippatos, H.N. Sabbah, H. Porchet, G. Valentini, and M. Gheorghiade. 2009. Istaroxime, a first in class new chemical entity exhibiting SERCA-2 activation and Na-K-ATPase inhibition: a new promising treatment for acute heart failure syndromes? *Heart Fail Rev* 14:277-87.

165.   Gobbini, M., S. Armaroli, L. Banfi, A. Benicchio, G. Carzana, G. Fedrizzi, P. Ferrari, G. Giacalone, M. Giubileo, G. Marazzi, R. Micheletti, B. Moro, M. Pozzi, P.E. Scotti, M. Torri, and A. Cerri. 2008. Novel analogues of istaroxime, a potent inhibitor of Na+,K+-ATPase: synthesis and structure-activity relationship. *J Med Chem* 51:4601-8.

166.   Arbabian, A., J.P. Brouland, P. Gelebart, T. Kovacs, R. Bobe, J. Enouf, and B. Papp. 2011. Endoplasmic reticulum calcium pumps and cancer. *Biofactors* 37:139-49.

167.   Gehrig, S.M., C. van der Poel, T.A. Sayer, J.D. Schertzer, D.C. Henstridge, J.E. Church, S. Lamon, A.P. Russell, K.E. Davies, M.A. Febbraio, and G.S. Lynch. 2012. Hsp72 preserves muscle function and slows progression of severe muscular dystrophy. *Nature* 484:394-8.

168.   MacLennan, D.H., and Kranias, E. G. 2003. Phospholamban: a crucial regulator of cardiac contractility. *Nature Reviews* 4:666-678.

169.   Bylund, D.B. 2007. Alpha- and beta-adrenergic receptors: Ahlquist's landmark hypothesis of a single mediator with two receptors. *Am J Physiol Endocrinol Metab* 293:E1479-1481.

170.   Banerjee, R.K. and A.G. Datta. 1983. Proteoliposome as the model for the study of membrane-bound enzymes and transport proteins. *Molecular and Cellular Biochemistry* 50:3-15.

171. Johnson, R.G., Jr. and E.G. Kranias. 1998. Cardiac sarcoplasmic reticulum function and regulation of contractility. Introduction. *Ann N Y Acad Sci* 853:xi-xvi.

172. Johnson, R.G., Jr. 1998. Pharmacology of the cardiac sarcoplasmic reticulum calcium ATPase- phospholamban interaction. *Ann N Y Acad Sci* 853:380-92.

173. Cornea, R.L., S.J. Gruber, E.L. Lockamy, J.M. Muretta, D. Jin, J. Chen, R. Dahl, T. Bartfai, K.M. Zsebo, G.D. Gillispie, and D.D. Thomas. 2013. High-throughput FRET assay yields allosteric SERCA activators. *J Biomol Screen* 18:97-107.

174. Feher, J.J. and F.N. Briggs. 1983. Determinants of calcium loading at steady state in sarcoplasmic reticulum. *Biochim Biophys Acta* 727:389-402.

175. Mueller, B., M. Zhao, I.V. Negrashov, R. Bennett, and D.D. Thomas. 2004. SERCA structural dynamics induced by ATP and calcium. *Biochemistry* 43:12846-54.

176. Stergiopoulos, V., P. O'Campo, A. Gozdzik, J. Jeyaratnam, S. Corneau, A. Sarang, and S.W. Hwang. 2012. Moving from rhetoric to reality: adapting Housing First for homeless individuals with mental illness from ethno-racial groups. *BMC Health Serv Res* 12:345.

177. Michelangeli, F. and J.M. East. 2011. A diversity of SERCA Ca2+ pump inhibitors. *Biochem Soc Trans* 39:789-97.

178. Tazzeo, T., F. Worek, and L. Janssen. 2009. The NADPH oxidase inhibitor diphenyleneiodonium is also a potent inhibitor of cholinesterases and the internal Ca(2+) pump. *Br J Pharmacol* 158:790-6.

179. Ariazi, E.A. and V.C. Jordan. 2006. Estrogen-related receptors as emerging targets in cancer and metabolic disorders. *Curr Top Med Chem* 6:203-15.

180. Clontech. 2006. Tet-On Advanced Inducible Gene Expression System User Manual. *Clontech*.

181. De Angelis, A.A. and S.J. Opella. 2007. Bicelle samples for solid-state NMR of membrane proteins. 2:2332-2338.

182. Clark, H.B. and H.T. Orr. 2000. Spinocerebellar ataxia type 1--modeling the pathogenesis of a polyglutamine neurodegenerative disorder in transgenic mice. *J Neuropathol Exp Neurol* 59:265-70.

183. Orr, H.T. 2012. SCA1-phosphorylation, a regulator of Ataxin-1 function and pathogenesis. *Prog Neurobiol* 99:179-85.

184. Menon, R.P., D. Soong, C. de Chiara, M.R. Holt, N. Anilkumar, and A. Pastore. 2012. The importance of serine 776 in Ataxin-1 partner selection: a FRET analysis. *Sci Rep* 2:919.

185. Aronson, D. and H. Krum. 2012. Novel therapies in acute and chronic heart failure. *Pharmacol Ther* 135:1-17.

186. Malik, F.I., J.J. Hartman, K.A. Elias, B.P. Morgan, H. Rodriguez, K. Brejc, R.L. Anderson, S.H. Sueoka, K.H. Lee, J.T. Finer, R. Sakowicz, R. Baliga, D.R. Cox, M. Garard, G. Godinez, R. Kawas, E. Kraynack, D. Lenzi, P.P. Lu, A. Muci, C. Niu, X. Qian, D.W. Pierce, M. Pokrovskii, I. Suehiro, S. Sylvester, T. Tochimoto, C. Valdez, W. Wang, T. Katori, D.A. Kass, Y.T. Shen, S.F. Vatner, and D.J.

Morgans. 2011. Cardiac myosin activation: a potential therapeutic approach for systolic heart failure. *Science* 331:1439-43.

187. Agafonov, R.V., I.V. Negrashov, Y.V. Tkachev, S.E. Blakely, M.A. Titus, D.D. Thomas, and Y.E. Nesmelov. 2009. Structural dynamics of the myosin relay helix by time-resolved EPR and FRET. *Proc Natl Acad Sci U S A* 106:21625-30.